

Manufacturing of Large Metallic Components through Wire and Arc Additive Manufacturing(WAAM)

Pushkar Kumar Pandey

A Thesis Submitted to
Indian Institute of Technology Hyderabad
In Partial Fulfillment of the Requirements for
The Degree of Master of Technology



Department of Mechanical and Aerospace Engineering

June 2019

Declaration

I declare that this written submission represents my ideas in my own words, and where ideas or words of others have been included, I have adequately cited and referenced the original sources. I also declare that I have adhered to all principles of academic honesty and integrity and have not misrepresented or fabricated or falsified any idea/data/fact/source in my submission. I understand that any violation of the above will be a cause for disciplinary action by the Institute and can also evoke penal action from the sources that have thus not been properly cited, or from whom proper permission has not been taken when needed.

Pushkar Pandey

(Signature)

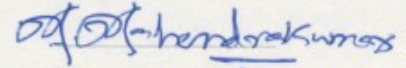
(Pushkar Kumar Pandey)

ME17MTECH11028

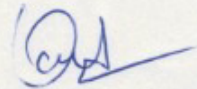
(Roll No.)

Approval Sheet

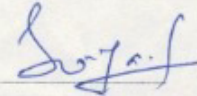
This Thesis entitled Manufacturing of Large Metallic Components through Wire and Arc Additive Manufacturing(WAAM) by Pushkar Kumar Pandey is approved for the degree of Master of Technology from IIT Hyderabad



(Dr. Mahendrakumar Madhavan) Examiner
Dept. of Civil Engineering
IITH



(Prof. N Venkata Reddy) Examiner
Dept. of Mechanical and Aerospace Engineering
IITH



(Dr Suryakumar S) Adviser
Dept. of Mechanical and Aerospace Engineering
IITH

Acknowledgements

I will first express my gratitude to my thesis advisor **Dr S Suryakumar** of IIT H for "Wire and arc additive manufacturing(WAAM) for large functional metal components". The door to Dr S. SURYAKUMAR's office was always open whenever I had any issue or any kind of doubts related to my project work. He motivated me in the right direction at tough times. I will also thank the people whose papers for literature survey I used to have the better depth about my research. I would like to thank manufacturing lab staff **Ramu G** and **Ramesh Boini** for their continuous support. Further I would like to put my heartfelt thanks towards **Nagallapati Vishwanath, Srinath Ellaswamy Gudur** and **Shashi Ranjan Mohan** for the continuous support. Also I feel extremely grateful to **Syed Quadir Moinuddin** for helping me throughout this work. Finally, I feel grateful to express my thankfulness to **My parents** and to **My friends** to empower me with continuous support while writing this thesis. This accomplishment seems hard to imagine without their help and support. **Thanks to the wind which has ever supported me.**

Dedication

I would like to dedicate this endeavour to my late Grandfather Shri Durgaprasad Pandey.

Abstract

Metal additive manufacturing have been in trend due to its ability to produce components at reduced cost and low buy-to-fly ratio. There are various techniques employed for metal additive manufacturing depending on energy source and type of raw materials used. Based on raw materials, metal additive manufacturing can be classified as wire-based, powder-based and sheet-based (laminated object manufacturing). Amongst these three, wire based systems have higher material efficiency and high deposition rates. They also better suited for continuous and uncluttered material supply. Hence, they are most suitable for large components. These wire based systems can be used in conjunction to different energy sources like Laser, Electron Beam and Arc. WLAM (wire and laser based additive manufacturing), EBAM (electron beam additive manufacturing) and WAAM (wire and arc based additive manufacturing) are examples of each of these energy sources respectively. In this study, Weld-deposition based WAAM is chosen.

The objective of this work is to fabricate large (greater than 1m in size) metallic components using WAAM process. Parameter study, kinematic setup for such working volumes and thermal analysis of deposition process to minimize distortions are some of the related aspects. Sample components in both multi-pass and single-pass geometries were also fabricated successfully. This work was mainly carried out for mild steel (ER70S6); some preliminary studies on extending this to IN625 are also presented. Overall, this thesis presents the suitability of WAAM in conjunction with a robotic or CNC type kinematic setup to produce large metallic components.

Contents

Declaration	ii
Approval Sheet	iii
Acknowledgements	iv
Abstract	vi
1 Introduction	6
1.1 Metal Additive Manufacturing	6
1.2 Applications of Metal Additive Manufacturing	8
1.3 Classification of Metal AM methods	9
1.3.1 Based on Energy source used	9
1.3.2 Based on form of raw material	11
1.4 Scope and Objective	12
2 Literature Review	14
2.1 Fabrication of Large Metal AM components	23
2.1.1 Laser based Additive Manufacturing	23
2.1.2 Electron beam based Additive Manufacturing	24
2.1.3 WAAM	25
2.2 Wire-Arc Deposition of Inconel 625	26
2.2.1 Distinctive properties and applications of IN625	26
2.2.2 Parameter control for IN625	28
3 Experimental Setup	31
3.1 Kinematic Setup for Weld-Deposition	31
3.2 Weld-Deposition Methodology	32
3.3 Initial Studies on Parameter Selection	32
3.4 Summary	33
4 Large Component Fabrication	34
4.1 Thick Multi-Pass Components	34
4.1.1 ϕ 250 mm cylinder	34
4.1.2 ϕ 900 mm cylinder	37
4.2 Thin Single-Pass Components	42
4.2.1 Simple Cylinder	44
4.2.2 Cylinder with Grooves	45

5	Thermal Analysis of the Deposition Process	49
5.1	Modelling procedure	49
5.1.1	Finite Element Modelling	49
5.1.2	Filler Element Modelling	50
5.1.3	Heat Source Model	51
5.1.4	Boundary Conditions	52
5.2	Result and Discussion	54
5.2.1	Temperature History of various points	55
5.2.2	Influence of Neighbourhood Deposition on previous pass	61
5.3	Heat Loss Rate and Dwell Time Estimation	65
5.4	Summary	68
6	Preliminary studies on weld deposition of IN625	69
6.1	Modification to the Deposition Setup	69
6.2	Parameter Study	70
6.2.1	Single Pass	70
6.2.2	Multi Pass	71
6.3	Fabrication of Simple Geometries	72
6.4	Issues and Challenges	73
7	Summary and Future scope	75
7.1	Summary of the Current Work	75
7.2	Future Scope	75
	References	77

List of Figures

1.1	Steps for AM process: (a) CAD model (b) Numerical slicing (c) Layer processing for a single layer (d) Layer processing for all layers and (e) Finished component [8].	7
1.2	AM fabricated Fuel nozzle for Jet Engine [11]	8
1.3	Titanium propellant tank [11]	9
1.4	Classification of metal AM	9
1.5	WLAM [16]	10
1.6	EBAM [12]	10
1.7	Welding based additive manufacturing [3]	11
2.1	Maximum temperature gradient in Y direction at different heights [24]	14
2.2	Y-direction maximum Temp gradient of the molten pool for different heights in same as well as different directions [24]	15
2.3	A typical HLM process [18]	15
2.4	Thermal cycle variation in a given layer [18]	16
2.5	Ultimate tensile strength along vertical direction for different values of current [18]	16
2.6	laser assisted(pulsed) MIG based additive manufacturing setup [23]	17
2.7	Pulse waveform of laser beam [23]	17
2.8	Surfaces at (a)Power=0 W (b)Power=200 W (c)Power=400 W (d)Power=600 W [23]	18
2.9	Effect of different laser powers on bead width [23]	18
2.10	High speed image of droplet transfer in CMT [14]	19
2.11	Location of a tensile test specimen [10]	19
2.12	WAAM of a angled wall [7]	20
2.13	Effect of TS on EWT and SW for ER4043 aluminium filler wire [7]	20
2.14	WAAM and inter layer rolling setup [5]	21
2.15	Microhardness at different locations [5]	21
2.16	Tensile properties of deposited interlayer rolled and heat treated 2219 alloy [5]	22
2.17	Turbine blade using WAAM 195 mm height(left) and impeller height was 70 mm. (right) [4]	22
2.18	Welding and milling [17]	23
2.19	Wing brackets for Airbus A350 XWB jets printed by concept laser [11]	23
2.20	An engine block fabricated using laser based AM courtesy-Concept Laser machine [11]	24
2.21	EBAM fabriacted component Ref- Lockheed Martin [13]	24
2.22	6 m long Al alloy spar fabricated using Robotic WAAM [20]	25
2.23	Top view(left) and side view(right) of Ti-6Al-4V spar wing structure using Robotic WAAM [21]	25
2.24	Fatigue resistance of IN625 & alloy 625 LCF [15]	26
2.25	TTT diagram of Alloy 625 [15]	27

2.26	Diagram of Alloy IN625 manufactured recuperator for a turbine engines [15]	27
2.27	Bellows produced using LCF IN625 (left) & Alloy Steel Boiler Tube Welded using alloy IN625(right) [15]	28
2.28	chemical composition of inconel 625	28
2.29	DOE prediction of current and travel speed effect on deposition rate [9]	28
2.30	Different arc length corrections [1]	29
2.31	Effect of arc correction parameter on depth,width and height of beads [1]	29
3.1	Schematic flow diagram of Robotic WAAM setup	31
3.2	Process flow diagram for WAAM	32
3.3	Parameter optimization for multi-pass circular beads	33
4.1	Path generation strategy for first layer	35
4.2	Fabrication process of medium scale components using Robotic WAAM	36
4.3	Deposition after 1st layer(left) deposition after 5 layers(right)	36
4.4	WAAM fabricated cylinder top view(left) and side walls(right)	37
4.5	Fabricated cylinder has 110 mm height(left) and 250 mm diameter with 10 mm wall thickness(right)	37
4.6	CAD model of fixture table to clamp the base plate	38
4.7	Position of clamps and fixture to avoid distortion with fabricated cylinder (980 mm diameter and 50 mm height)/initial trial with thinner wall thickness	38
4.8	Area filling strategy for first layer	39
4.9	Fabrication of large component	40
4.10	State of deposition after 1st layer,100 mm and 200 mm	40
4.11	Last layer deposition on left and finally deposited layer with 900 mm diameter and 240 mm height with 20 mm wall thickness	41
4.12	WAAM manufactured component before and after machining	41
4.13	Experimental setup for retrofitted CNC cum CMT deposition unit	42
4.14	Position of clamps and torch for initial setup	44
4.15	Fabrication of simple cylinder using WAAM	45
4.16	Fabricated simple cylinder	45
4.17	Fabrication of cylinder with grooves	46
4.18	Deposition after layer 1	46
4.19	Deposition after layer 50 mm deposition and 100 mm deposition	47
4.20	Deposition after layer 200 mm deposition and 300 mm deposition	47
4.21	Deposition at 400 mm height(left) finally deposited component(right) with 400 mm height and 250 diameter	48
5.1	Model for simufact welding analysis	50
5.2	Goldak's double ellipsoid moving heat source model (Goldak et al. , 1984)	51
5.3	Clamping boundary condition	52
5.4	Trajectories and initial boundary condition	53
5.5	Layout for lower layer(on left) layout for lower layer(on right)	54
5.6	Time-Temperature profile of particle 4 at the end of deposition	55
5.7	Variation of Goldak heat source temperature from center	56
5.8	Temperature profile of particle 3	56
5.9	Temperature profile of particle 1	57
5.10	Temperature profile of particle 2	57

5.11	Layout for lower layer(on left) layout for lower layer(on right)	58
5.12	Temperature profile of particle 12	59
5.13	Temperature profile of particle 9	59
5.14	Temperature profile of particle 5	60
5.15	Temperature profile of particle 6	60
5.16	Temperature profile of particle 7	61
5.17	Temperature profile of particle 8	61
5.18	Temperature profile of particles 3 and 4	62
5.19	Temperature profile of particles 1 and 2	62
5.20	Temperature profile of particles 7 and 8	63
5.21	Temperature profile of particles 5 and 6	63
5.22	Temperature of base plate at the end of layer 11 deposition	64
5.23	Temperature of base plate at the end of layer 11 deposition	64
5.24	Bead 1 of layer 1 deposition with external radius r_2 and internal radius r_1	66
5.25	Elemental layer deposition with thickness dh on base plate	66
6.1	Experimental setup for WAAM of IN625	69
6.2	Single bead deposition of In625 on In600 plates	70
6.3	multi-pass IN625 deposition at high/medium travel speed	71
6.4	multi-pass IN625 deposition at low travel speed	72
6.5	multi-pass IN625 deposition at low travel speed multi-pass(left) and multi-pass with mul- tilayer(3*3)	72
6.6	Deposition of thin wall of IN625	73

List of Tables

1.1	Source comparison [6]	12
1.2	Process comparison [6]	12
4.1	Parameters for WAAM fabrication of medium sized component	35
4.2	Parameters for ER70S-61.2 mm diameter for 4 multi-pass beads	39
4.3	CMT specifications	43
4.4	Chemical composition of ER70S-6(copper coated mild steel wire)	43
4.5	Parameters used for thin walled components fabricated using WAAM	44
6.1	Width and height for single deposited bead of Inconel 625	70

Abbreviation

AM- additive manufacturing

BAAM-Big area additive manufacturing

CMT-Cold metal Transfer

DDM-direct digital manufacturing

EBAM-electron beam additive manufacturing

EWT-Effective wall thickness

GMAW-Gas metal arc welding

HLM-hybrid layer manufacturing

KCP-kuka control panel

MS-mild steel

MIG-metal inert gas

PAW-plasma arc welding

PWHT-post welding heat treatment

TIG-tungsten inert gas welding

TS-travel speed

SMD-shaped metal deposition

STL-standard tessellation language

WAAM-wire and arc additive manufacturing

WLAM-wire and laser additive manufacturing

WFS-wire feed speed

Chapter 1

Introduction

1.1 Metal Additive Manufacturing

Metal additive manufacturing have been in trend due to its ability to produce components at reduced cost and low buy-to-fly ratio. There are various techniques employed for metal additive manufacturing depending on energy source and type of raw materials used. Based on raw materials, metal additive manufacturing can be classified as wire-based, powder-based and sheet-based (laminated object manufacturing). Amongst these three, wire based systems have higher material efficiency and high deposition rates. They also better suited for continuous and uncluttered material supply. Hence, they are most suitable for large components. These wire based systems can be used in conjunction to different energy sources like Laser, Electron Beam and Arc. WLAM (wire and laser based additive manufacturing), EBAM (electron beam additive manufacturing) and WAAM (wire and arc based additive manufacturing) are examples of each of these energy sources respectively. This section is about WAAM and its comparison with other powder and wire based systems and the application of metal additive manufacturing. Wire and arc additive manufacturing is a center of attraction now a days due to higher deposition rates, with added freedom of selection of power source as well its manipulation. The facility with the wire and arc manufacturing provided to get the desired properties at different locations is due to ability to change deposition parameters like current voltage and wire feed rates etc. Wire and arc additive manufacturing specially GMAW based has the potential to build large objects due to its ability to provide higher deposition rates. Arc based welding depositions is preferred over electron beam and laser based AM because it is more economical as well as faster.

In GMAW based additive manufacturing utilizes GMAW welding which consists of joining 2 metals by formation of arc between a consumable electrode wire (typically 0.8mm-1.5 mm diameter) and work piece by using an inert gas as protective shield and metal transfer to work piece takes place in 3 modes through- short circuit, globular or spray transfer. Short circuit transfer results at low arc current levels is suitable for thin walls production due to smaller weld pool through contact. Globular transfer occurs at mid-level arc current under gravity by large droplet formation and spray transfer at high arc current with influence of inert gas and is suitable for thicker walls and more penetration.

In WAAM wire and arc manufacturing components are made by deposition by bead of metal welds layer by layer using GMAW welding explained above and utilizing a position system like a CNC positioning system. Main advantage of wire and arc manufacturing additive manufacturing is high deposition rate so it is able to reduce manufacturing as well as lead time. Despite of higher deposition rates better economics and speed of the process GMAW based AM has some major areas of concern when implementing for bigger products issues being residual stresses due to temperature gradient because of successive

layer deposition layer stability due to slower solidification for larger layers, surface roughness which can go on accumulating due to scallops, substrate or base plate distortion as well as risk of welding defects.

Now a days various work are being done and are under research to prove the existing worth and potential of GMAW based AM for large scale components for its implication into aerospace, marine, petroleum and gas turbine industries for high temperature strength nickel alloy (INCONEL 718 and Inconel 625) as well as titanium alloy and complications and issues with its future implementation and challenges associated with it. The term AM has many variants for name like 3D Printing, Rapid Prototyping (RP),layered manufacturing and additive fabrication. Additive manufacturing application is limitless. Earlier Additive manufacturing was used in the form of Rapid Prototyping for producing prototype of actual working model. Now a days,AM is being used to fabricate functional user products in aircraft, dental restorations, medical implants, automobiles, and even fashion products. Additive manufacturing makes it possible to manufacture a 3D object out of 3D cad model by realizing one layer at a time. STL format is sliced and tool path generation strategies are made then each layer is realized at a time and thus layer by layer complete formation of the object is done. The basic steps for additive manufacturing is shown below.

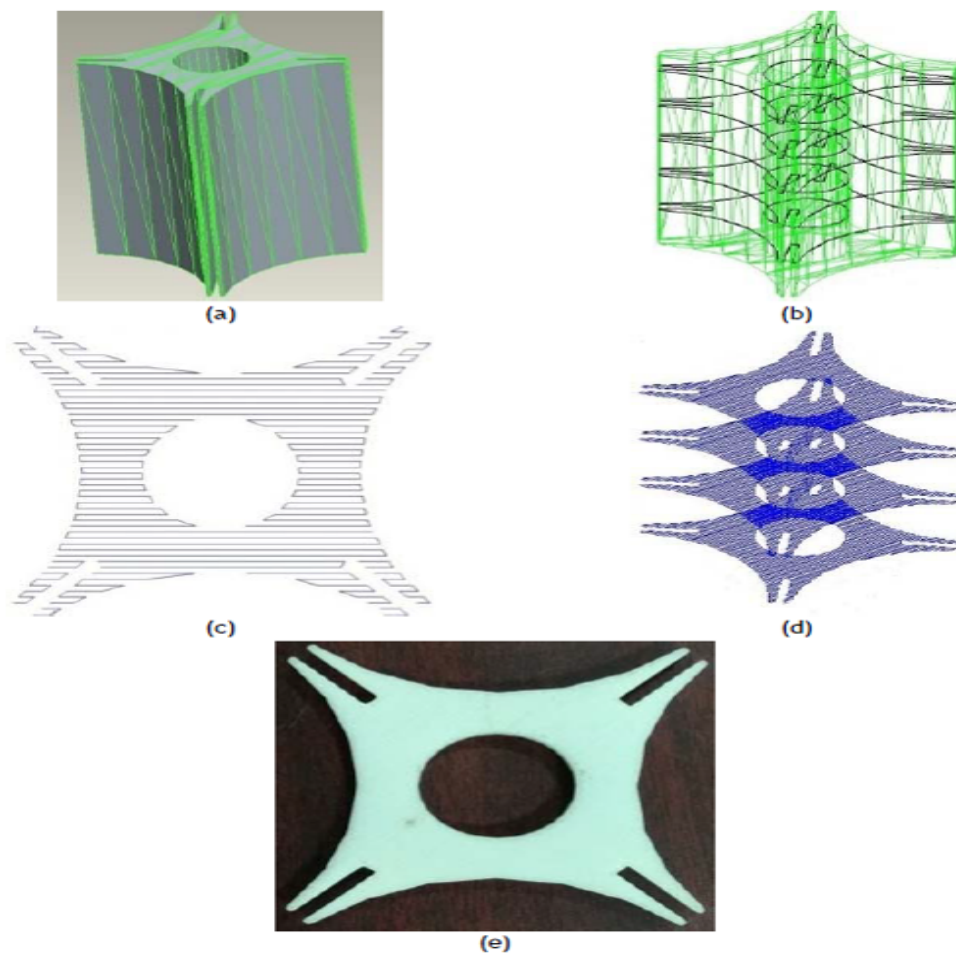


Figure 1.1: Steps for AM process: (a) CAD model (b) Numerical slicing (c) Layer processing for a single layer (d) Layer processing for all layers and (e) Finished component [8].

1.2 Applications of Metal Additive Manufacturing

Initially considered as sheer tool of prototyping and modelling AM has now expanded its domain of applications in so much wider domains. From initial prototyping or tooling to final product modern industries like architectural, medical, dental, aerospace, automotive, furniture and jewellery, new and innovative applications are constantly being developed. The major application of AM lies in following domains.

- Model and Prototype fabrication.
- Medical equipments,automobiles and aersospace sector.
- For job order short term production where tooling cost for conventional processes is higher
- Fabrication of complex geometries.



Figure 1.2: AM fabricated Fuel nozzle for Jet Engine [11]

Some other big area applications of metal AM involves in jet engines,rockets,oil and gas equipments,turbine blades,nuclear components,marine application etc. Also aircraft structures frames and parts can be manufactured using EBAM and WAAM techniques. Lockheed Martin tried to print satellite part using EBAM they tried conducting R & D in 3D-printing propellant tanks made of titanium which is capable of meeting higher demands of the same. They used the higher deposition rates of EBAM that resulted in reducing the fabrication time of fule tank for spacecraft by 80%.



Figure 1.3: Titanium propellant tank [11]

1.3 Classification of Metal AM methods

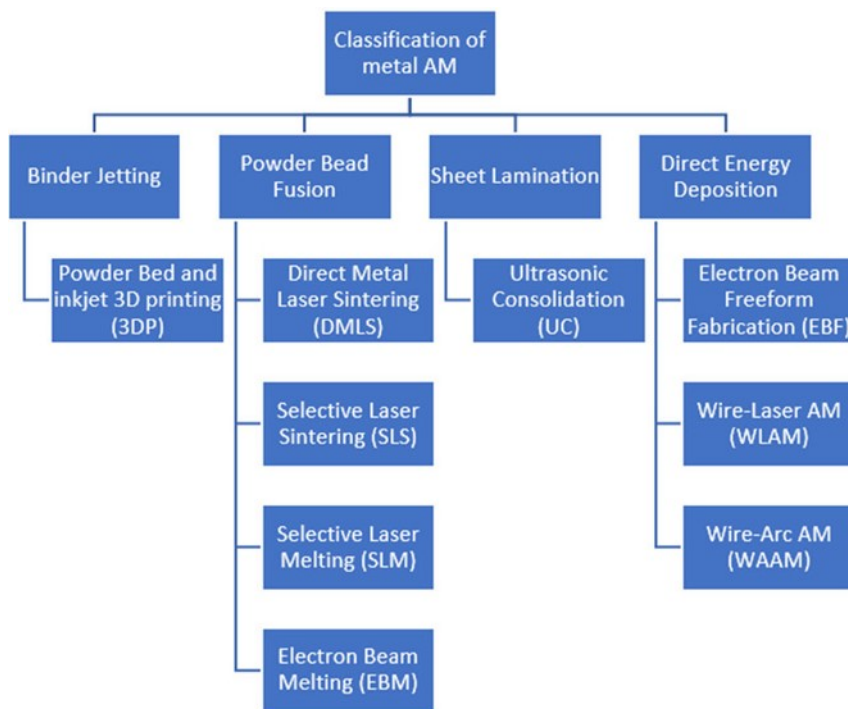


Figure 1.4: Classification of metal AM

1.3.1 Based on Energy source used

Additive manufacturing has been classified as laser based, electron Beam based and Welding and welding based additive manufacturing on the basis of power source. Later these processes can also be

classified on the basis of raw material basically in wire or powder form(for metals). Below are the process details of the above classified types of wire based AM and their comparison based on quality, cost speed and size characteristics.

Wire and Laser based Additive manufacturing(WLAM)

WLAM(wire laser additive manufacturing) is capable of producing complex 3D shapes, realized by feeding the wire into the pool of metal achieved through a laser. Highly dense parts can be manufactured of good quality of low to medium scale. Due to luxury of high power density small and intricate features can be achieved with near net shape using WLAM. Downside being cost and inability to produce bigger components.

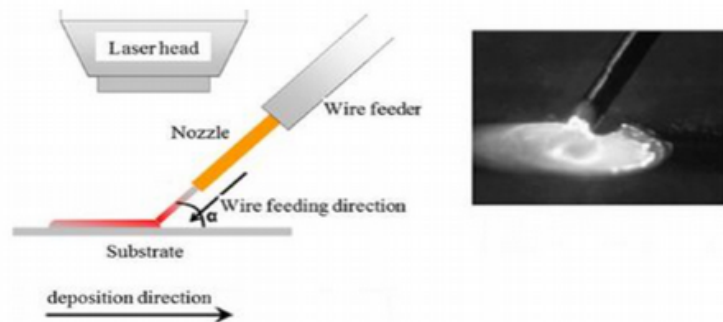


Figure 1.5: WLAM [16]

Electron beam additive manufacturing(EBAM)

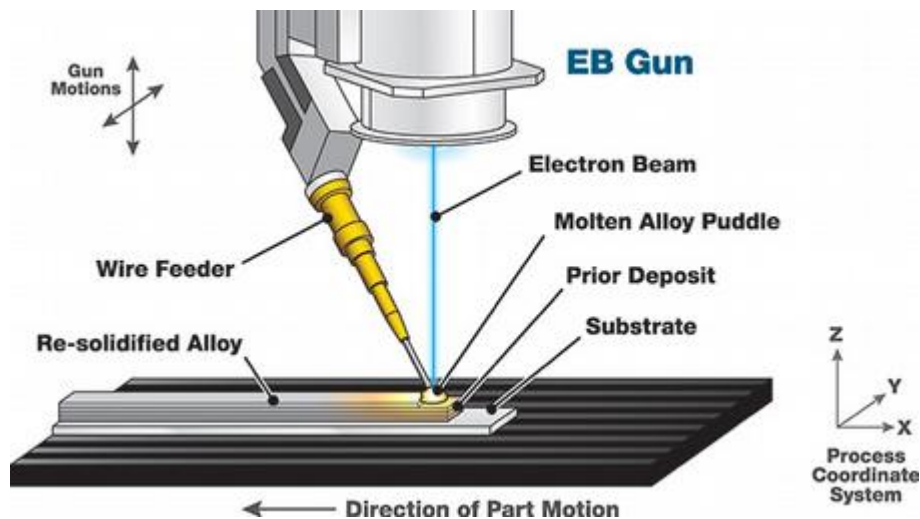


Figure 1.6: EBAM [12]

Wire based EBAM is better than powder based EBAM in terms of simplicity and deposition rates. Using electron beam as a heat source makes it possible to make bigger as well as complex and intricate parts. Also use to vacuum gives us the privilege to easily deposit highly reactive metals such as titanium which other wise would have required separate shield. The downside being the cost is higher as compared to WAAM and the essence of vacuum makes it bulky and costly.

GMAW based wire and arc additive manufacturing

In welding based AM manufacturing also properly known as WAAM ,heat supply unit is a welding power source. The (metal inert gas) welding gun is used to melt the wire and create the molten pool with the right selection of optimized parameter and correct tool path generation strategy layer by layer deposition is carried out. This is capable of creating parts of larger and complex parts with the proper control of dynamics at lower cost. The vital advantage of WAAM being its high deposition rate in comparison to all other processes which makes it faster and favourable. As shown in figure for simple rectangular deposition torch movement is shown in x direction(travel direction say) and subsequent layers are deposited in z direction(building direction say). ACM gas mixture(AR 80 % and carbon dioxide 20 %) Argon is used to provide inert gas shielding with more penetration and comparatively lesser spatter.

The most common blend is 75 % Ar / 25 % CO_2 for the simple reason is that it combines good penetration with reduced spatter. Running straight CO_2 gives the highest penetration depth, but it also creates a lot of spatter. The 75 Ar/25 CO_2 mix also provides more stability for other than flat position welding like V-up, H and OH. The reason being is that increased penetration when using 100 percent CO_2 shielding gas often makes these other than flat welds difficult for those who are not experienced in running hot and fast.

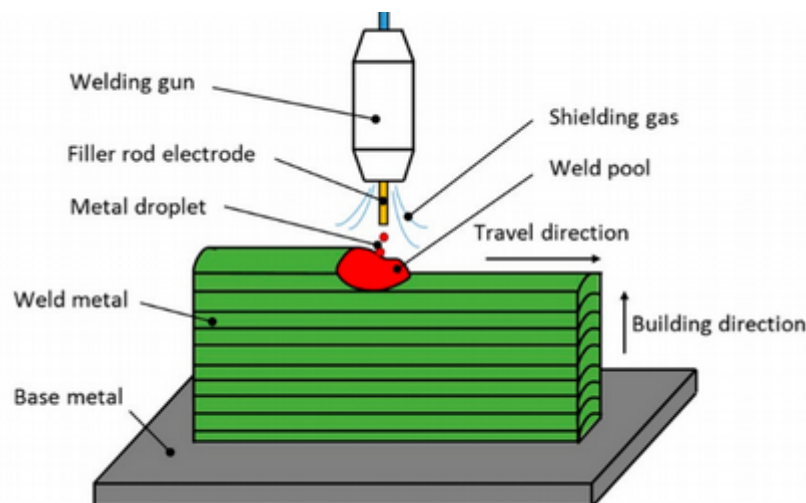


Figure 1.7: Welding based additive manufacturing [3]

1.3.2 Based on form of raw material

Various attributes have been used to compare the 3 processes for better estimation of GMAW based WAAM as compared to other powder based processes.

Ding [2] compared various wire feed additive metal additive manufacturing techniques and came with the distinguished characteristics of different wire feed processes. He justified the AM for its ability to be automated with the CAD/CAM environment resulting in reduced human intervention and saved production time. Powder bed technology was found to be geometrically more accurate than any other process with typical layer thickness of about 20-100 micrometers and dimensional accuracy of . 05 mm and roughness of around 10 micrometers but deposition rate is low 10 g/min limiting its application for large sized component. Wire feed AM however having 100 percent material efficiency which also makes it more environment friendly as compared to powders. WAAM has way more deposition rate around 330 g/min for stainless steel.

With increased deposition rates large components can be produced economically but accuracy and

Table 1.1: Source comparison [6]

Characteristic	Laser/EB	ARC
Quality of geometry	Near net	
Quality of material	similar	
Power efficiency	2-5 % laser and 15-20 % EB	>80 %
Material utilization	Powder efficiency 10-15%	Close to 100 % as wire is used
Speed	2/10 g/min	50-130 g/min
cost	Too expensive	Less expensive
size	Bulky	compact

Table 1.2: Process comparison [6]

Charateristic	Laser beam	Electron Beam	Arc
Source	photon	electron	metallic
Particle/EMV	EMV	not yet	particle
Energy density	less($10^6 w/mm^2$)	More($10^8 w/mm^2$)	very high
Efficiency	poor(2-5 %)	good(15-20 %)	excellent
Vcuum	not required	required	required

surface finish of parts decreases which has to be taken care still metal wires are of less cost which makes WAAM preferred.

1.4 Scope and Objective

It can be clearly visualized that the most of the fabrication and analysis related to WAAM for metals such as mild steel is restricted to small/medium components (typically 250 mm maximum) whereas the industry demands in fields of aerospace turbines, marine application as well as civil structures (bridge and columns) is for larger components the existing technology for manufacturing of these products is having lot of material wastage (very high BTF (buy to fly ratio) meaning they involve too much material wastage using GMAW AM to manufacture this product may drastically reduce the BTF ratio and hence will result in huge cost saving.

In aerospace and marine application big Inconel 625 components are needed due to their increased strength corrosion and fatigue strength at elevated temperature these component can be manufactured by WAAM and will result in huge reduction in cost (up to 80-85 percent of material reduction) and time, the components which by machine take 40-50 h would only take 15 hours of arc time.

Analysis and fabrication for fabrication of bigger alloy and mild steel component was to be done. Robotic WAAM has the immense capacity to fabricate bigger components due to larger working space and tool path generation capacity so it was exploited for this work to produce thicker multi-pass components of bigger size also due to more suitability of CMT for single pass and thin walled components, the thin walled components were deposited using CNC & CMT integration to fabricate large thin walled cylindrical component CNC providing required tool path and CMT as deposition unit.

Chapter 2

Literature Review

Previous work on WAAM

The control of distortion specially substrate or base plate distortion and residual stress being the cause of it is one of the major concern when looking for large scale WAAM process. The residual stress and the distortion is caused by temperature variation across the layers while moving in z direction to understand this variation temperature profile study of AM layers becomes important. Zhao [24] studied thermal analysis during single pass & multi-layer welding deposition he came up with the conclusion that temperature gradient decreased with the increasing layer height as shown in figure.

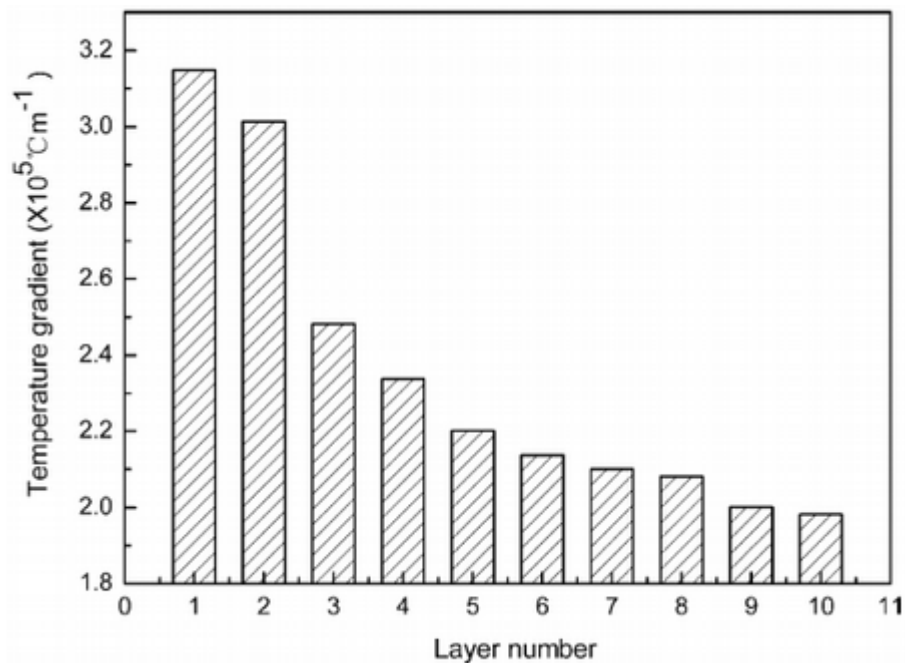


Figure 2.1: Maximum temperature gradient in Y direction at different heights [24]

zhao [24] also compared the same and reverse deposition directions to reveal that same deposition direction has greater temperature gradient than reverse deposition direction.

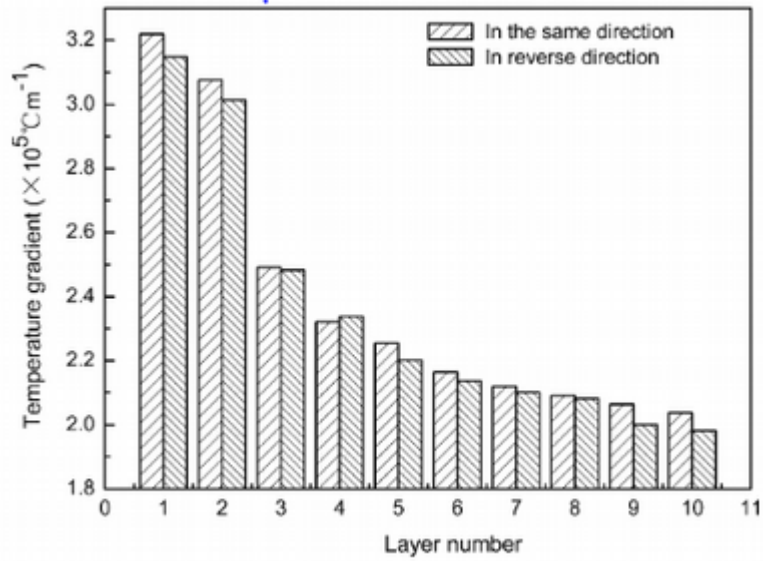


Figure 2.2: Y-direction maximum Temp gradient of the molten pool for different heights in same as well as different directions [24]

It was also concluded the heat spread in same cladding direction to be better as compared to reverse direction, and he stated that by optimizing the depositing direction the condition of heat diffusion could be improved.

S suryakumar [18] studied mechanical properties of objects made through weld deposition for metallic objects made through HLM(hybrid layer manufacturing) to analyse the hardness and tensile strength of WAAM manufactured metallic components.

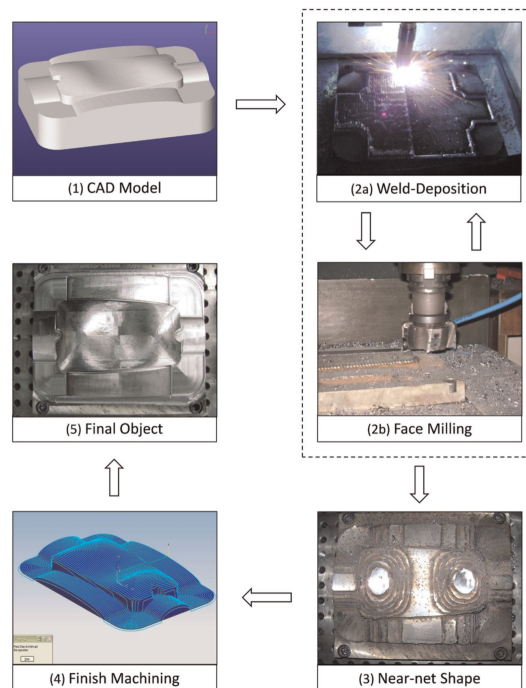


Figure 2.3: A typical HLM process [18]

Suryakumar [18] also tried to conceptualize the effect of thermal cycle on tensile strength and hardness

made through hybrid layer manufacturing.

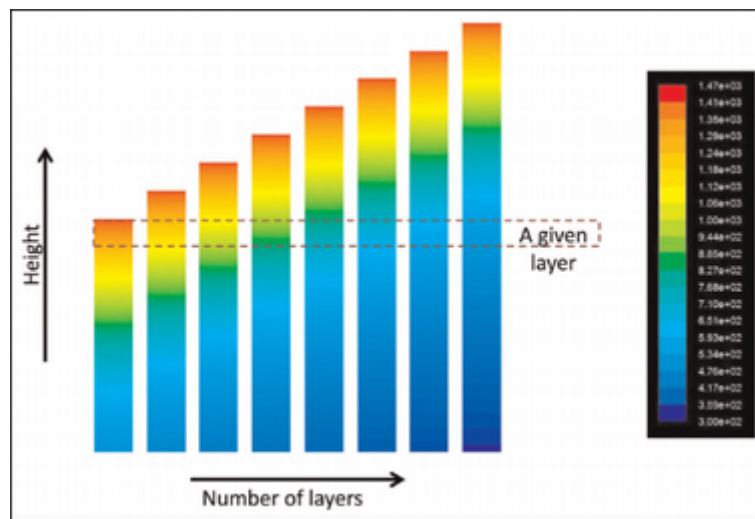


Figure 2.4: Thermal cycle variation in a given layer [18]

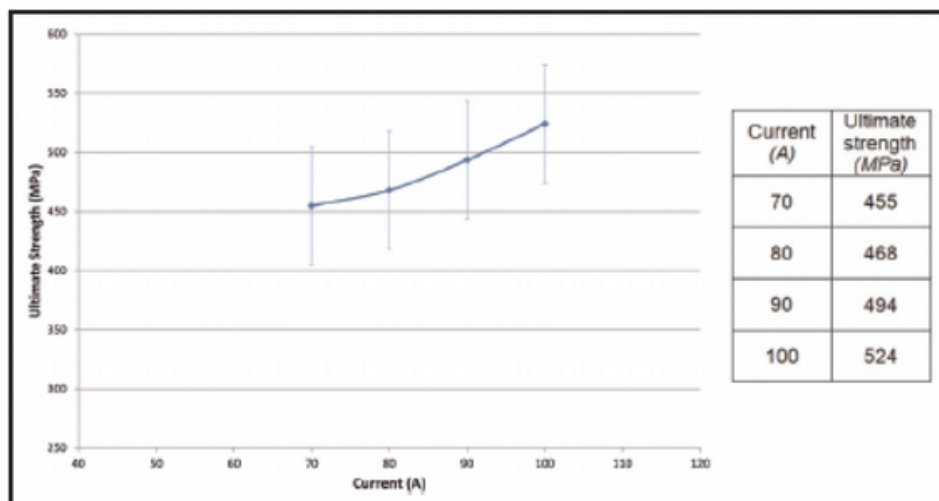


Figure 2.5: Ultimate tensile strength along vertical direction for different values of current [18]

Due to thermal variation across layers on increasing z height difference in maximum hardness he observed on the top layer while it was less in layers below top layers while for tensile stress it was same for horizontal while in vertical direction it was observed to be lower in vertical direction but it was possible to rectify it by increasing amperage. Also ability of HLM process to successfully produce composites where tensile strength of bond was found to be stronger than tensile strength of weaker material.

Xiong [22] studied the reason behind the poor surface quality in GMAW based AM manufacturing and he tried to study the crucial parameters which affect the surface quality and found interlayer temperature, wire speed and travel speed were important he found that increasing the interlayer temperature was attributed to increased surface roughness not only that but this even contributed to decreased layer height due to decreased heat conduction rate with increased layer height.

Xiong [22] also found that when travel speed(TS) was low that resulted in more height hence caused more stair stepping effect but increasing travel speed was limited to 420 mm/min as increasing travel speed beyond it caused poor surface quality due to spatter due to arc instability. While WFS (wire feed

speed) when increased caused more surface roughness due to mixing of layers and thus resulted unstable molten pool.

Zhang [23] suggested that using low power pulsed laser assistance for MIG based AM can result in reduced variation or fluctuation in width and height of bead also material utilization was claimed to be increased by 15 percent also for thin walled component better surface quality and stability was witnessed for ER5356 aluminium alloy wire and 6061 aluminium alloy plates(300mm*300mm*5mm).

The detailed process and results are given below the laser pulsed waveform was provided with typical MIG setting as shown in form of pulsed waveform as shown in the figure 1. 15 below.

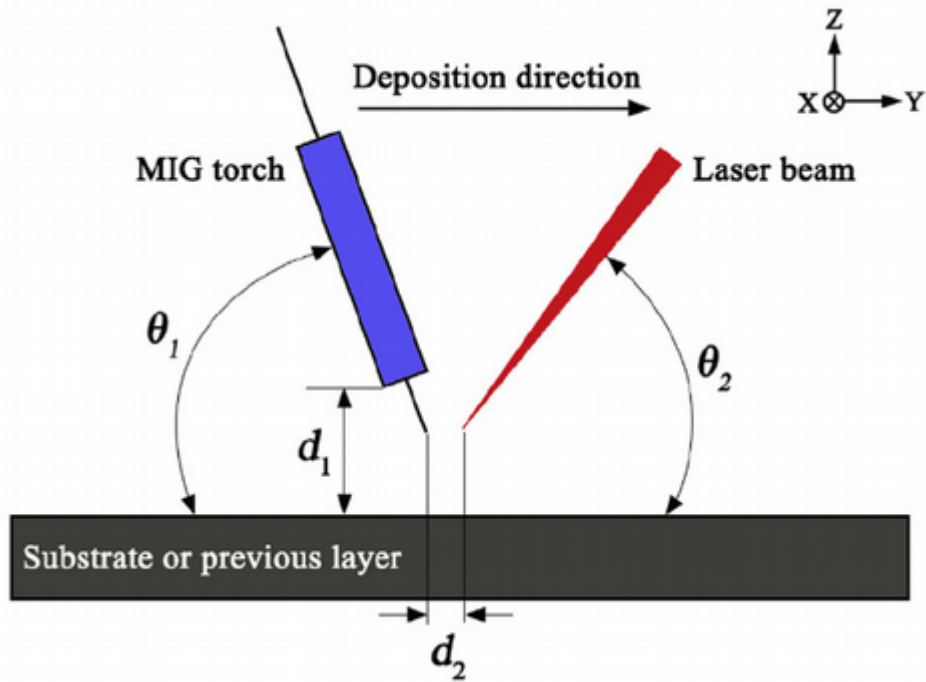


Figure 2.6: laser assisted(pulsed) MIG based additive manufacturing setup [23]

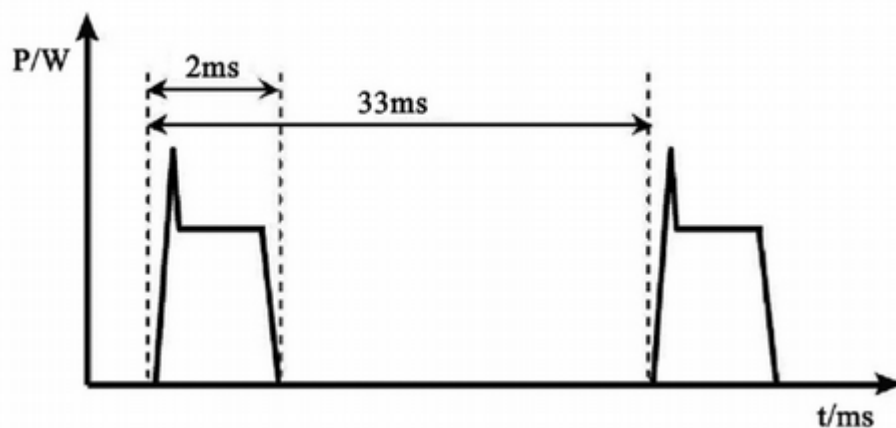


Figure 2.7: Pulse waveform of laser beam [23]

Zhang [23] also studied surface qualities at different laser powers at 0 watt 200 Watt 400watt 600 Watt in the figure given below in order to study the effect of varied laser powers on surface roughness

as well as on width of the thin walled component produced through laser assisted MIG based additive manufacturing.

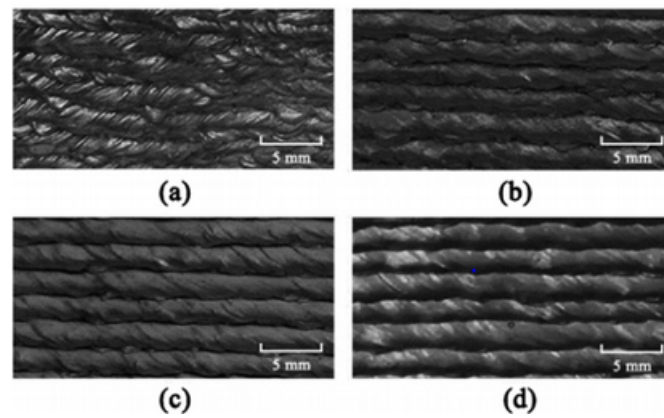


Figure 2.8: Surfaces at (a)Power=0 W (b)Power=200 W (c)Power=400 W (d)Power=600 W [23]

It can be observed from the figure below, as laser power is increased the width of bead decreases for 200 W and 400 W and the width is found to be increases again on increasing laser power from 400 W to 600 W but is still lesser than 0 W. Also is can be clearly observed that on laser assisted waveform the width of bead of thin walled component is relatively constant as compared to MIG at 0 laser power.

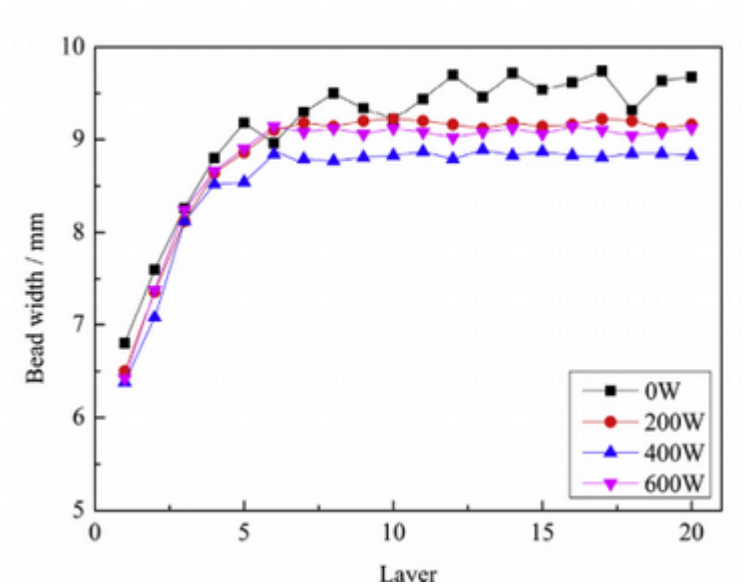


Figure 2.9: Effect of different laser powers on bead width [23]

Selvi [14] studied cold metal transfer for spatter reduction and welding characteristic of different materials using GMAW CMT.

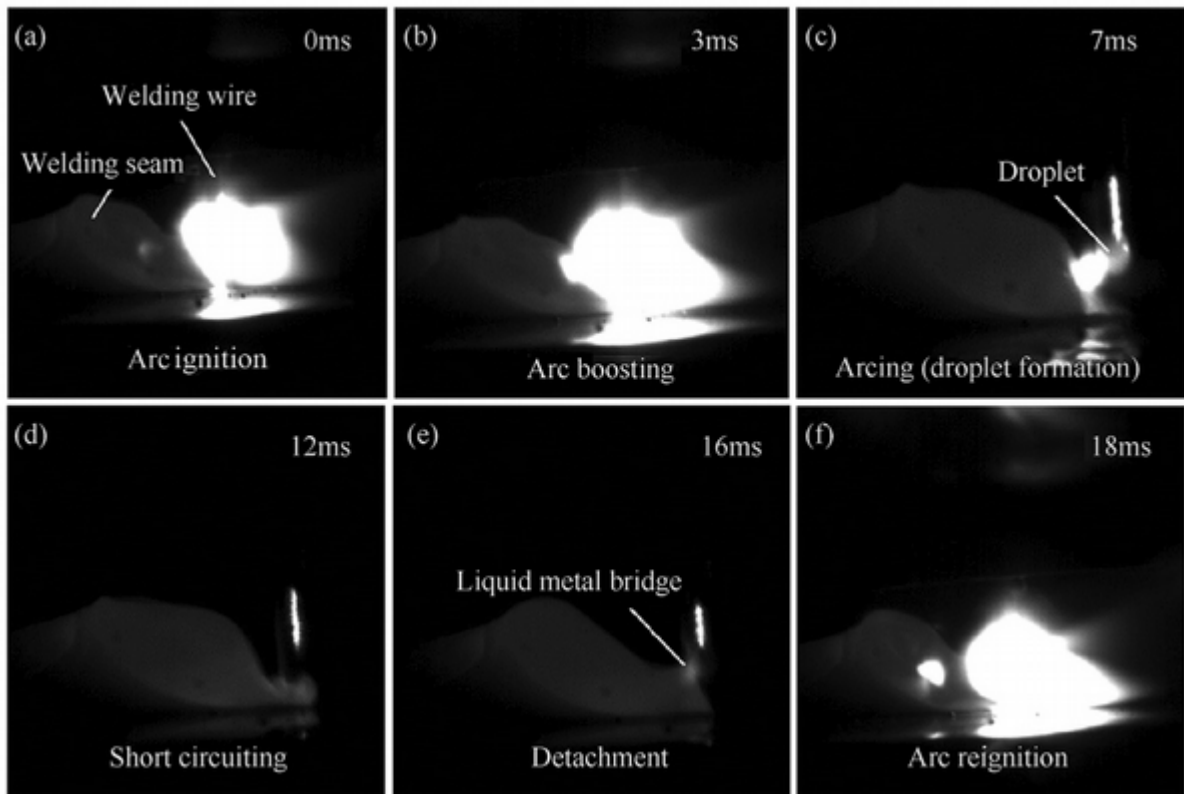


Figure 2.10: High speed image of droplet transfer in CMT [14]

It has several advantages such as low energy, spatter free, high WS . Although it is good for AM of thin walled components but there is a unfavourable possibility of incomplete fusion.

Posch [10] studied material properties of stainless steel blade Dimension of blade 200mm*220mm*10mm manufactured using WAAM using GMAW CMT(cold metal transfer) power source to analyse the better surface condition with CMT than typical GMAW process also he observed different yield strength in different direction for measurement which might be attributed to different grain orientation.

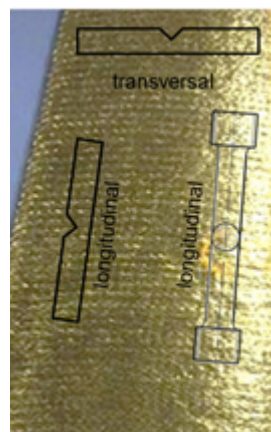


Figure 2.11: Location of a tensile test specimen [10]

Microstructure was comparable to typical GMAW process with no porosity and lack of fusion. Kazanas [7] focused on inclined position of welding torch using CMT to solve accessibility issues during

deposition he also studied effect of TS on quality of angled wall . He measured quality of walls using 2 variables : (i) effective wall thickness (EWT), which has been interpreted as the maximum thickness of wall(constant) which can be achieved after machining (ii) Surface waviness SW, which is the average maximum distance between peak to valley quantified using the profile of some given area of the wall.

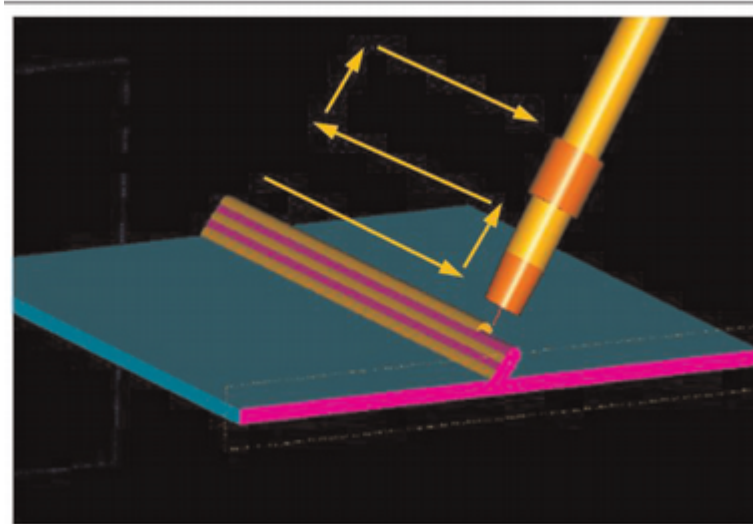


Figure 2.12: WAAM of a angled wall [7]

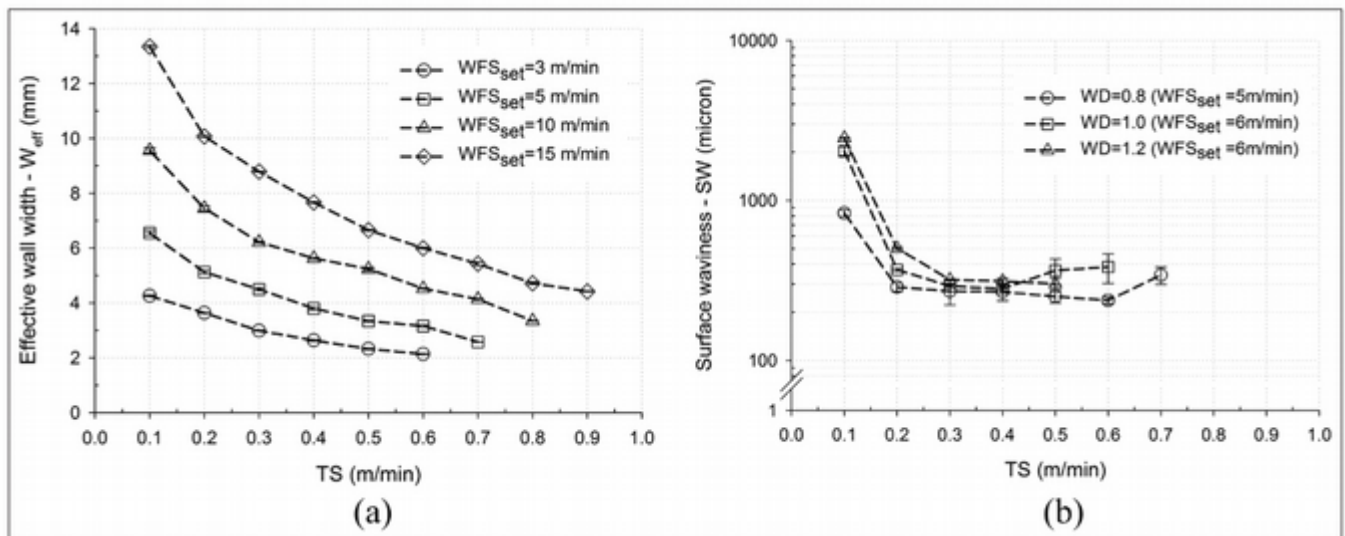


Figure 2.13: Effect of TS on EWT and SW for ER4043 aluminium filler wire [7]

Taberero [19] compared various WAAM based deposition processes like GMAW PAW and TOP TIG based on deposition rates (CMT 2.5 kg/hour, Top TIG 1 kg/hour and plasma 1.5 kg/hour) and concluded that for AISI 316L stainless steel, Ti6AL4V titanium alloy materials CMT is suited for large part with medium properties, TOP TIG is good for medium and small things, PAW better for medium/large with better quality but provided no information about size of objects produced.

Gu [5] studied effect of interlayer cold working and PWHT effect on the treatment on additively manufactured Al6.3Cu alloy during deposition he applied loads of 15 KN, 30 KN and 45 KN and

concluded that interlayer cold working with rolling can achieve UTS 314 MPA and YS 244 MPA but after T6 heat treatment they obtain a feat of UTS 450 MPA and YS 305 MPA better than wrought 2219-T6 alloy.

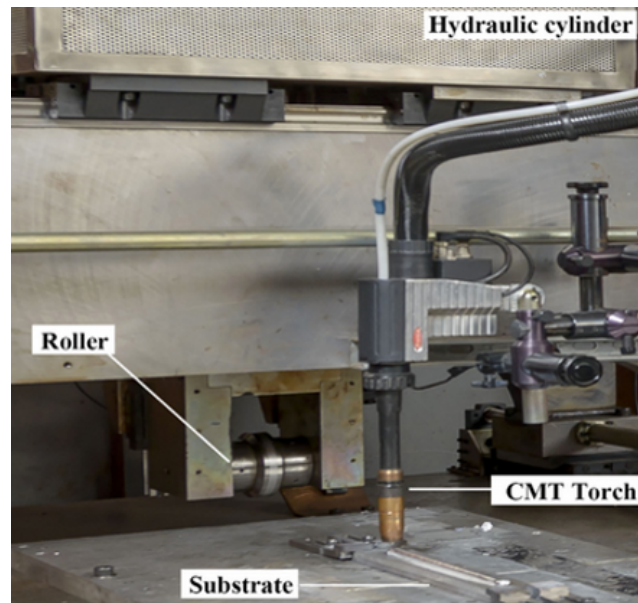


Figure 2.14: WAAM and inter layer rolling setup [5]

The microhardness and strength were increased with increasing rolling loads from 15 kN due to high density dislocation and fine sub grains with better orientation in rolled alloy. Tensile strength can be improved by heat treatment processes this is due to fine and uniformly distributed metastable precipitates.

Micro hardness and tensile properties of as deposited and rolled 2219 alloy at different loads

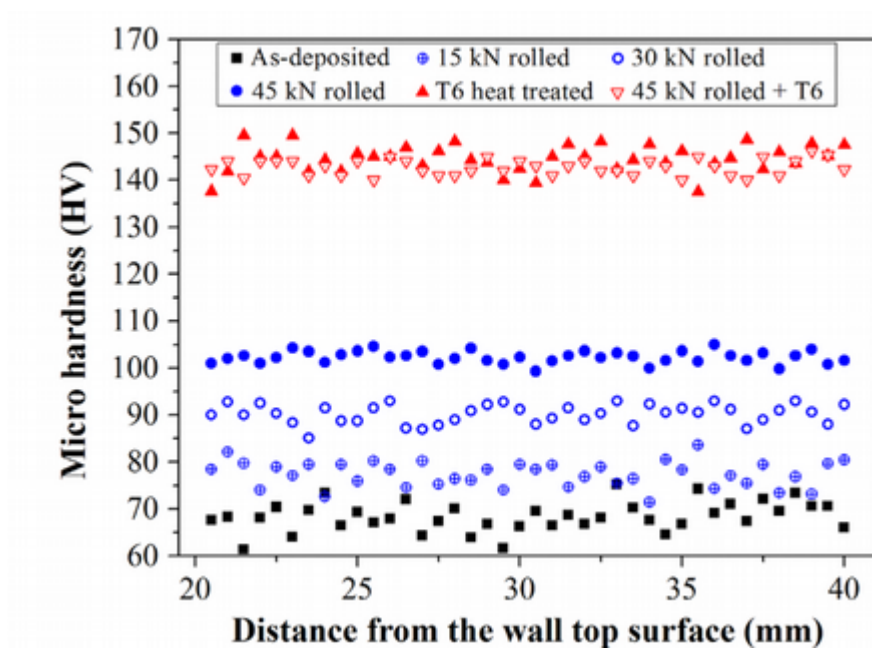


Figure 2.15: Microhardness at different locations [5]

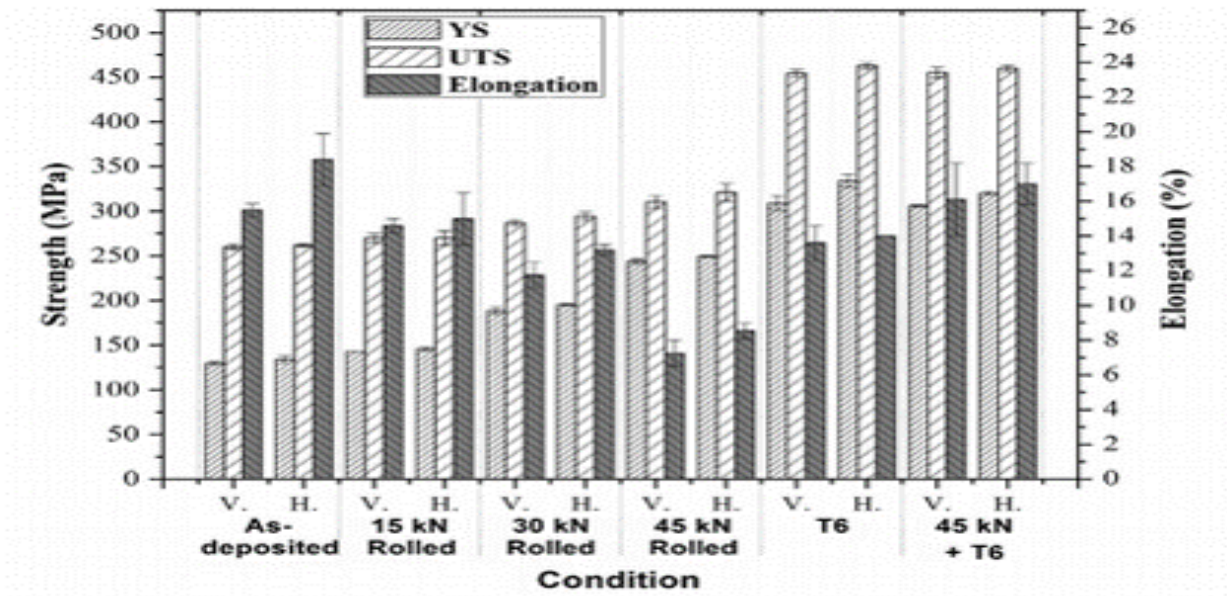


Figure 2.16: Tensile properties of deposited interlayer rolled and heat treated 2219 alloy [5]

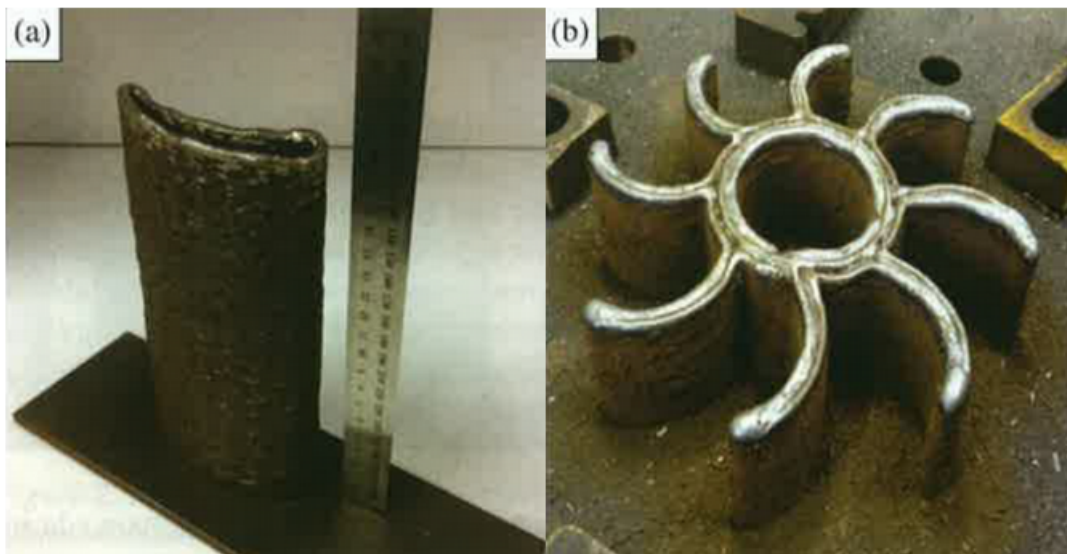


Figure 2.17: Turbine blade using WAAM 195 mm height(left) and impeller height was 70 mm. (right) [4]

Ding [4] used robotic MIG based AM For bigger components using suitable robot path and inter layer cooling of 60 seconds to avoid excess heat causing distortion and poor finish to fabricate components like turbine blades and impeller and generated net near shape after partial surface milling Max blade height was 195 mm and impeller height was 70 mm as shown above.

Welding and milling

Song [17] used 3d gmaw based welding and milling and thus by combination of deposition and subsequent milling he was able to get variation in layer thickness range between . 1 mm-1 mm thus facilitating adaptive layer height.

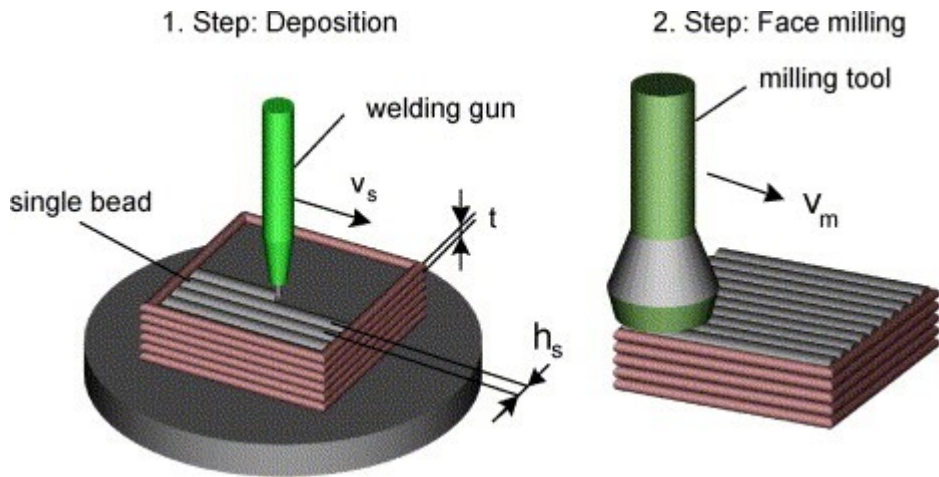


Figure 2.18: Welding and milling [17]

2.1 Fabrication of Large Metal AM components

Several efforts have been made to implement the metal additive manufacturing at large using all 3 power sources and they have been continuously expanding themselves in major industrial sectors here are some recent works in metal additive manufacturing based on power source.

2.1.1 Laser based Additive Manufacturing

Laser based Additive Manufacturing is already into industrial application where a Airbus has been using wing brackets fabricated 3D printed using laser by a company known as Concept Laser. Their first version Of 3D printer they claim is capable of printing parts up to 1 m long in at least two directions of materials such as titanium, aluminum and other metals.



Figure 2.19: Wing brackets for Airbus A350 XWB jets printed by concept laser [11]

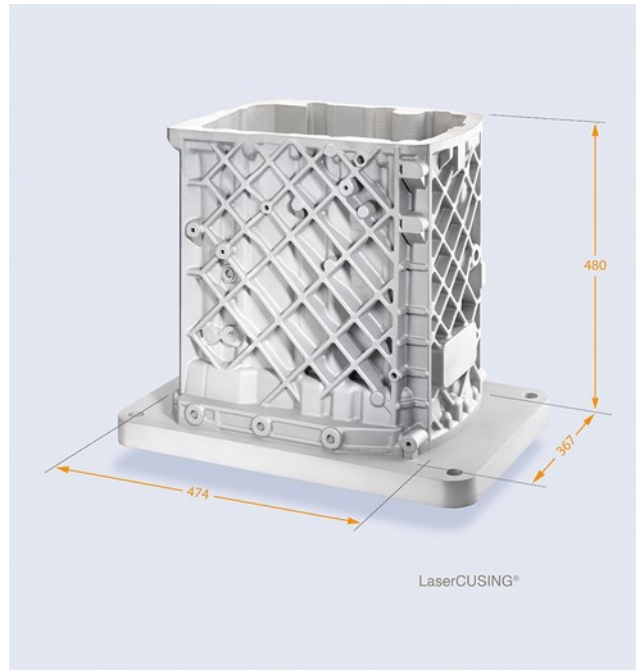


Figure 2.20: An engine block fabricated using laser based AM courtesy-Concept Laser machine [11]

2.1.2 Electron beam based Additive Manufacturing

The large scaled components fabricated using forging or casting can take from days to month to produce components which can be fabricated using EBAM in just few days another advantage being it can be used to fabricate the components of reactive metals and super alloys such as titanium and nickel based alloy due to luxury of inbuilt vacuum with it. Again its a high deposition rate process which can give the deposition from 30.8-11.34 kg/hour with flexibility and precision.



Figure 2.21: EBAM fabriacted component Ref- Lockheed Martin [13]

2.1.3 WAAM

In the more recent research at Cranfield University a 6 m length spar of Aluminium alloy was 3d printed using the WAAM process with an aerospace grade aluminium alloy. The 300-kg, 2 sided spar was fabricated in with 10-metre deposition setup, based on 2 industrial robots.



Figure 2.22: 6 m long Al alloy spar fabricated using Robotic WAAM [20]

One of the biggest challenge in fabrication of large scale metal and super alloy components fabrication using WAAM is heat management the the resulting distortion to overcome this S Williams [21] came with different building strategies and by selective approach for build direction with the minimized contact area with the substrate. He applied back to back building to cancel or minimizing the distortion, later he applied heat treatment before separation in order to release the existing residual stresses. By application of these building strategies and suitable distortion control management he was able to fabricate 1.2 m length spar structure with an excellent BTF of 2.2. Below is the figure showing his building strategy and fabricated component using WAAM.

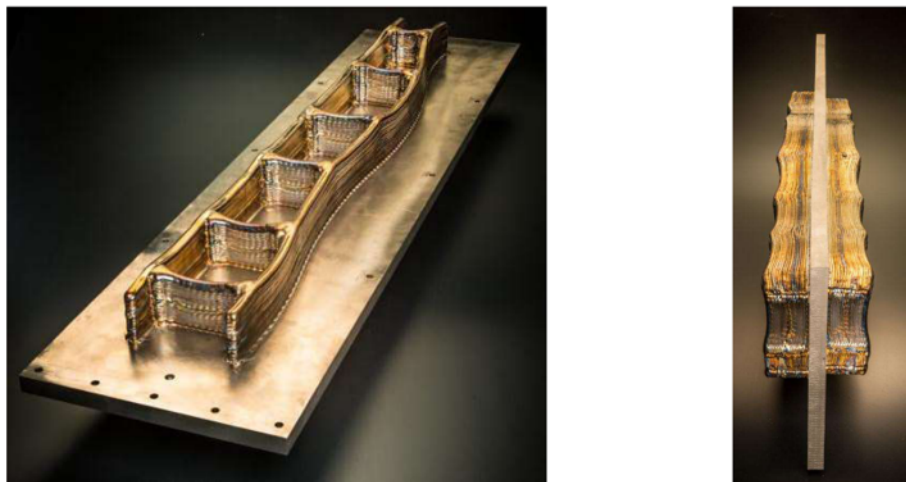


Figure 2.23: Top view(left) and side view(right) of Ti-6Al-4V spar wing structure using Robotic WAAM [21]

2.2 Wire-Arc Deposition of Inconel 625

Shoemaker [15] studied properties and application of Inconel 625 and Inconel 715 widely used for marine and petroleum industries and observed its high strength fracture toughness and fracture strength he also saw that with increasing the Ti fraction of the alloy while Nb is present, an alloy capable of being strengthened through heat treatment can be created.

2.2.1 Distinctive properties and applications of IN625

Alloy 625 has been recognised as a nickel-chromium alloy which is characterized through its content of molybdenum & niobium. It is also well known that the IN625 alloy has 2 main domains for use corrosion resistance at room to slightly higher temperatures and also for higher strength and creep and corrosion resistance at elevated temperatures [15]

Adding molybdenum reacts with the Nb to make the alloy matrix stiffer, thus enabling higher strength without heat treatment is needed. This alloy has also as great corrosion resistance. Alloy 625 is also being used in chemical processing, aerospace industry as shown below in fig below and marine engineering also oil and gas industry, for pollution control equipments and nuclear reactors as well. INCONEL 625 LCF is a potential variant of IN625 alloy here the melting can be controlled in a better manner in order to produce a notably cleaner microstructure. Further processing would be required to produce a finer grain size. It can also result in enhancing fatigue resistance where LCF stands for Low Cycle Fatigue. The alloy is e. g. used for bellows, aircraft exhausts and expansion joints. The alloy IN625 has good weldability and can be used to produce structures that have to go through cyclic fatigue at higher temperature.

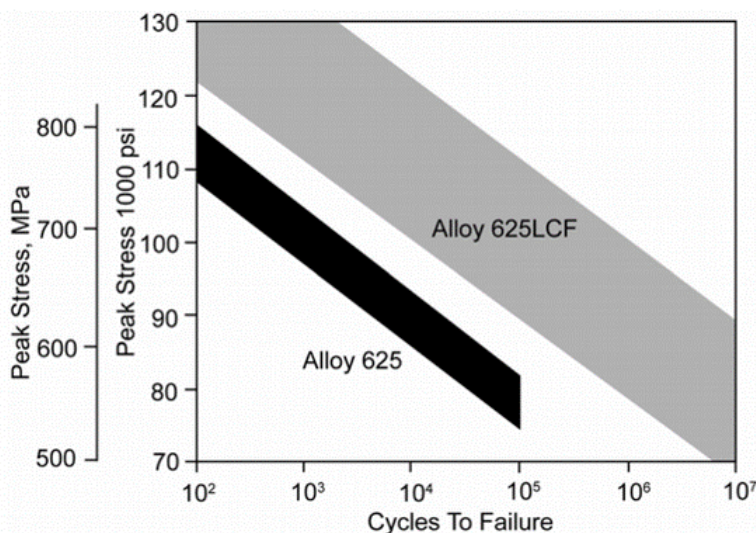


Figure 2.24: Fatigue resistance of IN625 & alloy 625 LCF [15]

Alloy 625 had sufficient strength due to its molybdenum and niobium presence. This alloy has corrosion resistance as well as creep resistance rupture resistance at high temperature. When alloy 625 (with 4 percent niobium) was heated in range of 649 -871 degrees it can precipitate Ni₃Nb dispersoid also various carbide particles M₆C were also found the effect of combined precipitation of these phases results in increasing the yield and tensile strength.

The TTT diagram of Alloy 625 [15] showing presence of laves and delta phases is shown below.

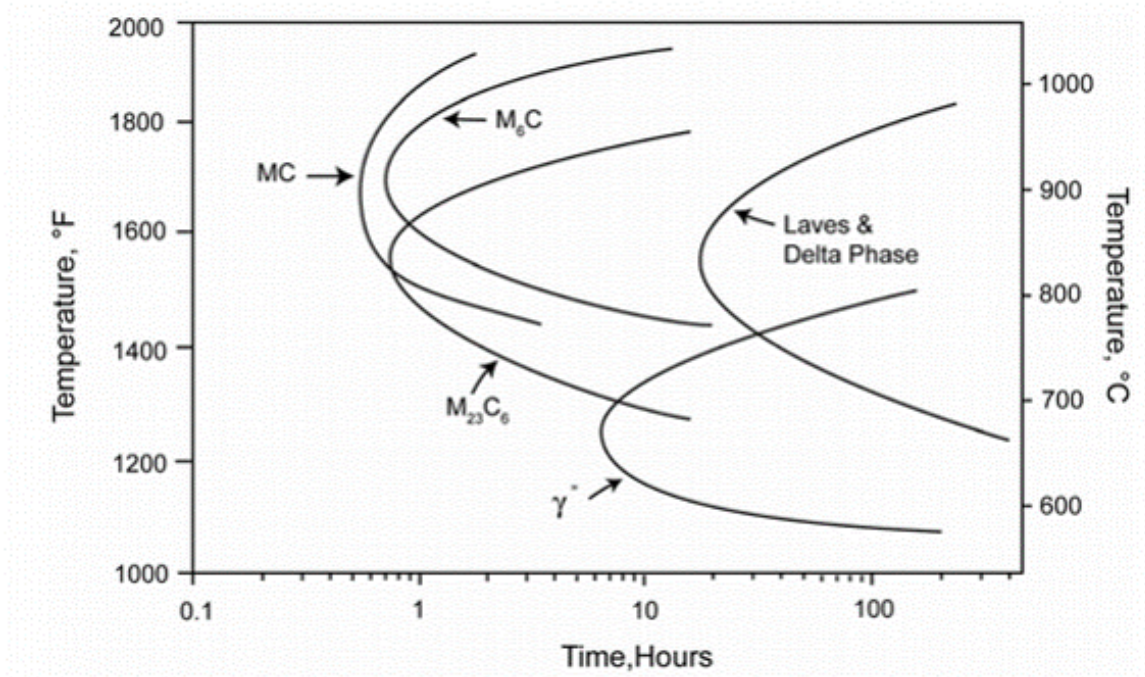


Figure 2.25: TTT diagram of Alloy 625 [15]

Applications of alloy 625

The alloy IN625 has good weldability and can be used to produce structures that have to be go through cyclic fatigue at higher temperature. IN625 has been used in chemical processing industries , aerospace industries and also in marine engineering oil and gas, for pollution control equipment and nuclear reactors.

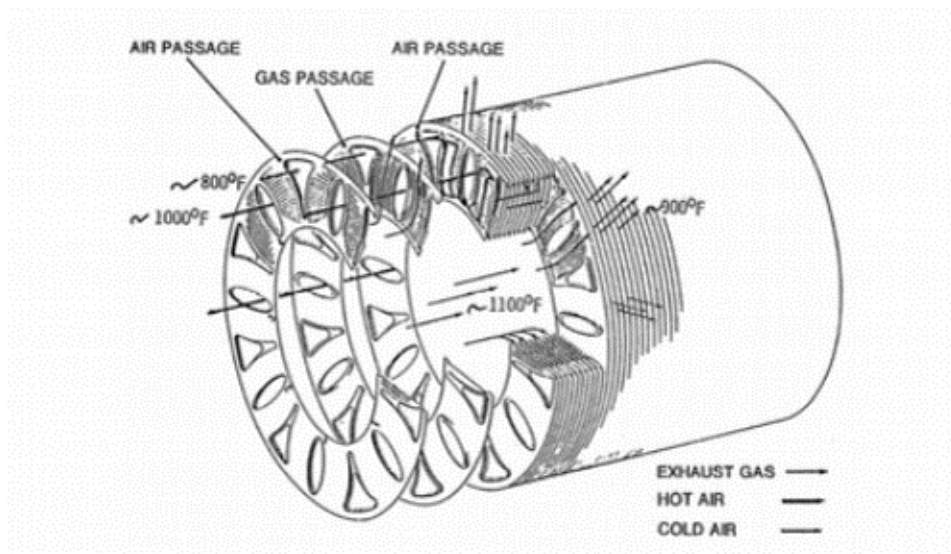


Figure 2.26: Diagram of Alloy IN625 manufactured recuperator for a turbine engines [15]

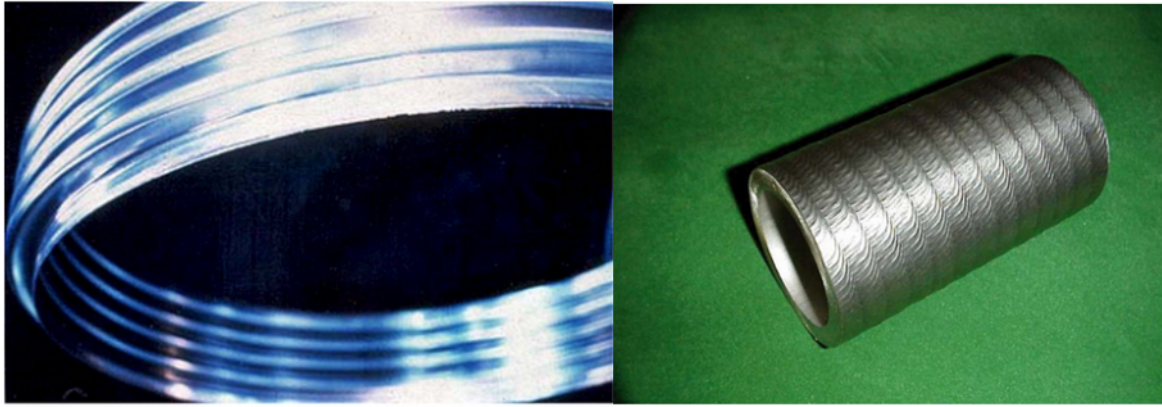


Figure 2.27: Bellows produced using LCF IN625 (left) & Alloy Steel Boiler Tube Welded using alloy IN625(right) [15]

2.2.2 Parameter control for IN625

Pinto [9] analysed 2 critical parameters current and welding speed for CMT based 3D printing of Inconel 625 alloy to critically examine their effect on deposition rate deposition efficiency build up rate average and hardness using DOE software for confirmation

Alloy 625	Ni	Cr	Fe	C	Mn	Si	Mo	Al	Ti	Nb	P	S
Min	bal	21.0	-	-	-	-	8.0	-	-	3.2	-	-
Max	bal	23.0	4.0	0.025	0.40	0.40	10.0	0.40	0.40	3.8	0.010	0.010

Figure 2.28: chemical composition of inconel 625

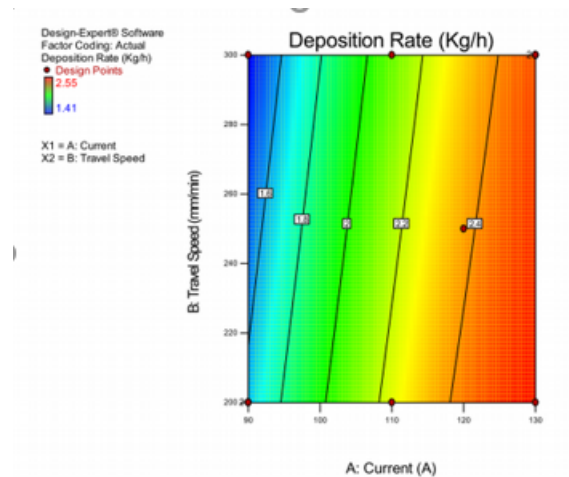


Figure 2.29: DOE prediction of current and travel speed effect on deposition rate [9]

That implies when torch speed is kept constant and current is increased automatically WFS increases and hence material deposition increases. While keeping every other parameter same when TS increases material deposition decreases. it was observed that for inconel 625 deposition speed was the most critical parameter to affect the deposition. At low speed deposition was observed to be more continuous than at higher speed for the other parameters unchanged .

Effect of Arc length correction on Cold metal transfer

In order to study the influence of the change in arc length correction on CMT welding cai [1] varied the arc length correction parameter from - 20 % to +10 % while other parameters kept unchanged. Cai [1] observed that weld depth decreases with the increasing the arc length parameter also he found that flatness of the weld(desirable for WAAM) was reduced. The same arc correction factor was later utilized for deposition of IN625 alloy as due to re-melting because of higher heat input makes its essential to control the bead geometry parameters and most important being the flatness of the bead which gets highly affected due to change in arc length correction. The application of arc length correction on cold metal transfer of IN625 will be discussed in chapter 6.

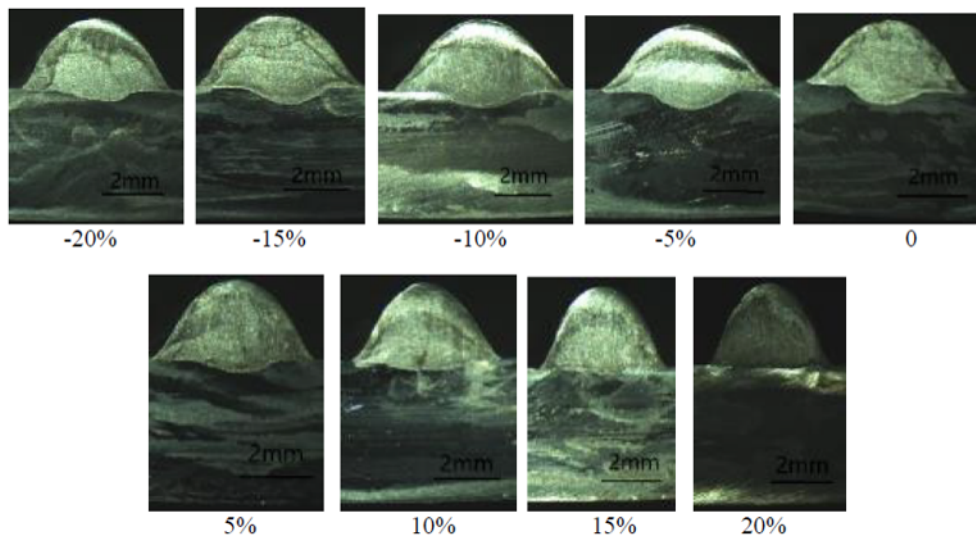


Figure 2.30: Different arc length corrections [1]

He also tried to study effect of arc length correction parameter on the width and depth of bead.

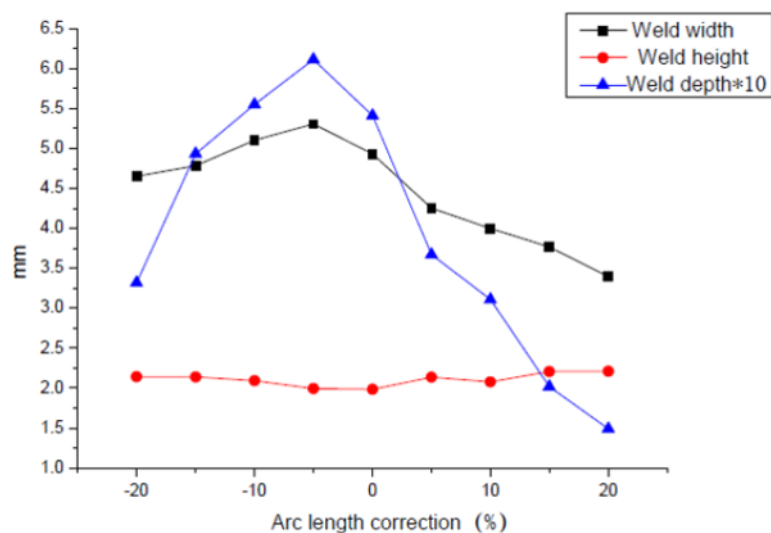


Figure 2.31: Effect of arc correction parameter on depth,width and height of beads [1]

From the figure 1. 33 is is evident that by changinf the arc length from -20 percent to +20 percentage cai [1] noticed that by increasing the positive arc length width and depth decreases and attains a maxi-

mum value at arc length correction of -5 percentage. While depth and width of the beads were found to be increasing in the range of the arc length correction of -20 % to -5 %.

Thesis overview

Chapter 3-Experimental Setup

This chapter involves study of Robotic WAAM setup and parameters study of fabrication of medium and large scale components.

Chapter 4-Large Component Fabrication

This chapter gives insights about fabrication of thicker as well as thin walled components using Robotic WAAM and CNC & CMT integration .

Chapter 5-Thermal Analysis of the Deposition Process

This chapter applies the simufact welding simulation to study the temperature profile of the multi pass and multilayer deposition and the effect of neighbourhood deposition on adjacent pass of a multi pass deposition. This chapter also works for the development of a mathematical model for calculating the interlayer dwell time for to reach steady state temperature.

Chapter 6-Preliminary Studies on Weld Deposition of IN625

This chapter studies the parameter optimization of single pass deposition of inconel 625 alloy on the inconel base plate,it also studies the parameter optimization of multilayer and multi pass inconel deposition. Finally it works to deposit thin wall of inconel 625 using optimized process parameters.

Chapter 7-Summary and Future Scope

This chapter gives the insights into the present achievement of this project and the future vision to be accomplished using WAAM for large metal components and super alloys.

Chapter 3

Experimental Setup

3.1 Kinematic Setup for Weld-Deposition

An Industrial 6 axis kuka kr 30 Robot is used as the basic kinematic setup. This is integrated with a weld deposition torch which is used to carry out the deposition through the robot programming path generation, the welding power source and the robot movements are controlled by a KCP(kuka Control Panel).

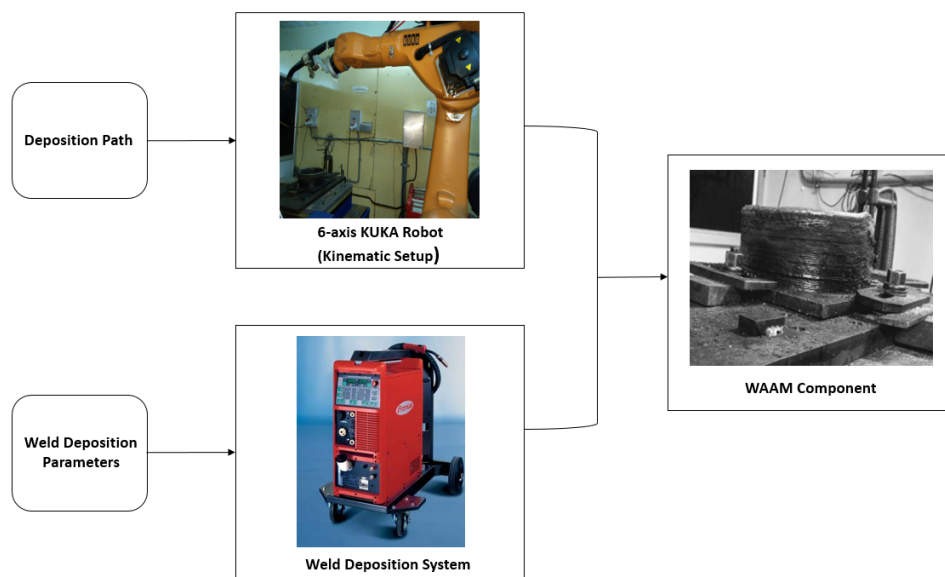


Figure 3.1: Schematic flow diagram of Robotic WAAM setup

Following are the components of the kinematic setup.

- 1- 6 axis Kuka Robot with integrated welding torch
- 2- Kuka control panel(KCP)
- 3- Welding power source
- 4- Robot controller(KRC2)
- 5- Table for clamping base plate

The tool path generation are given to the robot in the src file. motion details, welding on/off and tool home position etc are some details which are provided to the robot through this file. After the program have been fed into the controller it is shown in kuka control panel which controls the Robot movement

through the program fed into it. There are 3 modes in Kuka control panel viz. teach mode, jog mode and automatic mode. The dry run and program verification are done through jog mode while deposition is carried out at automatic mode only.

3.2 Weld-Deposition Methodology

3D object is sliced into layers fabricating each layer at a time as here the intention was to fabricate the cylinder each layer being a circular bead so robot path generation for a circle was carried out with proper welding parameters. MIG welding setup was used for deposition pulsed mode(GMAW-P) was used for droplet transfer because it can weld faster than globular and short circuit modes of transfer have good penetration, almost 90 percent less spatter than short circuit transfer and is also suitable for welding in all positions with high deposition than CMT and other modes of droplet transfers. Below is the diagram showing detailed process flow of Robotic WAAM. After the final component have been made some additional finish machining might be required.

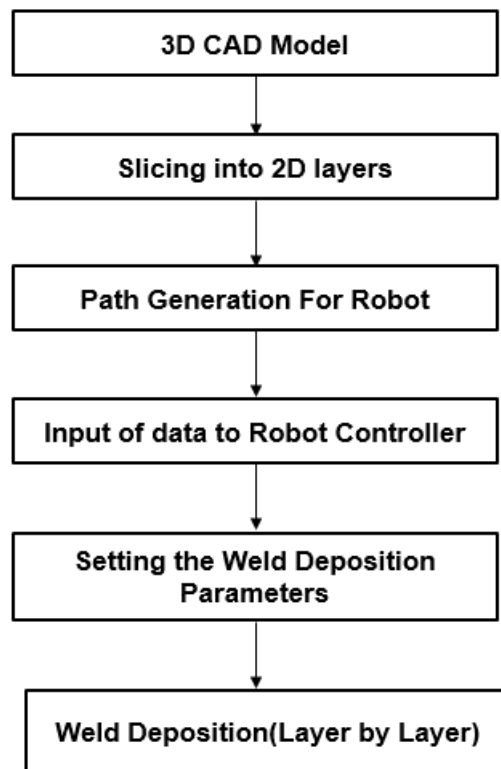


Figure 3.2: Process flow diagram for WAAM

3.3 Initial Studies on Parameter Selection

Before trying for of the larger components,parameters for small and medium scale components have to be understood hence in order to achieve parameter optimization and stable and quality product various trails were done at small scale first and then the best optimized parameters which resulted in least spatter,lesser material flow and stable successive beads with better quality were preferred for validation for medium scale components. To start with cylinder was aimed to be fabricated thus need for multi-pass circular bead optimization was required for this purpose "Tranplus Synergic 5000" welding source was utilized to start with synergic GMAW Pulsed mode to minimize spatter and better quality beads.

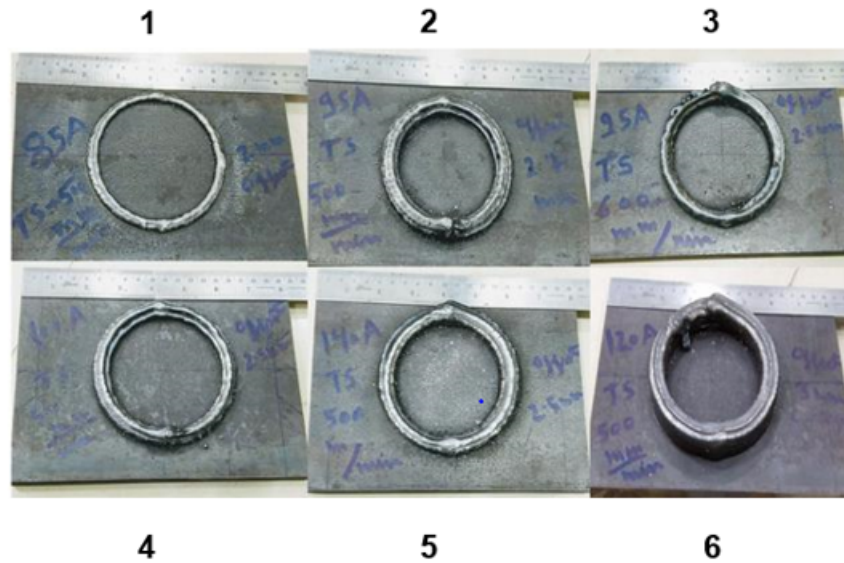


Figure 3.3: Parameter optimization for multi-pass circular beads

Fig shows the bead quality and overview for various set of parameters for 3 consecutive beads, Gas mixture of Ar 82 % and CO_2 18 % was used for the given ER70S-6 wire with 0.8 mm diameter with constant flow of 12 l/min ctwd was kept at 12 mm, in (fig 3.3 (1)) 85 ampere current was used in Torch travel speed was varied between 400 mm/min to 600 mm/min and it was observed that with all other parameters being same spatter was least and uniform bead was observed at 500 mm/min offset was taken 2/3 rd of bead width (2 mm offset for this case) the bead quality looked fine but thinner first layer was observed. For 2nd case (fig 3.3 (2)) 95 ampere current was used and stepover was accordingly increased to 2.7 mm with travel speed 500 mm/min this resulted in improper filling with gaps between beads as shown in fig, at same current i.e. 95 ampere and reducing offset to 2.5 mm at the same result between beads resulted in material flow after 2 layers because of bead instability due to reduced offset.

Increasing the current till 100 A and reducing the travel speed till 400 mm/min caused more spatter, waviness in first layers and thus unstable layers while with increasing current upto current 140 A and 600 mm/min TS resulted in thinner bead at reduced spatter with 2.5 mm offset.

With the above trails current was needed to be increased with proper proportion to offset to reduce spatter and material flow in order to get increased width and thus increased cylinder thickness thus current was increased till 120 Ampere and TS was kept at 500 mm/min and accordingly offset was increased to 3 mm, with this set of parameters first layer was of required thickness (10 mm) and stability for 5 layers so this set of parameters was selected (fig 3.3 (6)). Repeated experiments were performed with the above selected parameters in order to ensure repeatability and reproducibility.

3.4 Summary

This chapter involves the application of Robotic Welding setup for incorporating into WAAM, methodological study of Robotic WAAM by giving the detailed flow diagram for the Robotic WAAM fabrication, path planning strategy and the process parameter optimization for Robotic WAAM using MIG welding power supply. It mainly focusses upon multi-pass and multilayer deposition of the ER70SS-6 wire with 0.8 mm diameter (copper coated mild steel) using MIG welding and it also acts upon parameter study for various offset values.

Chapter 4

Large Component Fabrication

4.1 Thick Multi-Pass Components

Fabrication of thicker structures can be realised using WAAM with multi-pass deposition with the optimized parameters like offset between beads and current & travel speed. This was attempted to be done for medium and large scale the procedure shown below is to fabricate thicker sections using Robotic WAAM of the order of thickness from 10 mm-20 mm.

4.1.1 ϕ 250 mm cylinder

Though the parameter verification and optimization for multi-pass had been achieved through small scale trails but scaled up fabrication for the medium scale was needed to deal with issues like distortion, layer stability with increased component height as layer stability becomes critical at height due to plate distortion, residual stress due to differential temperature gradients. Considering the above issues a medium sized component of size 250 mm diameter and 110 mm height before moving to large scale components. A robotic tool path generation code was required for preferred area filling strategy to realize the actual deposition which was developed using circular algorithm and area filling strategy.

Parameters and Path Generation Strategy

Parameters used for small/medium scale components used in the table below are fed through RCU unit into the welding power source unit and are saved in form of a program later the same number program is fed into KCP(Kuka control panel) and is utilized for weld deposition. This is evident that ER70S-6 with 0.8 mm diameter gives relatively thinner beads thus in order to get thick walls for multi-pass becomes necessary.

Typical thickness of a single bead attained through the above parameters(Wire feed rate and travel speed) was 4 mm and layer height 2mm but here the desired wall thickness of the component was minimum 10 mm so one bead was not sufficient with the above parameters to achieve that wall thickness . Thus three beads could provide the desired thickness if optimized with the correct step over which have already been explained in earlier section.

Three passes were made order of the passes of robot movement for deposition and the start and end points are shown in the figure, it is to be noted that arc was made to stop after each pass and started instantaneously as soon as it has to start for the second pass.

Table 4.1: Parameters for WAAM fabrication of medium sized component

Parameters	Values
Filler material	ER70S-6 with 0.8 mm diameter
Travel speed	500 mm/min
Current	120 A
Contact tip to work distance	12 mm
Shielding gas used	82 % Argon 18 % CO ₂
Shielding gas supply	12 l/min
Step over distance	3 mm

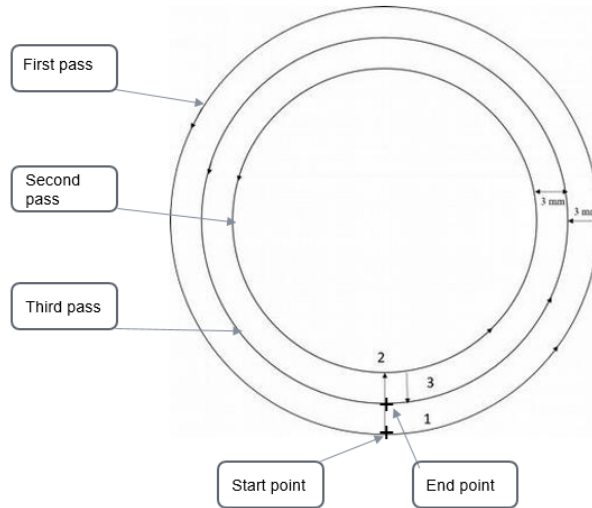


Figure 4.1: Path generation strategy for first layer

First layer consisted of 3 beads(intended to attain increased width) with 3 mm stepover between 2 consecutive circular beads. In order to ensure bead stability and to provide more time for cooling to earlier beads and thus for better stability after first bead,last bead were deposited and then next bead was deposited as shown in fig. The path generation was done using circular interpolation algorithm in KCP(kuka control panel) and z height was successively increased using orange edit software to deposit the cylinder.

There is a greater influence of area filling strategy in a multi-pass deposition as it has a direct influence on the temperature history of the adjacent bead and on the subsequent layers too. Like here we can observe that after first bead deposition(outermost bead or 1st pass) is done we move to the deposition of innermost beads this will give the outer bead time to reach the steady state temperature before the middle bead(3rd pass) deposition is carried out.

Deposition

Kuka Robotic welding station was utilized for carrying out the actual fabrication process as shown in figure 3. 3 after program was fed into kuka control panel the robot was switched to operate at automatic mode and the deposition was carried out.

Interlayer cooling time

Interlayer cooling time was given between layers in order to reach steady state temperature as for the small and medium scale components heat loss to through convection and radiation is less due to less surface area and base plate or the substrate is sufficiently heated up the heat accumulation causes the distortion of the plate. Also cooling time depends on the rate of conduction, convection and radiation which are directly dependent on area of exposure and here in AM area of exposure keep on adding up and so does the heat which causes the residual stress due to differential cooling and heating at different locations because of temperature gradient so different layers will have different cooling time which we will discuss in later sections in detail.



Figure 4.2: Fabrication process of medium scale components using Robotic WAAM

Below is the figure showing deposition after first layer and after 5 layers.



Figure 4.3: Deposition after 1st layer(left) deposition after 5 layers(right)

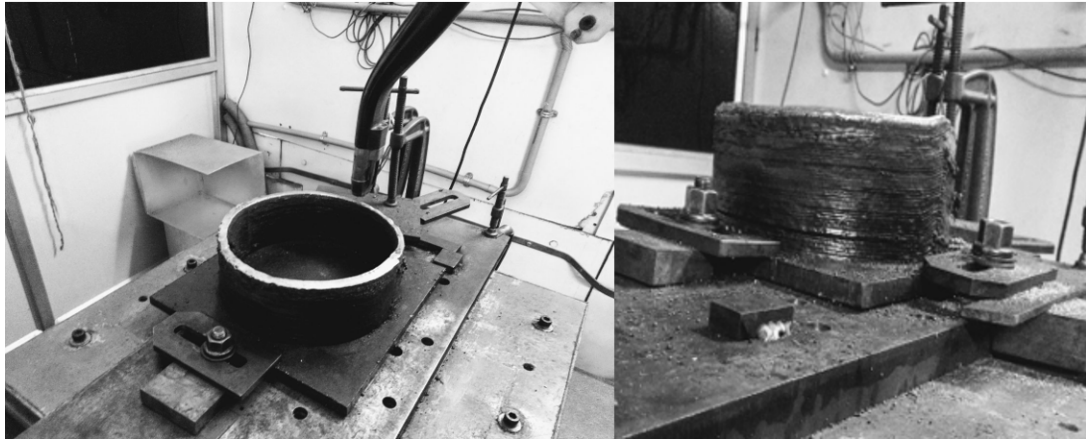


Figure 4.4: WAAM fabricated cylinder top view(left) and side walls(right)

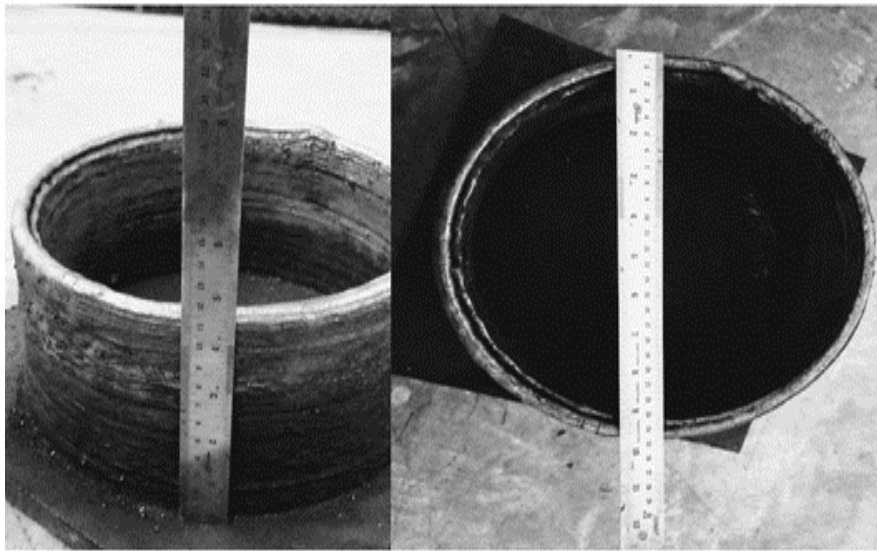


Figure 4.5: Fabricated cylinder has 110 mm height(left) and 250 mm diameter with 10 mm wall thickness(right)

4.1.2 $\phi 900$ mm cylinder

Experimental Setup for Large Scale Robotic WAAM

The single wire torch was used instead of twin wire welding torch by attaching it with modified fixtures. In a way here Kuka robot was only utilized for motion and deposition was carried out with retrofitted weld deposition MIG power source and torch with different fixtures. Welding on and off were carried out by using arduino relay switch.

Need for a bigger fixture table was realized with proper clamping to avoid the bending distortion so the table was fabricated to provide the C clamping at 8 locations the 1500 mm*1500 mm table with 415 mm height was used to clamp 1200 mm diameter and 8 mm thickness base plate.

The fixture table was designed considering the maximum accessibility of Robot movement along each direction and proper holding of the bigger base plates as well as best possible clamping to ensure minimal plate distortion due to higher heat generation in bigger components. Eight C clamps were used at 45 degrees to clamp the base plate as shown in fig below.

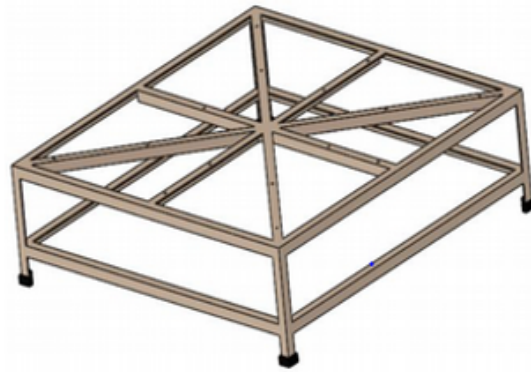


Figure 4.6: CAD model of fixture table to clamp the base plate

With the parameters validated for medium scale components explained earlier through this work an attempt to fabricate scaled up cylindrical component of 980 mm diameter was initiated and 25 successive layers were deposited with height obtained was 50 mm. It was observed that heat generation cum accumulation is more for bigger components and thus the bead stability was a issue as compared to small and medium scaled components also EWT(effective wall thickness) was around 8 mm (less due to heat accumulation at increased height) so need for increased EWT and better stability at increased was realised,for this purpose more deposition was needed so wire diameter was decided to be changed to 1.2 mm from 0.8 mm for ER705-6 wire.

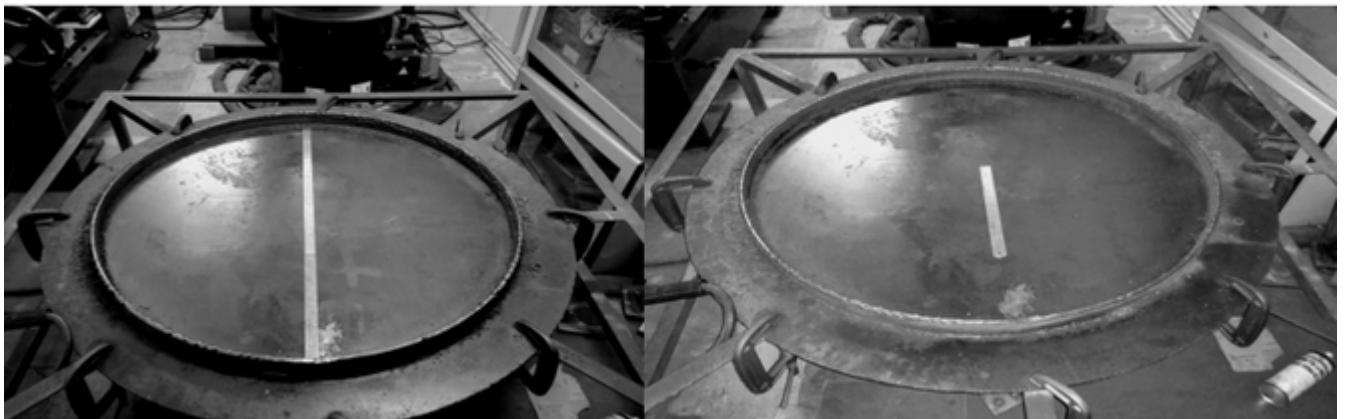


Figure 4.7: Position of clamps and fixture to avoid distortion with fabricated cylinder (980 mm diameter and 50 mm height)/initial trial with thinner wall thickness

Parameters selection and path planning

Parameter optimization for 1.2 mm diameter ER70S-6 wire was carried out in similar fashion like 0.8 mm diameter wire DOE(design of experiments) was used to conduct the experiments in an orderly manner and the parameters which provides the stable layer with no disbonding between adjacent beads. Based on qualitative analysis of bead stability and bonding between adjacent beads and successive layers the following parameters were selected.

Please note these parameters were varied upto 5 % according to need of the process current was

Table 4.2: Parameters for ER70S-61.2 mm diameter for 4 multi-pass beads

Parameters	Values
Filler material	ER70S-6 with 1.2 mm diameter
Travel speed	550 mm/min
Current	150 A
Contact tip to work distance	15 mm
Shielding gas used	82 % AR 18 % CO ₂
Shielding gas supply	12 l/min
Step over distance	5.1 mm

typically varied between 150-157 amperes to address the challenge of slight irregularities in the welding pattern. Gas supply was kept between 12-15 L/min and ctwd was maintained between 12-15 mm to take care of the any irregular glitch with the layer height. Four multi-pass beads were deposited for the first layer deposition. The deposition strategy for the layer 1 is shown below. Again in order to provide greater cooling time to earlier deposited beads and thus ensure greater bead stability it was decided to deposit outer and inner beads first and than next 2 beads were deposited for first layer. The offset between beads was 5.1 mm (2/3rd of bead thickness). Effective wall thickness obtained was 20 mm. The four deposited beads with this area filling strategy resulted in greater bead stability and relatively lesser affected by thermal history due to previously deposited beads for first layer.

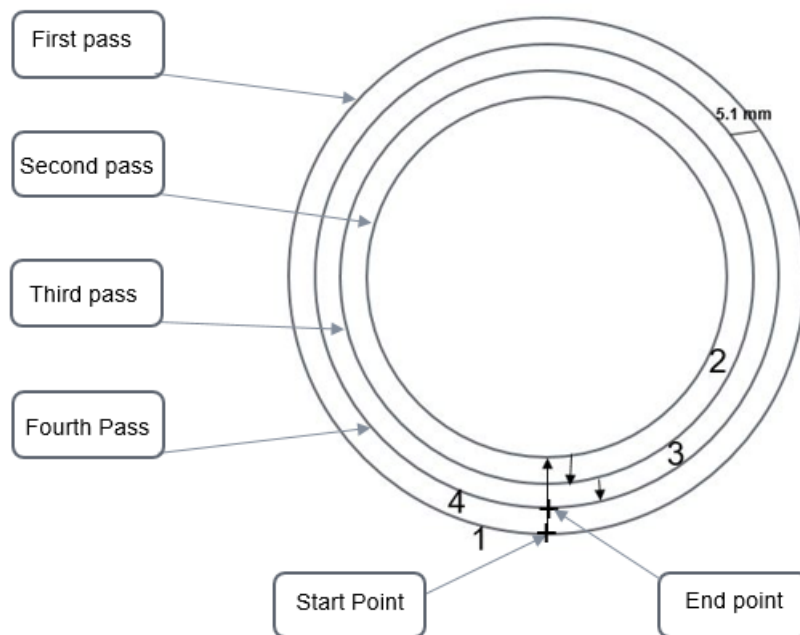


Figure 4.8: Area filling strategy for first layer

Large Component Fabrication

The fabrication was carried out with the above shown parameters and path planning. Each layer(4 passes each) was deposited using 6 axis Kuka robot with integrated MIG welding power supply,the fabrication process is shown in fig below.

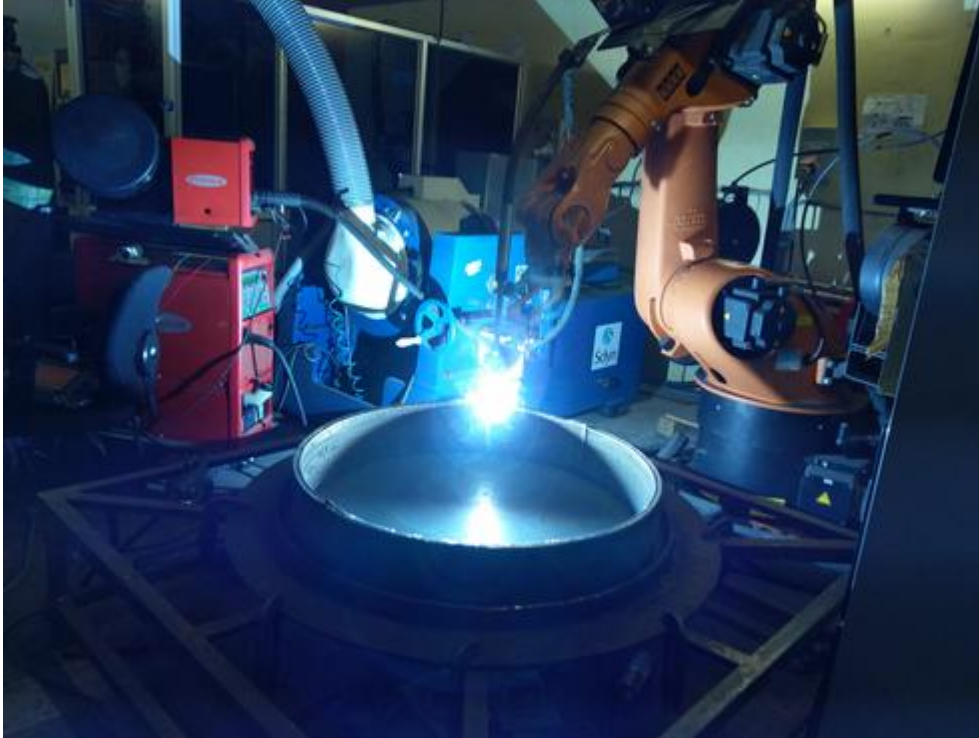


Figure 4.9: Fabrication of large component

The 900 mm diameter cylinder was intended to be deposited with 20 mm wall thickness the each layer was 2 mm height. Below is the state of deposition after first layer 100 mm and 200 mm the deposition was carried layer after layer with dwell time of 120 seconds to ensure each point may reach the same steady state temperature of 366 K. Minor Correction were needed to applied after few layer to ensure flat surface for the next layer to be deposited. Below is the figure of final deposition with total 125 layers were deposited and the total height obtained was 240 mm. The total number of beads deposited for complete component was 500(125*4). The time taken for each layer to be deposited was 20 minutes and 44 seconds with the travel speed 500 mm/min.



Figure 4.10: State of deposition after 1st layer,100 mm and 200 mm

It was also observed that as the deposition height increases the effect of heat conducted becomes less on the base plate and beyond 100 mm base plate becomes thermally stable and on further heating

base plate does not get sufficiently heated so the distortion is minimized after a certain height based on geometry



Figure 4.11: Last layer deposition on left and finally deposited layer with 900 mm diameter and 240 mm height with 20 mm wall thickness

The Metal additive manufacturing is capable of producing components with near net shape with some finish machining required after fabrication of the component the machining was carried out in order to get the finish machining and to observe if the surface contained any defects like porosity etc. Below is the state of component before and after machining and detachment from base plate.



Figure 4.12: WAAM manufactured component before and after machining

After machining the surface obtained was free from surface defects with EWT(effective wall thickness)obtained 14 mm. Total arc time taken for deposition of each layer was 20 min 46 seconds with travel speed of 500 mm/min across 900 mm diameter outer diameter and 860 mm inner diameter and two intermediate diameters with 5.1 mm offset between them and torch had to cover circular path for 4 multi-pass beads for each layer.

4.2 Thin Single-Pass Components

WAAM has its inherent capacity to fabricate component with overhangs which makes it able to fabricate large and complex components with intricate geometrical features. This ability was exploited with the help of proper tool path generation using CNC and retrofitment of CMT advanced power source to produce large and complex components.

Experimental setup for CNC and CMT integration

The Cold metal transfer weld deposition unit in integration with CNC center was used for deposition. CMT welding power source has ability to control high frequency push and pull mechanism through specially designed welding torch containing servo motor which enables wire motion in forward and backwards directions reducing heat input and controlling arc burning.

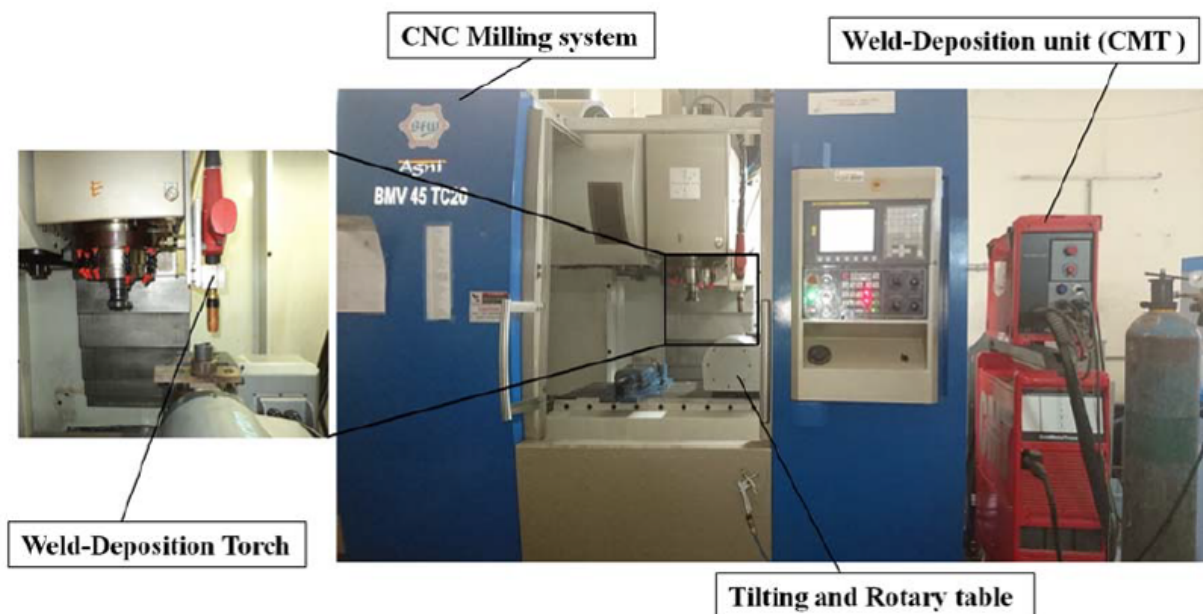


Figure 4.13: Experimental setup for retrofitted CNC cum CMT deposition unit

CMT is preferred over conventional MIG because of the following advantages.

- lesser heat input.
- lesser spatter than conventional MIG (globular and short circuit transfer).
- better arc control mechanism and arc stability.
- lesser distortion.
- better control over material transfer mechanism due to push pull feed system and thus better deposition

The cold metal transfer is the deposition medium here which is extension of short circuit transfer through droplet detachment using wire retracting by push pull mechanism where push enables the short circuit transfer after this based on controller feedback pull mechanism provides droplet detachment hence the

dependency of the metal transfer on electromagnetic force is reduced and this results in lesser spatter, lower heat input as compared to conventional MIG welding deposition. The detailed explanation about CMT setup is given in appendix. Below are the technical specification of the CMT.

Table 4.3: CMT specifications

Mains Voltage	3×400
Mains Frequency	50/60 Hz
Type of cooling	coolant
Mains fuse protection	35 A
Primary continuous current(100 %)	101-361 A
Primary continuous power	12.4-13.9 KVA
Degree of efficiency	88-91 %
Welding Current range MIG/MAG	3-500 A
Open Circuit voltage	68-78 V
Open Circuit voltage	68-78 V
Working voltage MIG/MAG	14.2-39 V
Dimensions l/w/h(in mm)	625/290/475
Weight(in Kg)	35.6

ER70S-6 wire(copper coated mild steel) with 0.8 mm wire diameter was used and because of its superior mechanical properties like hardness and tensile strength.

Table 4.4: Chemical composition of ER70S-6(copper coated mild steel wire)

Element	Percentage
Carbon	0.075
Manganese	1.22
Sulfur	0.014
Silicon	0.67
Phosphorus	0.01
Iron	Remaining

4.2.1 Simple Cylinder

The mild steel base of dimension 300*300*20 mm was used as the substrate plate was clamped at four corners as shown to arrest any distortion during deposition. The CMT welding torch was fixed near to the spindle head using fixtures and moves in z direction with cnc movement and carries out deposition thus CNC is utilized as positional interpolator.

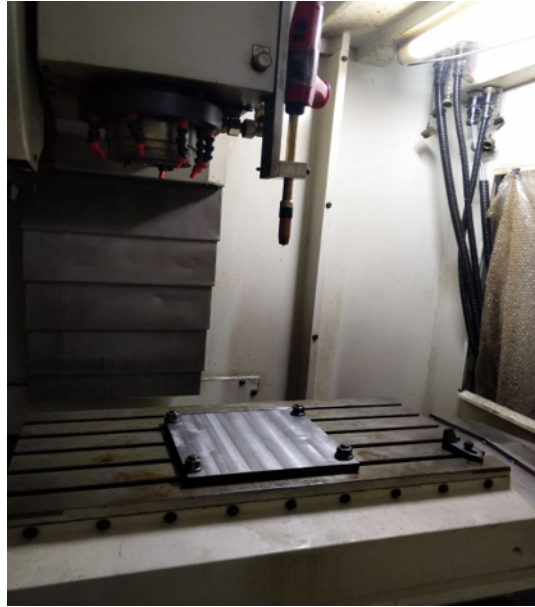


Figure 4.14: Position of clamps and torch for initial setup

Parameters selection and path planning

A Matlab code was used to generate the G code for fabrication of component with internal protrusion this involved angular shifting of coordinates of each layer with increasing z height for a given height. The parameters used for the process are given below these parameters were used based on previous literature work [18] and with experiments conducted before the actual deposition.

Table 4.5: Parameters used for thin walled components fabricated using WAAM

Parameters	Values
Filler material	ER70S-6 with 0.8 mm diameter
Travel speed	550 mm/min
Current	120 A
Contact tip to work distance	10 mm
Shielding gas used	82 % AR 18 % CO ₂
Shielding gas supply	12 l/min

The parameters shown above were used for deposition of thin walled component single layer was

deposited at 300 seconds of dwell time was given to each layer ,with dimension the wall thickness 4 mm and layer height of 10.8 mm.

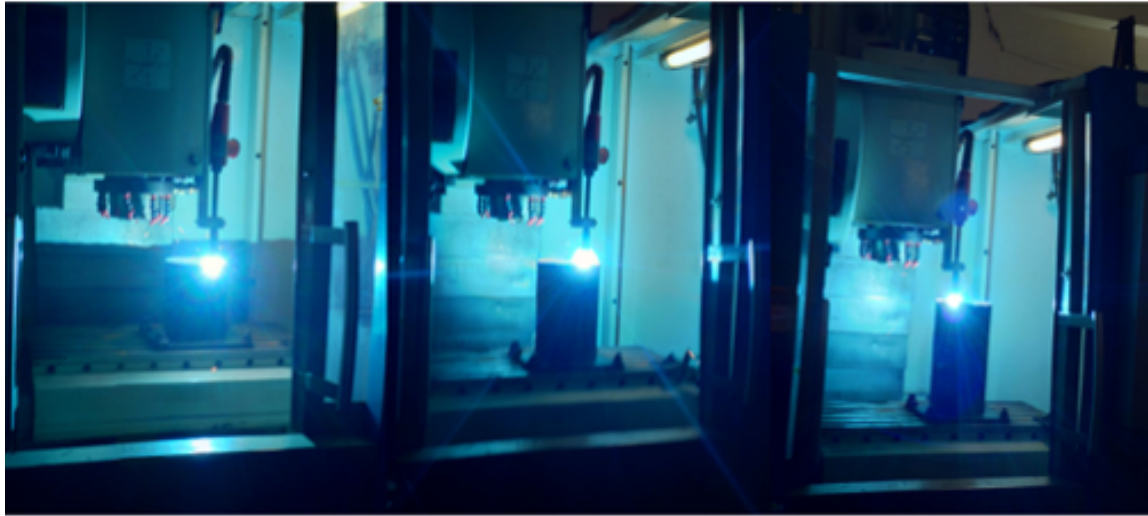


Figure 4.15: Fabrication of simple cylinder using WAAM

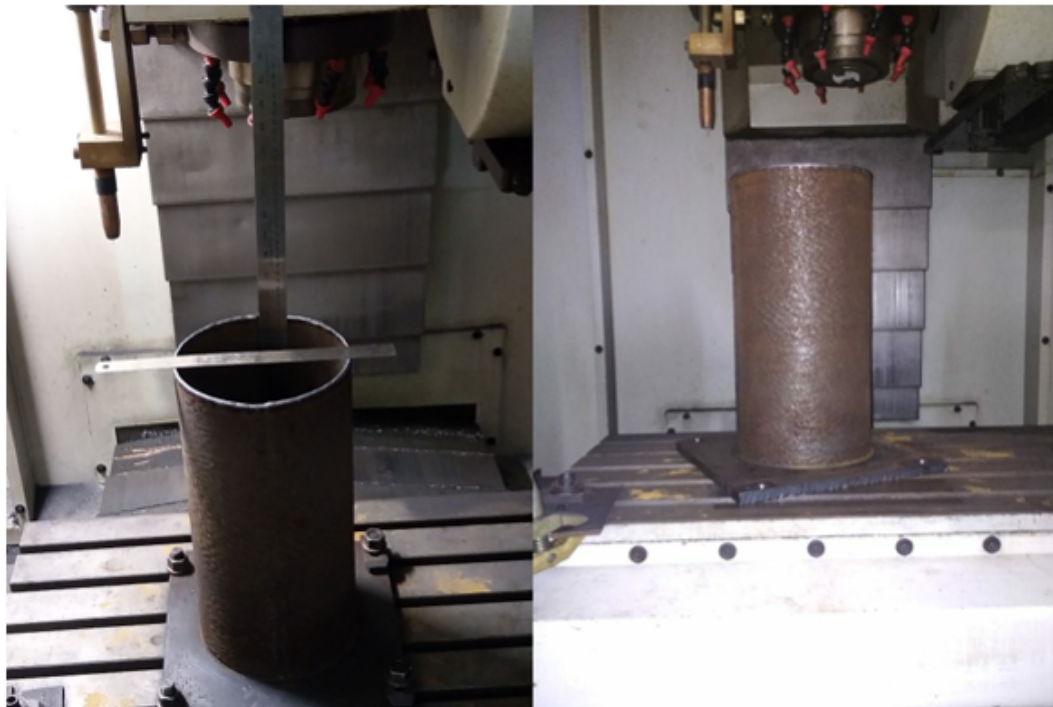


Figure 4.16: Fabricated simple cylinder

4.2.2 Cylinder with Grooves

Fabrication was done layer by layer with CNC movement being synchronized with welding supply on off. The CNC bed movement provided x,y movement and z movement of CNC spindle head provided torch movement in z direction with increased layer height. Below is the figure showing step by step deposition after certain heights. First layer consists of 4 grooves at 90 degrees each,after first layer each

groove was provided with angular shift with increased z height and thus next layers were deposited with updated coordinates with increased z height.

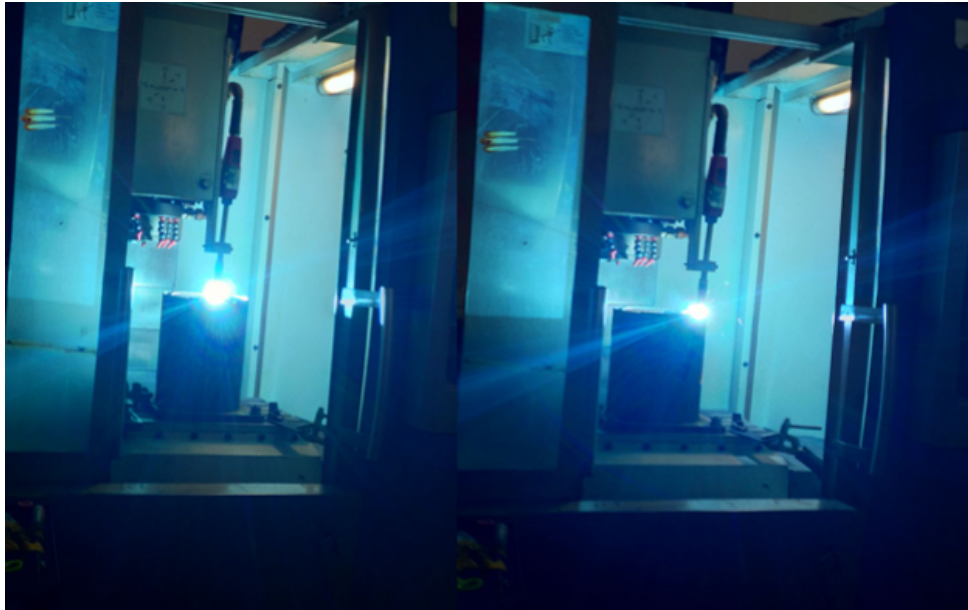


Figure 4.17: Fabrication of cylinder with grooves



Figure 4.18: Deposition after layer 1

First layer deposition is shown in figure 4.18 has 250 mm diameter and layer height 10.8 mm ,grooves have diameter of 25 mm,four grooves as shown in figure are at 90 degrees each.

The arc time taken for the deposition of each layer with travel speed of 550 mm/min and each layer of height 10.8 mm,50 mm was deposition was accomplished with 30 layers deposition thus the arc time taken for the deposition of 50 mm was 45.5 minutes at travel speed of 550 mm/min similarity arc time for the deposition of 100 mm ,200 mm, and 300 mm was 83 min,166 min,250 min respectively. The final component of 400 mm height,250 mm diameter with 25 mm 4 grooves and wall thickness was deposited in 225 layers with total arc time taken for deposition was 5.69 hours.



Figure 4.19: Deposition after layer 50 mm deposition and 100 mm deposition



Figure 4.20: Deposition after layer 200 mm deposition and 300 mm deposition

It is to be mentioned that after the deposition of 200 mm height, base plate has reached in thermal equilibrium with surroundings which means that base plate has reached room temperature and after 200 mm deposition in here the temperature of substrate or the base plate does not get increased on further deposition. This indicates that on further increase in height would not result in base plate distortion hence with proper clamping and with initial cooling if initial base plate distortion can be arrested WAAM can produce larger components easily without much distortions using CMT and CNC integration. Below is the finally fabricated component using WAAM with Cold metal transfer based WAAM.

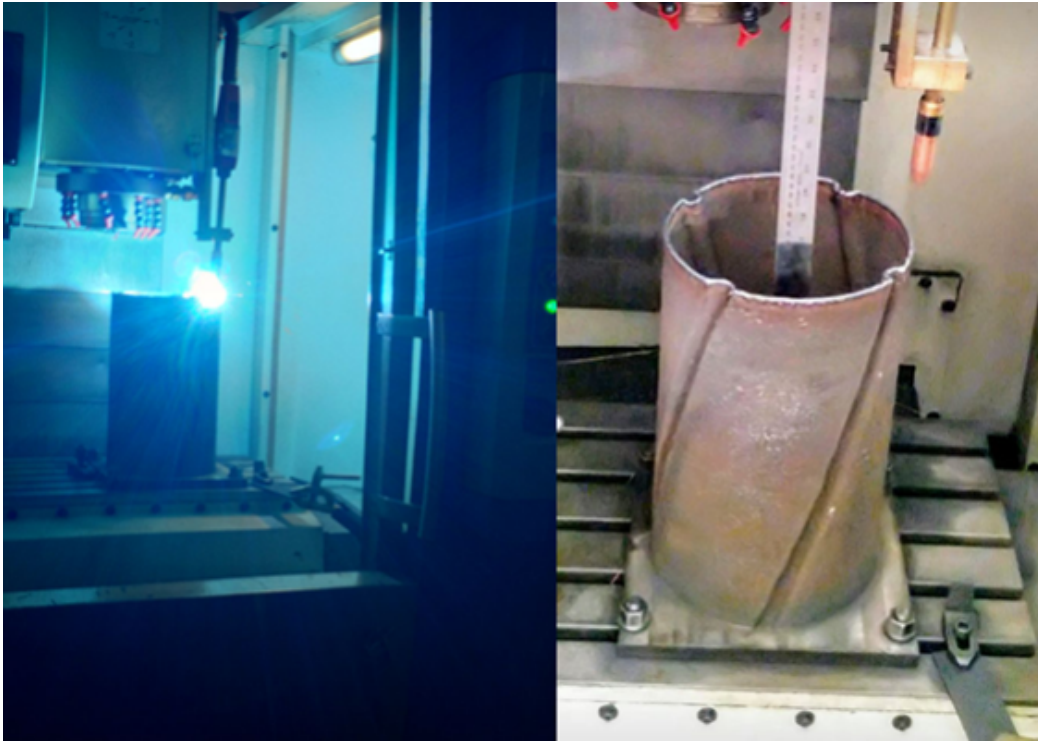


Figure 4.21: Deposition at 400 mm height(left) finally deposited component(right) with 400 mm height and 250 diameter

Chapter 5

Thermal Analysis of the Deposition Process

Thermal study and analysis is one of the most crucial aspect for design of thermally driven wire and arc additive manufacturing. This section takes into account the thermal behaviour of the big cylindrical WAAM manufactured component with multi-pass welds and successively deposited layers. This analysis consists of two parts first part deals with simulation analysis of the deposition process and second part involves the prediction of dwell time or interlayer cooling time to reach steady state temperature. The simulation was carried out in the MSC simufact welding software.

5.1 Modelling procedure

A thermo-mechanical analysis has to be carried out in 2 steps. The first step involves of transient state thermal history analysis(time-temperature analysis) from which the nodal temperature history is carried utilized for the mechanical analysis. This is helpful in prediction of thermal stress and distortion. Below is the model which was input for the analysis in the simufact welding software. The thermo-mechanical FEM analysis is has following variables in terms of deign of the simulation

5.1.1 Finite Element Modelling

Component was modelled using abaqus which has relatively better good mesh control than MSC apex and other meshing . Nastran Exported files in *. bdf format are the only type of format accepted which has mesh data i. e. node coordinate and element data compared to *. iges has vertex, line, area data and *. stl which creates surface to triangles which are not acceptable due to poor quality mesh which exploit the simulation.

In this model shown above, all the components were modelled in Abaqus and exported to *. bdf files and then imported and assembled in Simufact Welding.

Following are the essential mesh used for finite element analysis in simufact welding.

- Essential elements : linear and quadratic elements.
- Linear: uses two nodes over edge and interpolates solution linearly
- Quadratic: flexible and gives better result than linear. More computational time for quadratic elements as more no of PDE equations are to be solved. Commonly used element shape : tetrahedron and hexahedron (brick).

- Tetrahedron: geometrically flexible and convenient for complicated 3D meshing.
- Hexahedron : better computational efficiency and accuracy. Fully integrated linear brick element is overly stiff in bending and modal analysis. This is called shear locking which leads to error in the results.
- 3D block under pure bending should experience curve or shape change but Fully integrated linear brick doesn't respond in similar fashion. It experiences tensile at one surface and compressive at another layer but edges of linear element do not bend.
- To prevent the shear locking reduced linear integration is used which employs one point less than the full integration at each point. This provides flexibility and prevents incorrect shear stress error like pure bending.
- In some cases element becomes under stiff and gives absurd results known as hour glass effect. The FEA software has hourglassing control internally.
- to have precise results fine mesh with reduced integration is used where high distortion is anticipated.

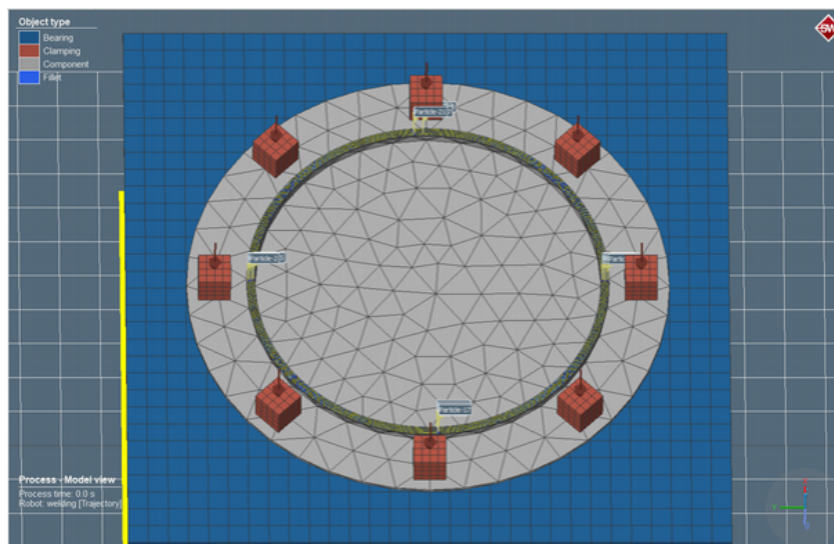


Figure 5.1: Model for simufact welding analysis

5.1.2 Filler Element Modelling

- The filler element scenario is an assumption that all the elements of filler elements are present with properties assigned.
- This causes an error in estimation of temperature during heat transfer through elements. It may also predict incorrect plastic deformation.
- The nature of the weld deposition is carried out using “element birth and death technique” and “quiet element approach” for simulating deposition precisely.
- Element birth and death technique : initial stage of analysis of all the elements of filler element are deactivated and as the process progresses the elements activates as per the user.
- This is provided by a subroutine file which saves lot of computational time and increases accuracy.

- Quiet element approach: all the elements are present in the initial stage itself. However, these elements are assigned to certain material properties that do not effect the whole model. A low value of stiffness and thermal conductivity properties are assigned at the initial stage and actual filler material properties are assigned when heat source reaches position of interest.
- This technique although is more comfortable but takes more computational time as calculation is to be done for whole model.

5.1.3 Heat Source Model

Heat source modelling is most crucial aspect for any welding based modelling process. For an incompressible body heat flow is characterised by flow from higher temperature to lower temperature. The heat flow thus occurring in transient in nature and this transient temperature variation $T(x,y,z,t)$ drives the physical attributes of the welded component and characterize melting and solidification melting and remelting and HAZ . mechanisms through which micro-structures of the weld change, and therefore control the changes, it is crucial to understanding the heat distribution from the torch, and the dissipation of this heat through welding geometry. For welding processes in which the momentum transfer effect of the arc on the weld pool is large, Goldak et al. (1984) derived a model to describe the volumetric heat flux acting on a substrate due to arc. In order to overcome the discrepancy between the predicted and measured temperature gradients in front and behind the arc, two ellipsoidal heat sources were combined as shown in Figure,the front half of the source is the quadrant of one ellipsoidal source and the rear half of the heat source is the quadrant of another ellipsoidal heat source.

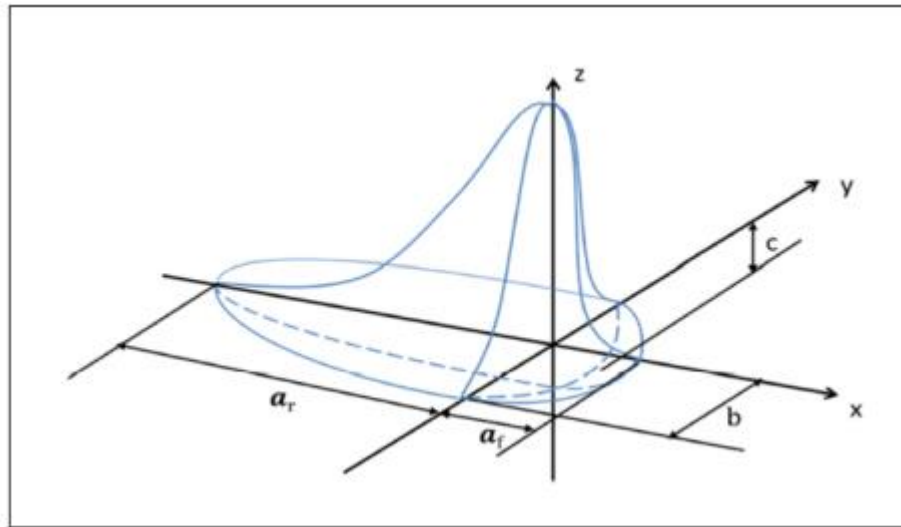


Figure 5.2: Goldak's double ellipsoid moving heat source model (Goldak et al. , 1984)

heat distribution at front is given by

$$q_f = \frac{6\sqrt{3}Qf_f}{\pi\sqrt{\pi a_f b c}} \exp^{-3\left\{\left(\frac{x^2}{a_f^2}\right) + \left(\frac{y^2}{b^2}\right) + \left(\frac{z^2}{c^2}\right)\right\}}$$

heat distribution at rear is given by

$$q_r = \frac{6\sqrt{3}Qf_r}{\pi\sqrt{\pi a_r b c}} \exp^{-3\left\{\left(\frac{x^2}{a_r^2}\right) + \left(\frac{y^2}{b^2}\right) + \left(\frac{z^2}{c^2}\right)\right\}}$$

Where, (a_f) and (a_r) are the front and rear length of the ellipsoid, respectively, b is the width and c is the depth of the heat source model respectively. Q is the energy input w. r. t the efficiency. The

factor (f_f) and (f_r) are the distribution of power at the front and rear of the heat source respectively and is related as $(f_f) + (f_r) = 2$. The Goldak's heat source model is most utilized model for moving heat source and can be flexibly used with the change in weld parameters a,b and c, which can be calculated using the metallographic images. Below are the goldak heat source parameters selected for the simufact welding simulations for the analysis of thermo-mechanical modelling.

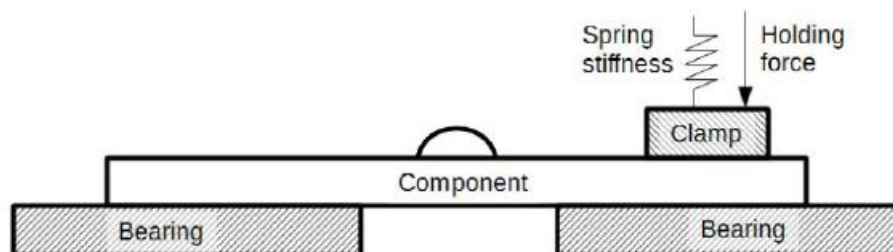
- Front length $a_f = .001002$ m
- Rear length $a_r = .00334$ m
- Width $b = .00334$ m
- Depth $d = .00167$ m

Below are the welding parameters selected for experimental as well as simulation work these parameters were selected based after modelling and material selection .

- velocity = 0.00916667 m/sec
- Current = 150 A
- Voltage = 21.3
- Efficiency = 0.9

5.1.4 Boundary Conditions

- The boundary conditions are a set of differential equations assigned at the boundary region of the model.
- The major heat losses due to conduction, convection and radiation are necessarily included in the model.
- The constraining conditions like clamping and the base plate are modelled as spring elements and the rigid surface is owing to less deformation.
- The release of clamping is simulated by the dispensation of the spring elements displacement boundary condition. The governing equation for heat transfer energy balance is:



Clamping Boundary condition

Figure 5.3: Clamping boundary condition

$$\rho C(DT/dt) = -grad.q(r, t) + Q(r, t)$$

ρ is the material density, C is the specific heat capacity, T is the temperature, t is the time, Q is the heat source, r is the relative reference coordinate, and q is the heat flux vector, calculated as

$$q = -K.grad(T)$$

where k is the thermal conductivity of the material.

Order	Trajectory	Length [m]	Start welding [s]	End welding [s]	Welding time [s]	End time [s]
1	Trajectory	2.80951	0.0	306.492	306.492	306.492
2	Trajectory-2	2.77812	306.492	609.56	303.067	609.56
3	Trajectory-3	2.7467	609.56	909.2	299.64	909.2
4	Trajectory-4	2.71497	909.2	1205.38	296.179	1205.38
5	Trajectory-5	2.80951	1205.38	1511.87	306.492	1511.87
6	Trajectory-6	2.77812	1511.87	1814.94	303.067	1814.94
7	Trajectory-7	2.7467	1814.94	2114.58	299.64	2114.58
8	Trajectory-8	2.71497	2114.58	2410.76	296.179	2410.76

General information
 Robot type: **Standard**
 Solution: **Thermomechanical**
 Simplified approach: **Disabled**

Welding filler
 Initial temperature: 293.15 K

Robot timings
 Start time: 0.0 s
 End time: 2410.76 s
 Total working time: 2410.76 s
 Total trajectory length: 22.0986 m

Selected trajectory
 Name: Trajectory

Trajectory timings
 Pause (start): 0.0 s
 Lead time: 0.0 s
 Welding time: 306.492 s
 Follow-up time: 0.0 s
 Pause (end): 0.0 s
 Sum: 306.492 s

Welding-parameter
 Name: Heat-source
 Heat source: Conventional
 Specification mode: **Transient (indirect power)**
 Velocity: 0.00916667 m/s
 Current: 150.0 A
 Voltage: 21.3 V
 Efficiency: 0.9
 Energy per length
 Gross: 3485.45 J/cm
 Net: 3136.91 J/cm

Figure 5.4: Trajectories and initial boundary condition

- Key points for the FE modelling of the weld based AM process based on the literature survey
- Temperature-dependent mechanical and thermal properties are needed for performing simulation, especially yield stress and thermal conductivity. Phase change effects can be ignored.
- Goldak's heat source model is better for accurately simulating the physics of the welding process.
- Boundary conditions for the thermal analysis includes convection and radiation. If any cooling system is introduced, an equivalent convection coefficient can be used.
- Dense meshing should opt in weld vicinity zone. For large deformation to prevent, the shear locking reduced integration elements scheme can be considered.
- Element birth technique is better for simulating weld deposition process precisely.

Below is the time for each trajectory as the parameters(eg. velocity) was same for each layer in simulation and experiments time taken for each deposition will be as experimental.

5.2 Result and Discussion

While fabricating components using WAAM the first layer is deposited on base plate at room temperature while next layers are being deposited at a temperature much higher than room temperature ie. the temperature of previously deposited beads with other perspective every layer is subjected to different heating loads which may result in residual stresses and change in properties so while depositing the estimation of interlayer cooling time is required to reach the steady state temperature which is needed to be calculated for the deposition of the next layer. Also for bigger metal component(steel here) it is evident that after 70 layer or so the latest deposited layer does not much affect the base plate as it has reached the height which brings it to thermally stable state with respect to base plate thus for this analysis base plate was maintained at room temperature ie. 300 K. Following assumption were used for the simulation and modelling.

- The thickness of the component is assumed to be same throughout the process.
- The base plate and bottom of the weld-bead is maintained at room temperate.
- The properties of depositing material such as density, specific heat and thermal conductivity etc. are assumed as constant throughout the process.

This analysis also considers the time temperature analysis of the mutipass multilayer bead deposition to examine what is the temperature reached after each layer deposition and whether the there is any need of interlayer cooling time considering recrystallization temperature of steel. Moreover this analysis takes into account the effect of deposition at a point on neighbourhood point to consider the temperature influence at these points and the need and prediction of dwell time for subsequent layers.

For this analysis 10 layers were considered to be previously deposited(of the same material and at room temperature) and 11th and 12th layers(2 layers) were deposited simultaneously above 10 th layer layout and parameters of deposition are shown below.

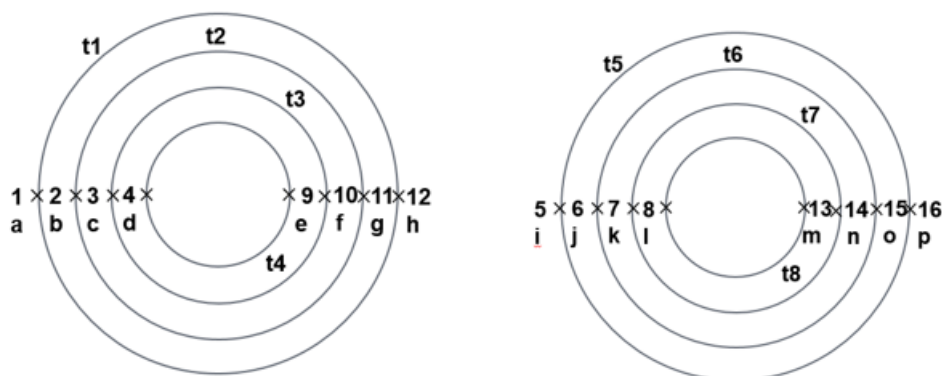


Figure 5.5: Layout for lower layer(on left) layout for lower layer(on right)

This layout considers the points of analysis during deposition across trajectories of deposition t1 t2 t3 t4(of bottom layer deposition) and t5 t6 t7,t8(of top layer deposition)at which temperature profile has to be considered. For instance points 1,2,3 and 4 were the points taken on 4 beads(4 passes of deposition) of the lower layer while 5,6 and 7 and 8 were the points taken on 4 beads of the multi-pass upper layer

whereas the point 9,10,11 and 12 and points 13,14 15 and 16 were the points of diametrically opposite ends of lower and upper layers respectively.

- The modelling was done in abaqus using median axis algorithm with approximate global size 2.5 (grid size) and the assembly and models were imported to siufact welding in . bdf format.
- Circular trajectories were selected on the beads and clamping boundary conditions were applied to arrest degrees of freedom of the substrate/base plate due to heating loads.
- Goldak moving heat source model was selected for deposition.
- The base has been maintained at room temperature ie. 300 K.

5.2.1 Temperature History of various points

The time temperature analysis was done to analyse the temperature profile with time. The total time for deposition was 2405.76(for 2 layers) and the first layer deposition took exactly half the time ie. 1205.38 seconds the Time-temperature plot was constructed using csv file for the points taken on the trajectory.

The total deposition for two layers took 2410.76 seconds while first layer took half of its time ie. 1205.38 seconds. Time temperature analysis of lower layer was done as shown in Figure below the particle at which the Goldak heat source is at the end of the deposition of first layer(lower) at the end of deposition of lower layer ie. particle 4 was considered.

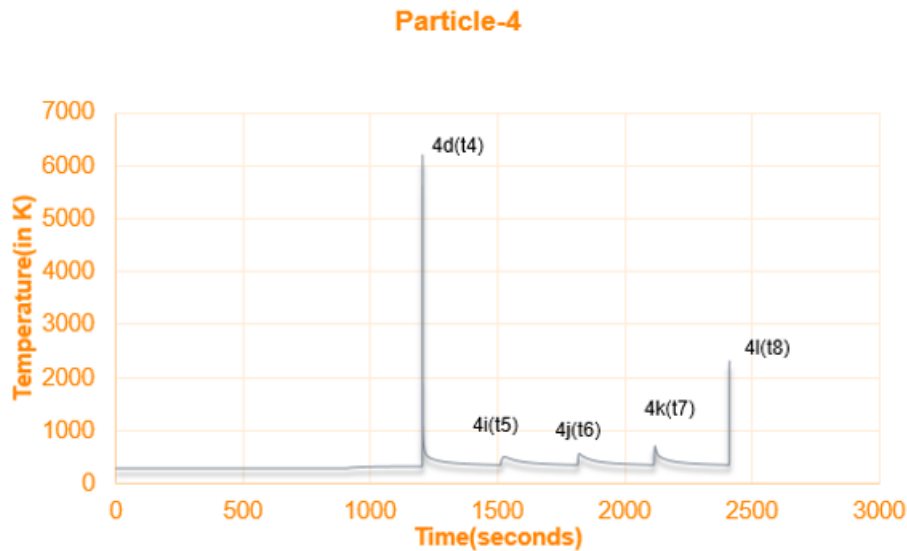


Figure 5.6: Time-Temperature profile of particle 4 at the end of deposition

It can be inferred that at a particular node/point the temperature reaches a maxima when Goldak heat source is at that point also to mention that as Goldak moving heat source is a negative exponential function of space and at origin ie. at exact location temperature tends to infinite thus it does not give the exact temperature at origin of Goldak heat source. Actual temperature is the temperature of Goldak moving heat source at adjacent node ie. 2.5 mm in x direction the actual peak temperature can be calculated using Goldak heat equation and balancing it wrt transient heat equation and by substituting

the Goldak parameters and time step. The maximum temperature thus obtained is 3000 K. Below is the variation of temperature of Goldak heat source from center. Considering movement in a straight line.

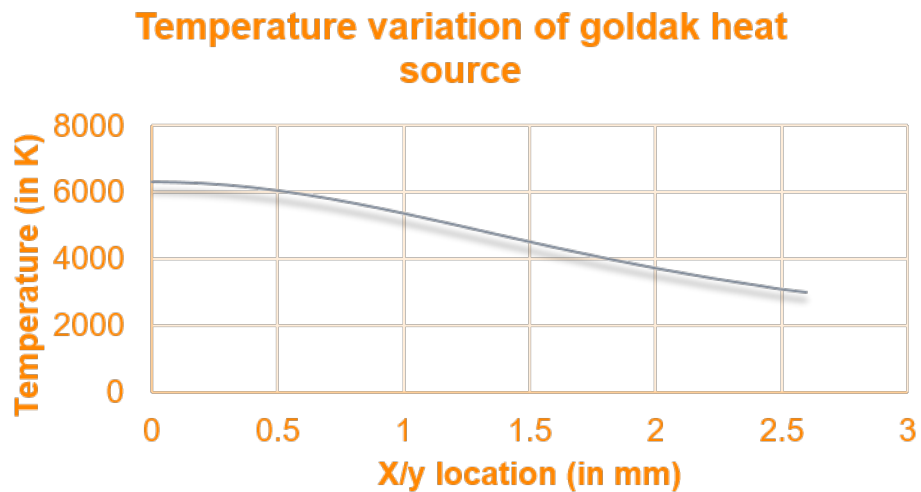


Figure 5.7: Variation of Goldak heat source temperature from center

It can be seen in figure below that there are two peaks first peak is at 1205.38 when Goldak heat source is at particle 4 (at the end of the deposition of layer 1) while the second peak is when the Goldak heat source is just above the particle 4. Similarly the temperature profile of other particles on adjacent beads of multi-pass were studied for lower layer. Temperature profile of particle 3 i.e. the adjacent to the particle 4 is shown below. It is to be noted that at the end of deposition of layer 1 the Goldak heat source is at particle 4 (deposition at trajectory 4 is carried out).

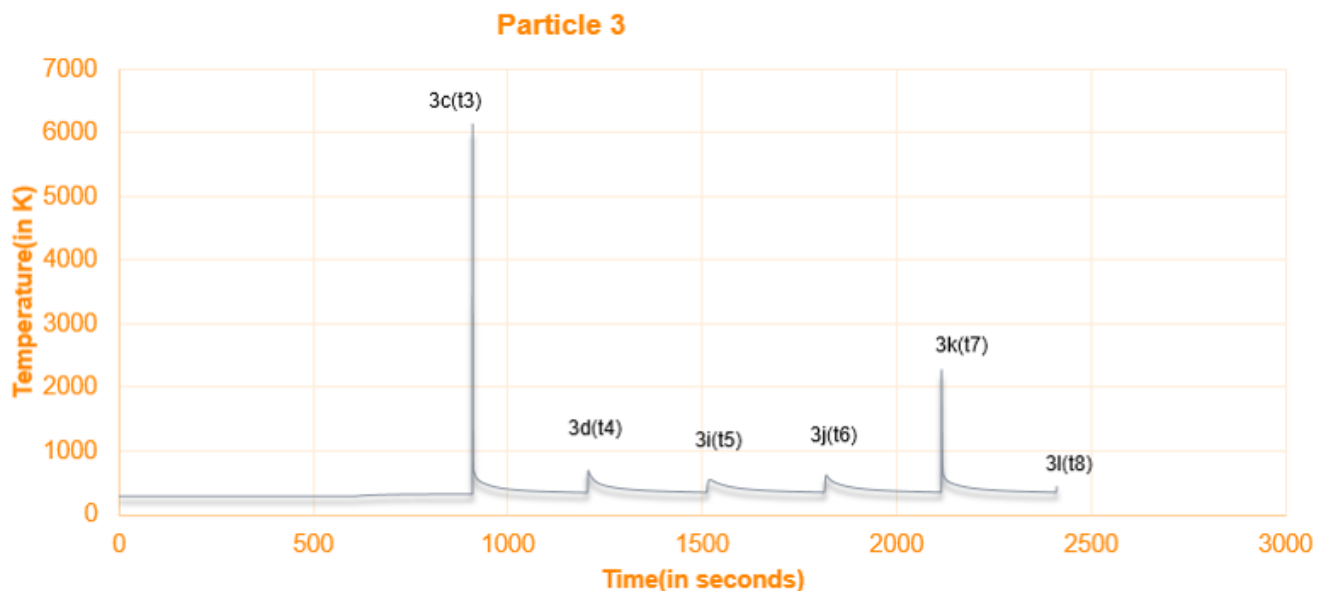


Figure 5.8: Temperature profile of particle 3

It can also be observed from the temperature profile of the particle 3 and 4 (on 3rd and 4th bead or trajectory) the first two peaks (maxims) represent the presence of Goldak heat source at that particle

and the particle or node just above that particle while there are also more peaks depending upon the history of that particle. The temperature profiles of the particles 1 and 2 on beads 1(first pass) and bead 2(second pass) can be shown below.

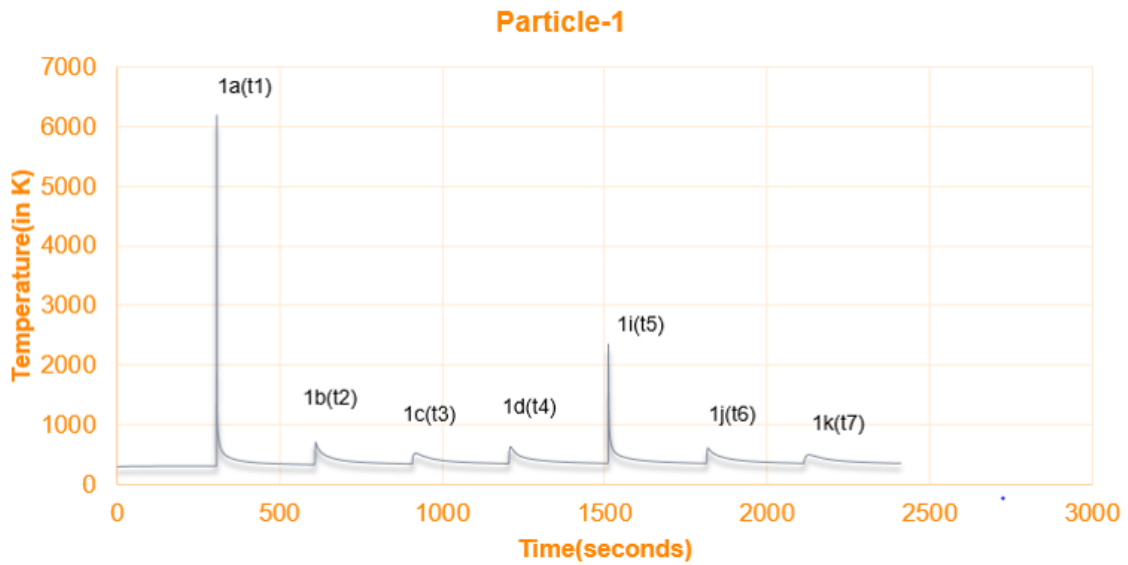


Figure 5.9: Temperature profile of particle 1

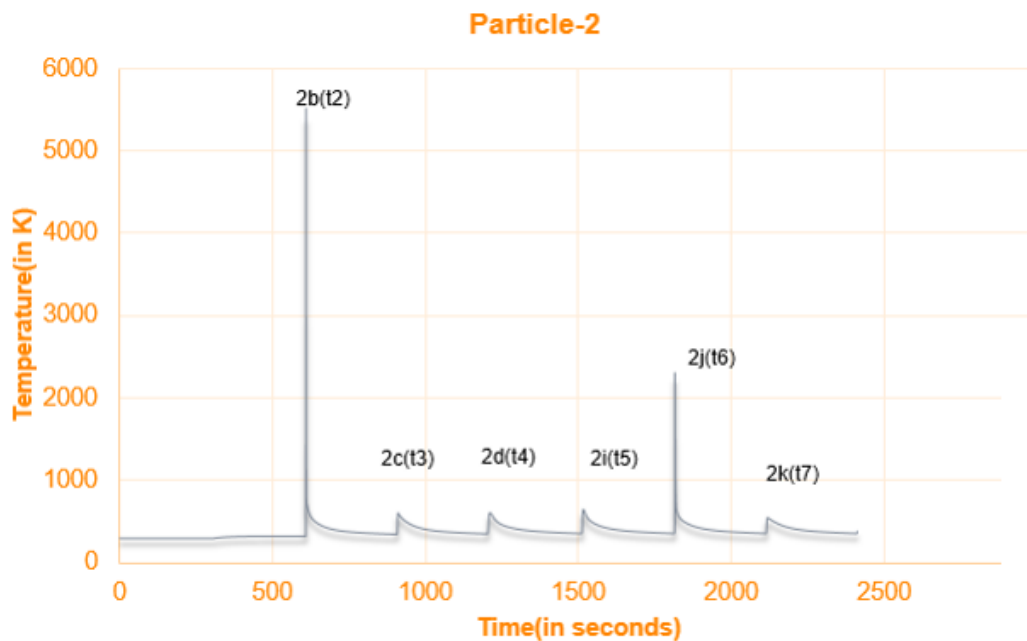


Figure 5.10: Temperature profile of particle 2

It is evident from the particle taken for analysis on the trajectories of lower layer below are the observation. Except when the Goldak heat source is at particle and at the node just above it which causes the singularity of Goldak heat source. Also it is to be noted that peak 1d(t4) ie. the peak temperature of particle 1 when the deposition is carried out at trajectory 4 ie higher than the peak 1d(t4) the reason of this increase is after the completion of lower layer deposition no cooling time was

provided also at the end of deposition of layer 1 due to more temperature difference between particle 4 (on the trajectory t4 ie. 4th pass the) and the particle 1 heat gets conducted from trajectory 4 to adjacent trajectories so the temperature of the particles on the adjacent trajectories increases and as soon as the next layer deposition is started this temperature gets added to give this slightly **higher peak this is mainly attributed to jump of goldak heat source from particle 4 to particle 1.**

- At the end of deposition of first layers ie. 1205.38 seconds.
- Temperature of particle 1=384 K.
- Temperature of particle 2= 428 K.
- Temperature of particle 3= 631 K.
- Temperature of particle 9= 378 K. (diametrically opposite to particle 4 ie. the particle at which Goldak heat source is at the end of deposition of layer 1).

Particle 3 has higher temperature as it is just at the adjacent left to the particle 4.

- At the end of deposition of 2 layers ie. 2410.76 seconds.
- Temperature of particle 1= 363 K.
- Temperature of particle 2= 379 K.
- Temperature of particle 3= 447 K.
- Temperature of particle 9= 378 K.

Temperature profile of the particles on the diametrically opposite ends

The temperature profiles of the particles selected at the opposite ends on the trajectories is equally important as they are unaffected by their conduction due to sudden jump of the Goldak heat source. The temperature profiles of the particle 12 diametrically opposite to particle 1 on trajectory 1 (t1), is shown in fig. As evident from figure first 4 peaks are due to first layer deposition and last four peaks are due to deposition at top trajectories. Below are the trajectories to understand the temperature variation across particles at diametrically opposite ends.

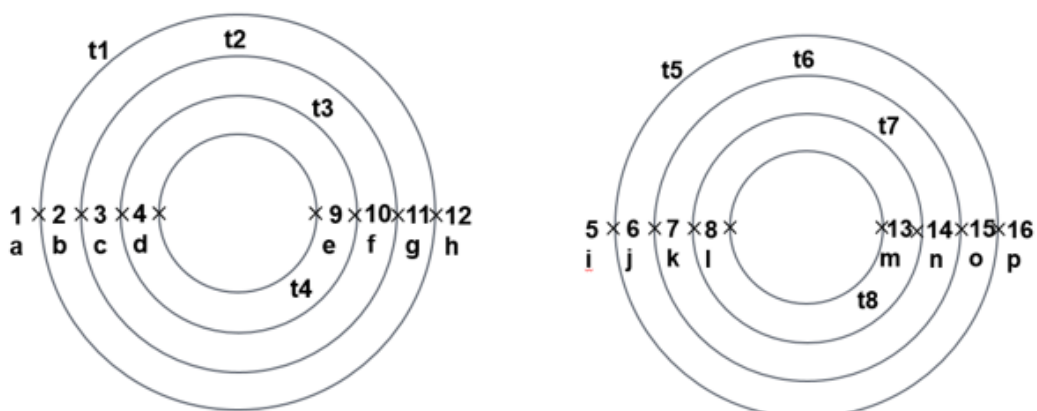


Figure 5.11: Layout for lower layer (on left) layout for lower layer (on right)

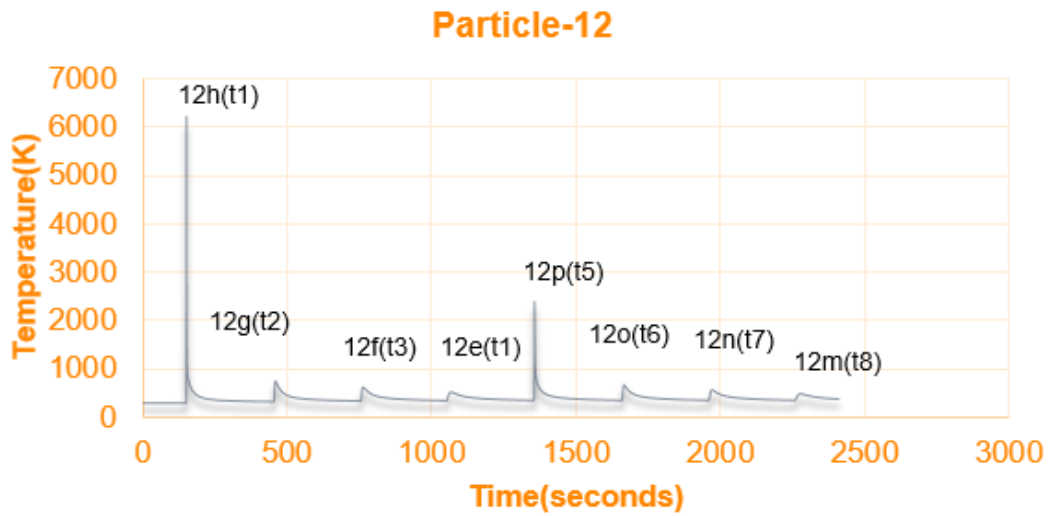


Figure 5.12: Temperature profile of particle 12

The temperature profile of particle 9 as shown is on trajectory 4(t4) diametrically opposite to particle 4. Peaks get increasing as the heat source is deposition on the top layers and it gets its second highest peak 9m(t8) when the Goldak heat source is right above particle 9.

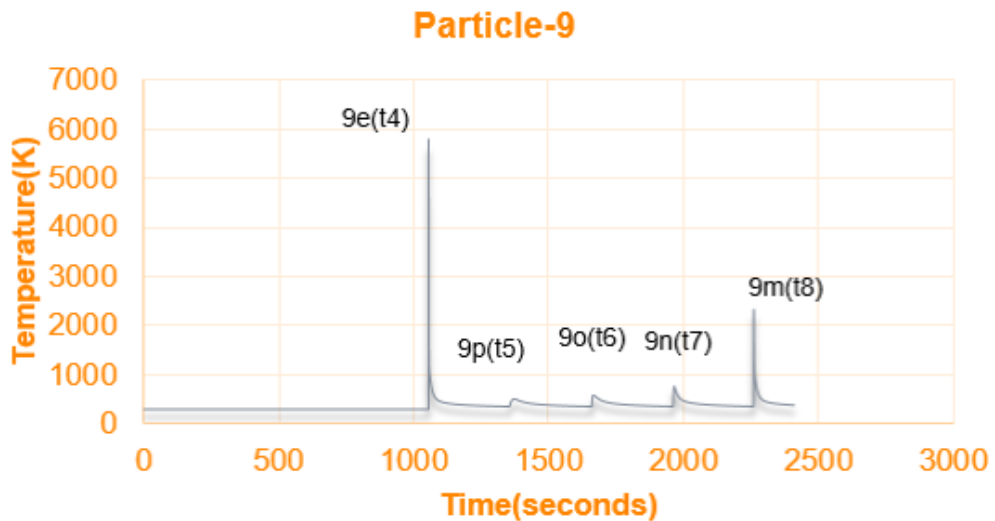


Figure 5.13: Temperature profile of particle 9

similarly the temperature profile of the particles selected on top layer trajectories(4 passes) was studied.

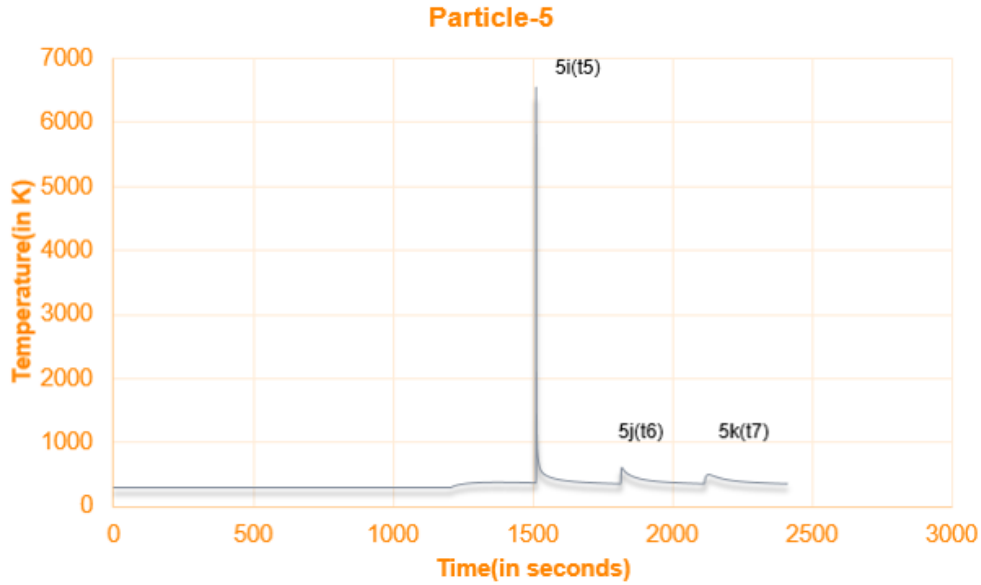


Figure 5.14: Temperature profile of particle 5

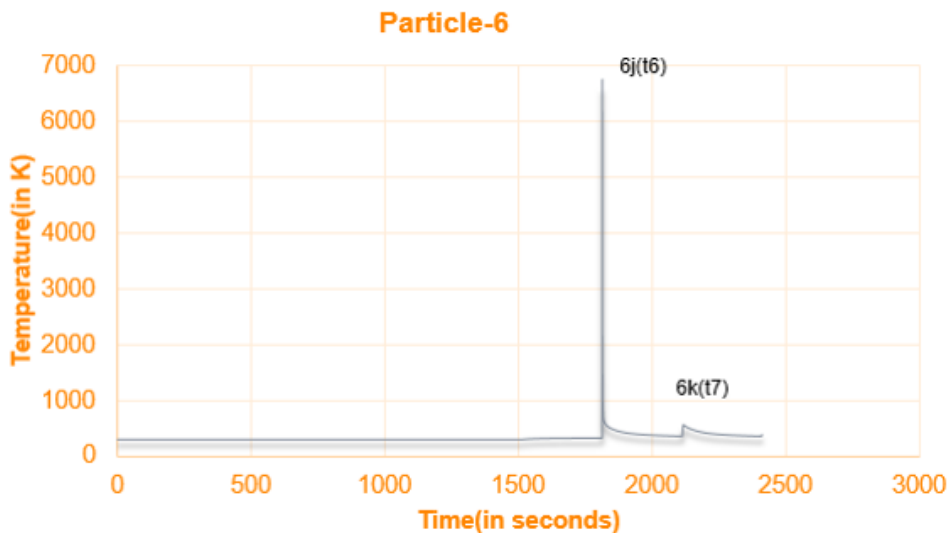


Figure 5.15: Temperature profile of particle 6

It is shown in graphs of particles 5, 6 and 7 and 8 at the top layer particle 5 was deposited first thus it experiences a slight rise in temperature when the deposition is being carried out at its adjacent beads(Goldak heat source) or pass ie. particles 6,7 and particle 8 (3 lower peaks) Similarly particle 18 sees rise due to deposition at particles 7 and 8(on trajectory t7 and t8)(2 lower peaks) and particle 7 sees only one lower peak ie. slight rise when goldak heat source is at particle 8.

- Temperature variation of upper layer at the end of deposition ie. 2410.76 seconds.
- Temperature of particle 7 = 453.28 K(just adjacent left to point of Goldak heat source ie. particle 8, bead 3 on top layer trajectory 7).
- Temperature of particle 6 = 382 K(left to particle 7, bead 2 of the top layer, trajectory 6).

- Temperature of particle 5=361 k(left to particle 6,bead 1 of top layer trajectory 5).
- Temperature of particle 13=382 K(opposite end of goldak heat source ie. diametrically opposite to particle 8)

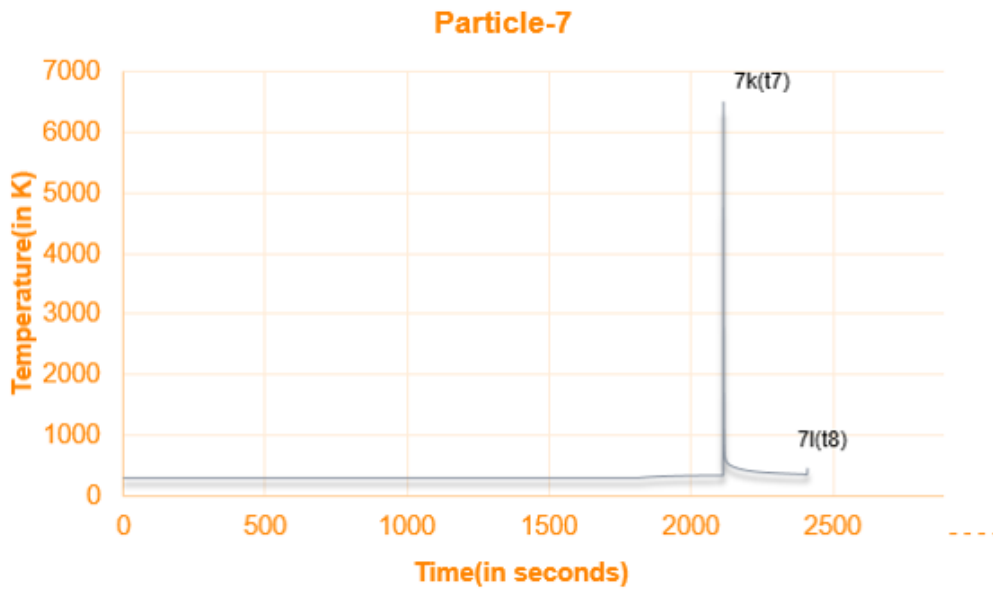


Figure 5.16: Temperature profile of particle 7

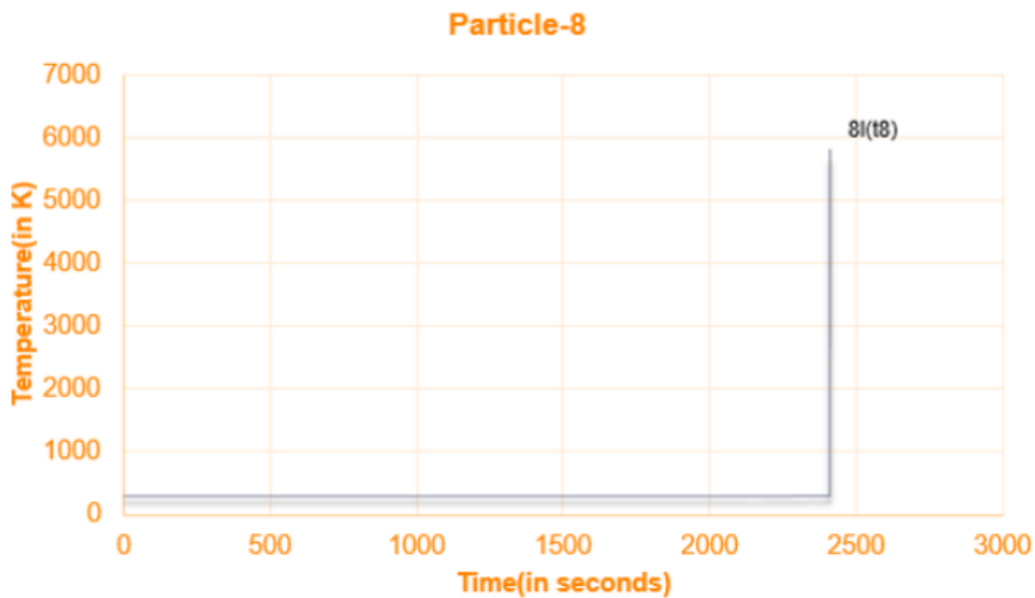


Figure 5.17: Temperature profile of particle 8

5.2.2 Influence of Neighbourhood Deposition on previous pass

The other smaller peaks are equally crucial as for multi-pass deposition while first being goes on depositing the adjacent bead goes for cooling and as the deposition is being carried out at one particular

location it is necessary to monitor the other peaks(of adjacent beads)in order to analyse the effect of deposition of one pass in a multi-pass and mutlilayer additive manufactured component comparison of 2 temperature profiles was drawn.

The temperature profiles of individual particles was combined for both bottom and top layer based on their profiles it was to be inferred whether or not the lower peaks for the adjacent passes/beads reach the recrystallization temperature of steels.

below are the graphs showing comparison of the temperature profiles of the lower layer.

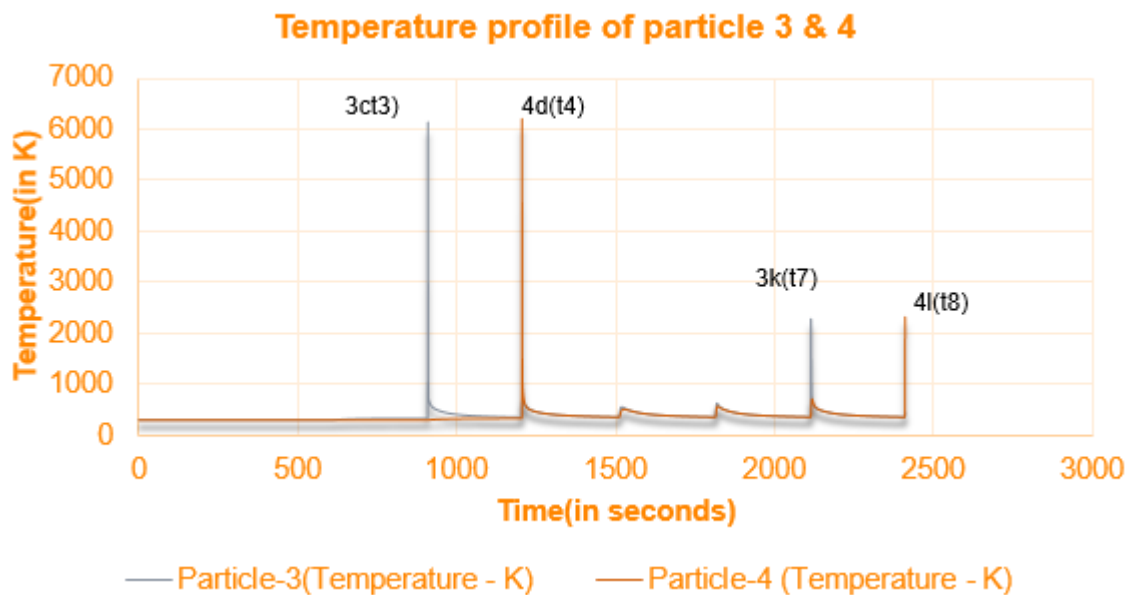


Figure 5.18: Temperature profile of particles 3 and 4

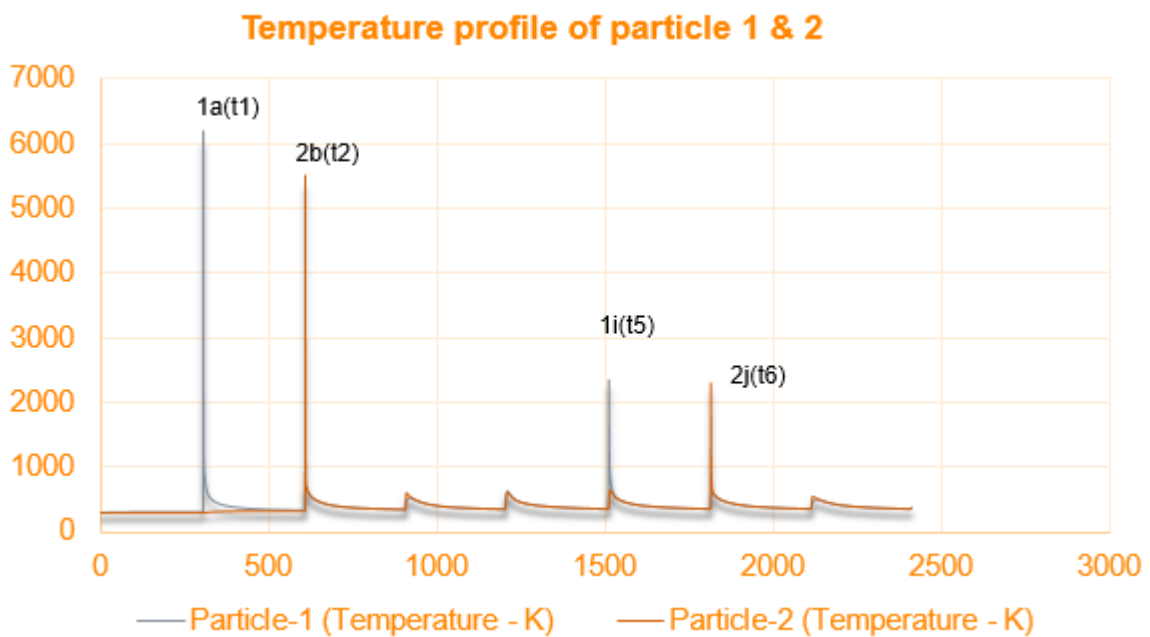


Figure 5.19: Temperature profile of particles 1 and 2

With the help of this comparison we know that the the bead adjacent to the application of Godak heat source ie. the deposition gets influenced most. Thus if we can closely observe the other peaks(except top two peaks which are at the center of Goldak heat source) we can have the knowledge **if the other peak temperatures are above recrystallization temperature of steel that may result in grain deformation which may negatively affect the mechanical properties like strength and hardness.** Maximum temperature peak of the node adjacent to the point of application of Goldak heat source(at the adjacent bead during a multilayer deposition) is 710 K (in the bottom layer) which is below recrystallization temperature of steels ie. 1073 K.

Below is the comparison of temperature profiles of top layer.

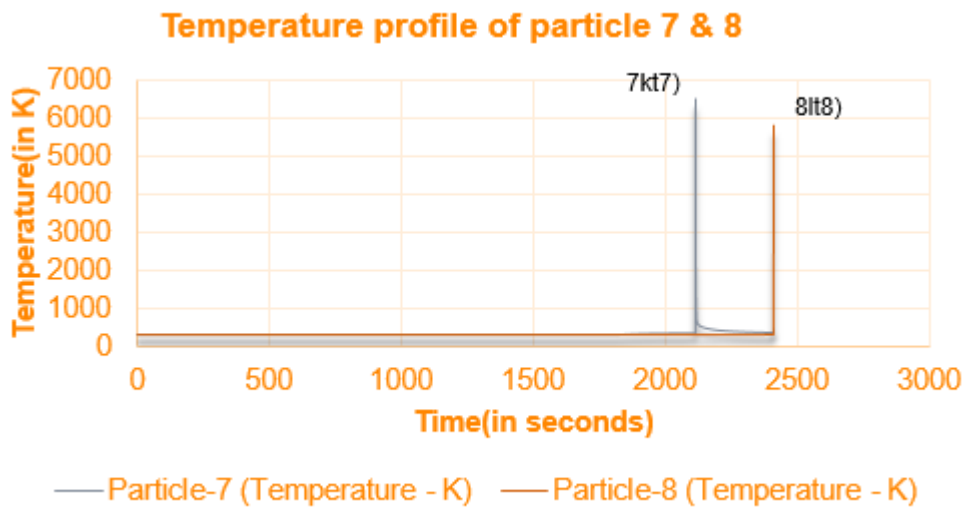


Figure 5.20: Temperature profile of particles 7 and 8

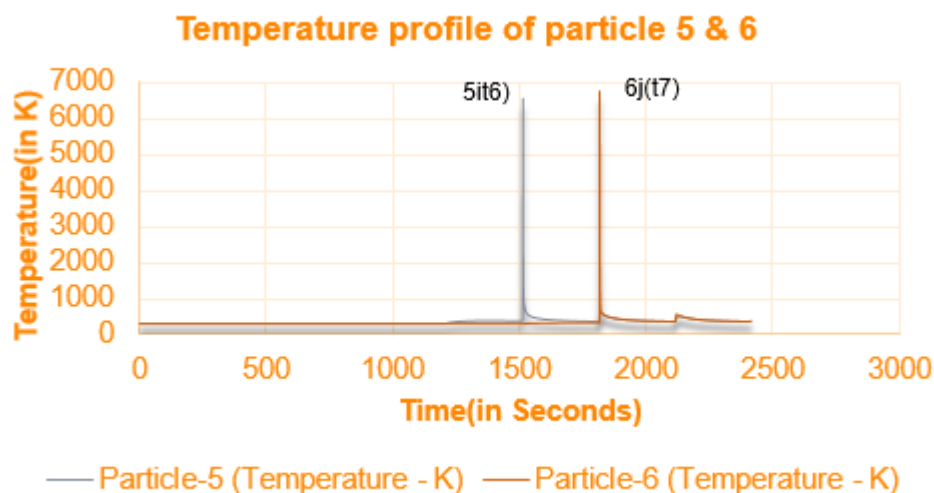


Figure 5.21: Temperature profile of particles 5 and 6

Maximum temperature peak of the node adjacent to the point of application of Goldak heat source(at the adjacent bead during a multilayer deposition) is 710 K (in the bottom layer) and 600 K (at the top layer) ,which is far below the recrystallization temperature of steel ie. 1073 K.

Base plate temperature after deposition

The base plate temperature as per experiments and simulations were found to be decreased as the height of deposition increases, the base plate temperature was analysed for simulations at various points near beads after the deposition of 11th and 12 layers. Below is the temperature of base plate near the deposited bead after 11th layer being deposited at the end time 1205.38 seconds. As evident maximum temperature at the end of 11th layer is 370 K and at other points the temperature of the base plate is in close proximity to steady state temperature.

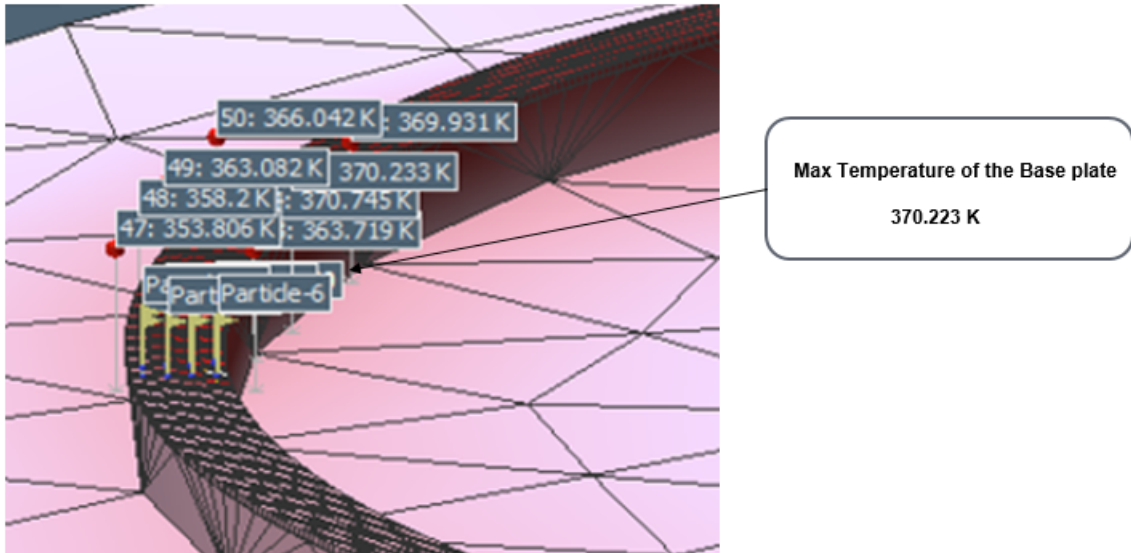


Figure 5.22: Temperature of base plate at the end of layer 11 deposition

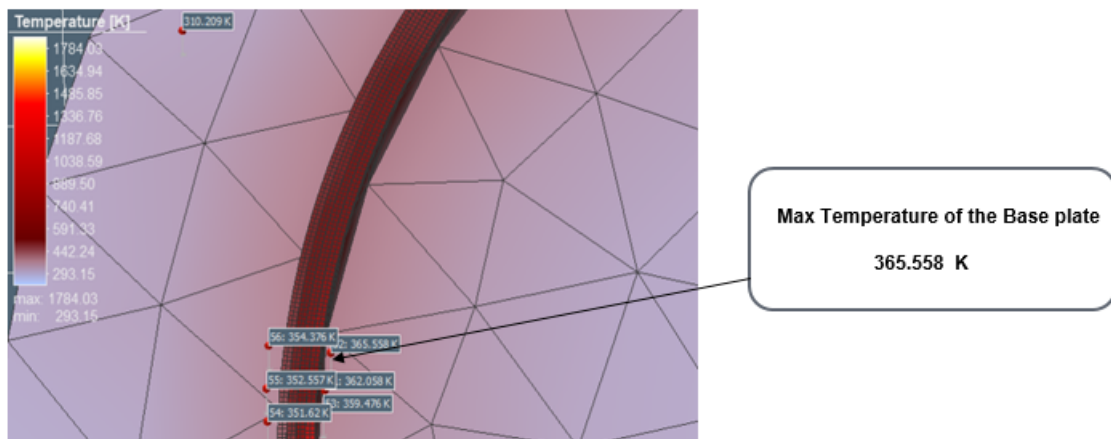


Figure 5.23: Temperature of base plate at the end of layer 11 deposition

It can be seen from figure 5.22 above the temperature of the base plate after 2 consecutive beads 11th bead and the 12th beads is being deposited simultaneously and the temperature measurements recorded are at the end of deposition of 12th layer 2410.76 seconds. The maximum temperature observed is lesser than 11th layer the temperature of the base plate at the end of deposition is 365 K.

5.3 Heat Loss Rate and Dwell Time Estimation

The simulation after the WAAM fabricated bigger component helps to conclude that maximum temperature obtained is 700 K across all multipass layers and in order to avoid recrystallization the maximum temperature before deposition of next layer should at some minimum temperature to avoid re-melting and recrystallization, this temperature is known as steady state temperature, so after each layer certain dwell time is needed to be given in order to reach that steady state temperature for this analysis steady state temperature is considered to be 366 K. Based on the geometry of the cylindrical deposition and based on the deposition pattern a model was tried to be developed to estimate the time required to reach steady state temperature. This model has been based on some practically feasible assumption like we know after deposition of N number of layers (After sufficient height deposited say 100 mm) the base plate temperature reaches thermally stable state with respect to current layer being deposited, thus it does not get affected significantly as height increases further and thus it minimizes the base plate distortion to least possible extent. So in this model the base plate temperature is assumed to be at room temperature and to justify this first like simulation 11 th and 12 th bead interlayer cooling time/dwell time is calculated and compared with the simulation result if similar simplified mathematical models are developed and exploited to predict the cooling time a lot of computational cost and fabrication time can be saved. A Matlab has been developed and used to calculate the cooling time for 11th and 12th bead as same was compared with the simulation result and could be applied to actual automated experiments to get the optimized dwell time between layers. This model also has the versatility of consideration multi-pass beads which helps mitigating the the complexity of dwell time calculation for multi-pass and multilayer deposition. Below is the predicted thermal mathematical model for prediction of dwell time for a cylindrical component with k number of successive beads and subsequent deposition in z direction with total deposited height H. The first layer consists of k number of beads and the heat transfer mode for the first layer for heat loss is radiation conduction and convection. The values of the parameters are given below.

$T_w = 2000 \text{ K}$ (deposition temperature)

$T_s = 366 \text{ K}$ (preheat temperature)

$T_a = 300 \text{ K}$ (atmospheric temperature)

$T_b = \text{Temperature of deposition at } H \text{ height}$

$h = 1.9 \text{ mm}$ (layer height)

$N = 125$ (number of layers)

$H = N * h$ (total wall height)

$h_{cv} = \text{convective heat transfer coefficient} = 10 \text{ w/m}^2\text{K}$

$K = \text{thermal conductivity} = 30 \text{ w/mK}$

$\rho = \text{density of depositing material} = 7850 \text{ kg/m}^3$

$$C_p = 685 \frac{J}{KgK}$$

Heat loss rate

The heat loss through the component is through conduction convection and radiation.

For the above analysis the individual beads can be considered of as cylindrical beads with thickness dh and values of internal and external radius as r_{2k-1} & r_{2k} respectively and height dh as shown in figure for such individual bead.

Where k is number of beads deposition for layer 1, for 1st bead deposition

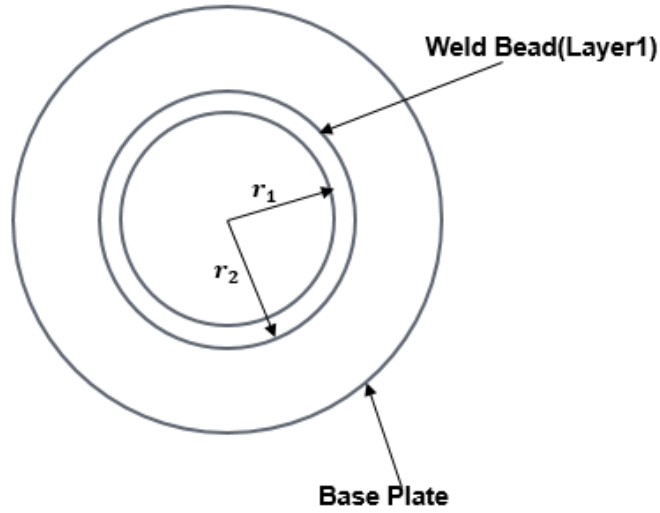


Figure 5.24: Bead 1 of layer 1 deposition with external radius r_2 and internal radius r_1

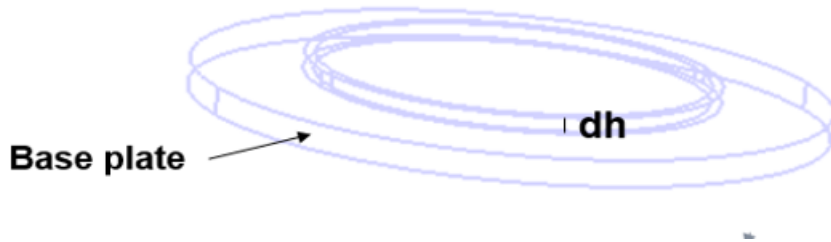


Figure 5.25: Elemental layer deposition with thickness dh on base plate

Here are the assumptions undertaken for the above analysis

1. The thickness of the component is assumed to be same throughout process.
2. After a given layer is deposited, the top surface of the wall is allowed to cool down till it reaches 93°C (pre heating temperature of low carbon steel for avoiding thermal cracks) to deposit the next layer.
3. The base plate and bottom of the weld-bead is maintained at room temperate.

The total heat loss through the component

$$Q = q_{conduction} + q_{convection} + q_{radiation} \quad (5.1)$$

Heat loss through conduction

$$q_{conduction} = 2 \times \pi \times K_{conduction} \sum_1^k \frac{1}{\ln\left(\frac{r_{2k}}{r_{2k-1}}\right)} \int_0^H (T - T_a) dh \quad (5.2)$$

Where

$$T = (T_b - T_a) \times \frac{h}{H} + T_a \quad (5.3)$$

substituting T from Equation 5.3

$$q_{conduction} = 2 \times \pi \times K_{conduction} \sum_1^k \frac{1}{\ln\left(\frac{r_{2k}}{r_{2k-1}}\right)} \int_0^H \left(\left((T_b - T_a) \times \frac{h}{H} + T_a \right) - T_a \right) dh \quad (5.4)$$

On integration and simplification

$$q_{conduction} = \pi \times K_{conduction} \times H \times (T_b - T_a) \quad (5.5)$$

For convection and radiation

First bead convection/radiation will depend on 2 radius and successive bead will depend on single internal radius as the previously deposited bead will act as a shield for the outer layer to get exposed to convection and radiation that is why considering heat loss through convection and radiation for multiple beads first bead is first exclusively considered and then heat loss through subsequent beads are taken into account.

$$q_{convection} = 2 \times \pi \times h_{cv} \times (r_2 + r_1) \times \int_0^H (T - T_a) dh + 2 \times \pi \times h_{cv} \sum_2^k r_{2k-1} \int_0^H (T - T_a) dh + A \quad (5.6)$$

where $A = N \times \pi \times h_{cv} \sum_1^k (r_{2k}^2 - r_{2k-1}^2) \times (T_b - T_a)$ is convection from the top surface and N is number of layer deposited.

On substituting for T

$$q_{convection} = 2 \times \pi \times h_{cv} \times (r_2 + r_1) \times \int_0^H \left((T_b - T_a) \times \frac{h}{H} + T_a - T_a \right) dh + L$$

Where $L = 2 \times \pi \times h_{cv} \sum_2^k r_{2k-1} \int_0^H \left((T_b - T_a) \times \frac{h}{H} + T_a - T_a \right) dh + A$

on integrating and simplification

$$q_{convection} = H \times \pi \times h_{cv} \times (T_b - T_a) \times \left\{ (r_2 + r_1) + \sum_2^k (r_{2k-1}) \right\} + A \quad (5.7)$$

Heat loss through radiation

$$q_{Radiation} = 2 \times \pi \times \epsilon \times \sigma \times (r_2 - r_1) \int_0^H (T^4 - T_a^4) dh + 2 \times \pi \times \epsilon \times \sigma \times \sum_2^k r_{2k-1} \int_0^H (T^4 - T_a^4) dh + B \quad (5.8)$$

where $B = N \times \epsilon \times \pi \times \sigma \sum_1^k (r_{2k}^2 - r_{2k-1}^2) \times (T_b^4 - T_a^4)$ radiation from top surface.

On substituting values of T $q_{Radiation} = 2 \times \pi \times \epsilon \times \sigma \times (r_2 - r_1) \int_0^H \left(\left\{ (T_b - T_a) \times \frac{h}{H} + T_a \right\}^4 - T_a^4 \right) dh + 2 \times \pi \times \epsilon \times \sigma \times \sum_2^k r_{2k-1} \int_0^H \left(\left\{ (T_b - T_a) \times \frac{h}{H} + T_a \right\}^4 - T_a^4 \right) dh + B$ On simplification and integration of above equation

$$q_{radiation} = 2 \times \pi \times \epsilon \times \sigma \left[\left\{ (r_2 + r_1) + \sum_2^k r_{2k-1} \right\} \right] \times M$$

$$\text{where } M = \left[0.2 \times (T_b - T_a)^4 + T_a (T_b - T_a)^3 + 2T_a^2 (T_b - T_a)^2 + 2T_a^3 (T_b - T_a) \right] + B$$

and $B = N \times \epsilon \times \pi \times \sigma \sum_1^k (r_{2k}^2 - r_{2k-1}^2) \times (T_b^4 - T_a^4)$ is radiation from top surface. Heat input in through the process is given by

$$q_{input} = \rho \times V \times c_p \times \frac{dT}{dt} \quad (5.9)$$

Where $\rho = \text{density of material}$, $V = \text{volume of deposition}$ and

$$c_p = \text{specific heat}$$

$$q_{input} = \rho \times \pi \times (r_2^2 - r_{2k-1}^2) \times H \times C_p \times \frac{dT}{dt} \quad (5.10)$$

For heat balance

$$q_{input} = Q_{total}$$

$$\rho \times \pi \times (r_2^2 - r_{2k-1}^2) \times H \times C_p \times \frac{dT}{dt} = q_{radiation} + q_{convection} + q_{conduction}$$

As discussed earlier, the time taken to reach 366^o (top surface of the deposited layer), the above equation has to be solved for t

$$\int_0^t dt = \int_T^{366} - \frac{dT}{(q_{radiation} + q_{convection} + q_{conduction})} \rho \pi (r_2^2 - r_{2k-1}^2) H C_p \quad (5.11)$$

Where t=time taken by top layer to reach 366 K. Heat balance considering the conduction through the layers of cylinder with heat loss through radiation and convection as zero. While deposition of next layer (say (N+1)th layer) the currently deposition layer of height h at temperature T_w and the previously deposited layers at average temperatures as shown below to the base plate maintained at room temperature T_a.

And T_b can be calculated by

Which is the temperature just after deposition of next layer which has to be waited to reach steady state temperature.

$$\left(\frac{T_b + T_a}{2} \right) H = (T_w \times h) + \left(\frac{T_a + T_s}{2} \right)$$

T_s = preheat temperature (366 K)

T_w = welding deposition temperature(2000 K)

T_a = Room Temperature(300 K)

h=height of one bead H=total height of the component

5.4 Summary

This chapter involves the thermal analysis of the large WAAM fabricated cylindrical component with the help for simufact welding software by selecting the point across its trajectories on its lower and upper layers deposited and studying the temperatures of the those particles. It also investigates the effect of neighbourhood deposition on the adjacent beads and studies the time required to reach steady state temperature for base plate on subsequent deposition. In later part of the work a thermal model was developed to predict the interlayer cooling time between successive layers to make it reach at steady state temperature.

Chapter 6

Preliminary studies on weld deposition of IN625

It has been discussed in chapter 2 the alloy 625 offers strength, fatigue resistance, and resistance to aqueous corrosion at elevated temperatures. And, it is capable of offering higher strength and creep strength, rupture, and hot corrosion resistance at higher or elevated temperatures. Alloy 625 has also the capability of maintaining a great tensile strength as well as ductility, and impact strength and toughness at higher or cryogenic temperature range. Due to excellent excellent weldability and resistance to hot cracking it is one of the becoming the first choice of WAAM. This work deals with parameter selection and optimization of Inconel 625 for multi-pass and multilayer WAAM and also attempts to deposit thin wall.

6.1 Modification to the Deposition Setup

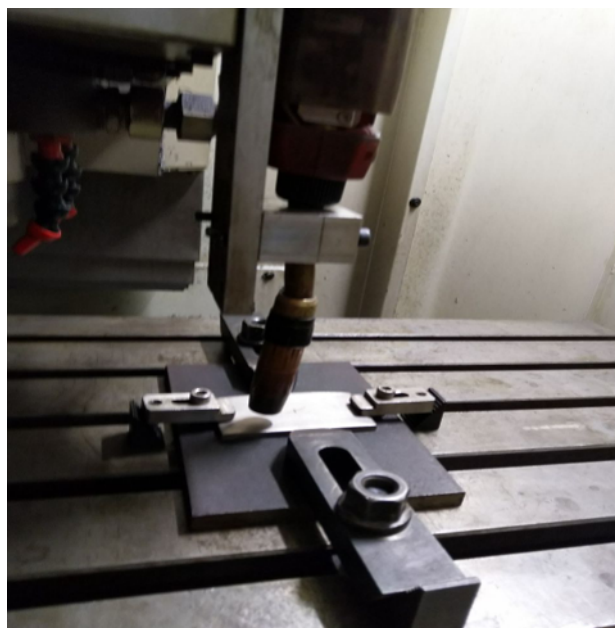


Figure 6.1: Experimental setup for WAAM of IN625

Due to better suitability of the process CMT was used for Inconel 625 and for this purpose integration of CMT with the CNC for weld-deposition was carried out this retrofitment utilizes the precise movement of CNC bed with welding torch being fixed the x,y and z movement is carried out by cnc with deposition accomplished through VR 7000 CMT advanced power source.

Inconel 625 wire with 1.2 mm diameter was used on base plate of inconel 600 with dimensions 100*50*5 mm.

6.2 Parameter Study

6.2.1 Single Pass

First attempt was to establish stable single pass bead and to measure its width and height in order to proceed for multi-pass and multilayer WAAM. For this purpose wire feed rate was varied between 6.1 m/min-6.5 m/min. Current was varied between 161 A- 171 A. Travel speed was typically kept between 500 mm/min-600 m/min. Inert gas used was 100 percent Argon with gas flow rate of 12 l/min and contact tip to work distance(ctwd) was kept 10 mm throughout.



Figure 6.2: Single bead deposition of In625 on In600 plates

At 161 ampere current and 600 mm/min travel speed 6 mm width and 2.5 mm height was obtained while 171 ampere current gave 7 mm width and 2.3 mm height. Also for decreased travel speed of 500 mm/min the height of the bead of increased to 2.7 mm while width was 6.3 mm for 171 amperes. At this parameters range of 161 A- 171 A most of the welds were continuous and uniform for single bead deposition based qualitative study.

Table 6.1: Width and height for single deposited bead of Inconel 625

WFS(m/min)	Current	Voltage	Table feed(mm/min)	Width(in mm)	Height(in mm)
6.1	161	12	600	5.9	2.5
6.1	161	12	500	6.1	2.7
6.5	171	12.5	600	60.8	2.4
6.5	171	12.5	500	60.8	2.7

6.2.2 Multi Pass

The single beads deposition parameters were tried for multi-pass welding at high and medium travel speeds.



Figure 6.3: multi-pass IN625 deposition at high/medium travel speed

Here are the observations based on attempt of the deposition.

- With high speed (700 mm/min) in cmt mode no proper fusion between beads.
- With medium speed(500 m/min-700 m/min) more height of deposition waviness was evident.
- Less heat input(less current and high speed) caused no bonding and continuous bead if given a delay between successive offset layers was given.

Multi pass welding of Inconel 625 at low speeds

The lack of fusion and disbonding being dominant at higher speed ,in order to get stable and proper bonding and fusion IN625 multi-pass deposition was tried to be carried out at lower travel speeds. For the experiments the current was kept constant at 161 amperes and travel speed was varied between 250 mm/min-500 mm/min. Based on geometry of the single bead the offset was kept between 3.3 mm-5 mm a Design of experiments(DOE) full factorial design model was used to develop the model for the set of experiments.

- Dis-bonding between layers at higher speed was observed.
- Re-melting was observed at certain locations due to excessive heat during the process.
- The time difference between successive beads played a crucial role towards their bonding during Fusion.
- At 161 ampere current and 250 mm/min travel speed with 4.4 mm offset with 4 consecutive beads, flat and uniform beads were observed except re-melting at start-end points due to more heating.



Figure 6.4: multi-pass IN625 deposition at low travel speed

Further in order to deal with re-melting and disbonding parameters were needed to be modified with current of 161 ampere the travel speed was now varied between 350 mm/min- 380 mm/min and arc correction was set to -4 % from -25 % at the bottom right as shown in figure 6.5 it was evident that changing arc length correction at the corner helped to control width and depth of the beads and helped in controlling the heat input during the deposition of mutipass beads thus arc correction felicitates in situ deposition control,ctwd was kept 12 mm and gas supply was kept at 12 l/min. 3 multi-pass beads were deposited(on left) as shown in figure below and 3 layers like this were deposited(on right).



Figure 6.5: multi-pass IN625 deposition at low travel speed multi-pass(left) and multi-pass with multi-layer(3*3)

6.3 Fabrication of Simple Geometries

A thin wall of Inconel 625 was deposited on IN625 plate of dimensions 100*50*5 mm using current range 153 A- 161 A. At torch speed 350 mm/min. The layer height of 4 mm was obtained and thus 8 layers were deposited total height deposited was 35 mm. At these parameters continuous beads were obtained without any material flow and disbonding. The deposition at low speed resulted in better stability of beads for thin wall. Below is the figure showing simple thin wall of IN625 deposited using WAAM.



Figure 6.6: Deposition of thin wall of IN625

6.4 Issues and Challenges

Surface and Material Quality

Though high deposition is the significant advantage of WAAM but it carries with itself the excessive heat input which results in residual stresses and distortions, so while aiming at large scale implementation of WAAM residual stresses and distortions are the major concerns. To minimize the residual stresses and distortion major experimentation and simulations will be required. The surface quality is highly dependent on the process parameters like current used, travel speed, wire feed rate and also wire diameter. Post welding heat treatments can be done to release the residual stresses and pre heating should be preferred to avoid surface cracks and distortions so for enhancing surface quality the further strategies and methods are needed to be developed.

Automatic Path Planning

Now a days work have been done only for producing simpler structures at large scale using WAAM because of lack in manipulators and slicing strategies so there is immense need of algorithm to automatically generate the sliced path for any complex structure. For WAAM the quality and accuracy of individual layers is crucial for successful deposition of next layer but there is the kind of unpredictability in the bead geometry due to less accurate process and due to spatter and material flow so sensors are needed to automatically calculate the bead geometry and layer height so that adaptive slicing strategy can be implemented. Thus we can visualize that automatic path planning is still is a major challenge for manufacturing of bigger WAAM structures.

Monitoring and Process Control

GMAW based WAAM is still lacking predictability and repeatability because for sensitive parameter variation even slightest change in wire feed rate during the process due to small irregularity can cause bad surface quality so in order to ensure the stability of previously deposited layer the automatic control of factors like interlayer temperature and layer height are important.

Minimizing Machining

Because of poor accuracy and stair stepping effect an integrated milling system is to be used after each layer which results in more time consumption so there is a need to optimize the bead geometry in order to reduce the stair stepping effect and thus minimal finish machining to get the net shape without any surface defects with optimal surface quality.

Residual Stress and Distortion

Residual stress causes bad tolerances as well as premature failure due to non-uniform heating and cooling although residual stress can be minimized by post processing still they cause major loss to tolerances. The most useful technique to arrest distortion is to control the building up of the residual stress during the process due to heating and cooling simultaneously involved in AM bigger component the residual stress can become more severe and cause the warping and the bending distortion in the

substrate and the component so to address this issue and minimized bending distortion of the substrate proper cooling should be provided during the process and PWHT should be done to deal with the residual stress involved in the process.

Chapter 7

Summary and Future scope

7.1 Summary of the Current Work

This work starts from established WAAM technology and aims to scale up its capabilities both in size and material options for fabricating large scale metal and super alloys components.

Parameter optimization and path planning strategies were studied for the medium scale components (ϕ 250mm) with Robo path generation and GMAW-P process optimization. After successful fabrication of medium scale components using WAAM, the kinematics and setup for fabrication of bigger metal components has been taken up. The setup has been fabricated and optimized with respect to working volume for maximum utilization of 6 axis Robot kinematics. Subsequently, trials were carried for the fabrication of bigger metal components.

The challenges in the fabrication of bigger metal components were studied and the parameters were fine tuned to control the layer instability and material flow. This would ensure that the fabrication of the bigger metal components can be realized with improved quality such that minimum finish machining is required. Based on this knowledge, a large metal component (ϕ 900mm) was successfully fabricated.

The above mentioned components were comparatively thick needing multi-pass fabrication. Subsequently, thin components needing single-pass deposition were fabricated. Single-pass components are much more challenging as the weld-beads have to exactly align with each other and there is no room for cross-flow. Hence, a cold metal transfer (CMT) system was employed for the weld-deposition as it offers continuous and consistent weld-deposition. Using this, a large cylindrical columnar structures with helical grooves was successfully fabricated on the CNC kinematic setup.

In a multi-pass fabrication, the order of the passes become important as they will influence the thermal state of the component under fabrication. Too much of heat accumulation at one point might lead to erosion and molten metal flow in that spot. Hence, the thermal analysis of the deposition process was also carried out. Effect on temperature profile of adjacent pass was studied during neighbourhood deposition. A thermal model was developed for prediction of interlayer dwell time between layers for the deposition of next layer.

Some initial trials were done for multi-pass and multi-layer deposition of Inconel 625 alloy.

7.2 Future Scope

As most of the studies on the mechanical properties of the WAAM components are on small scale samples, a study of how these properties change when scaled up in size will be of relevance.

A better understanding of the temperature profile during weld-deposition can be arrived at by em-

ploying enhanced instruments for better recording and control of temperature data of base plate and the subsequent layers.

Some generic and universal guidelines can be evolved for a wider set of geometries so that simulations can be minimized.

The fabrication of IN625 is being subjected to too much of heat and further studies will be required to obtain better accuracy products.

Bibliography

- [1] Menglei Cai, Chenhui Wu, and Xin Gao. The influence of arc length correction on welding in cmt welding. In *IOP Conference Series: Earth and Environmental Science*, volume 170, page 042106. IOP Publishing, 2018.
- [2] Donghong Ding, Zengxi Pan, Dominic Cuiuri, and Huijun Li. Wire-feed additive manufacturing of metal components: technologies, developments and future interests. *The International Journal of Advanced Manufacturing Technology*, 81(1-4):465–481, 2015.
- [3] Donghong Ding, Zengxi Pan, Stephen van Duin, Huijun Li, and Chen Shen. Fabricating superior nial bronze components through wire arc additive manufacturing. *Materials*, 9(8):652, 2016.
- [4] Donghong Ding, Chen Shen, Zengxi Pan, Dominic Cuiuri, Huijun Li, and Nathan Larkin. Robotic wire and arc additive manufacturing: Innovative fabrication for large metal components. *Australasian Welding Journal*, 60:8–9, 01 2015.
- [5] Jianglong Gu, Jialuo Ding, Stewart W Williams, Huimin Gu, Jing Bai, Yuchun Zhai, and Peihua Ma. The strengthening effect of inter-layer cold working and post-deposition heat treatment on the additively manufactured al–6.3 cu alloy. *Materials Science and Engineering: A*, 651:18–26, 2016.
- [6] KP Karunakaran, Alain Bernard, S Suryakumar, Lucas Dembinski, and Georges Taillandier. Rapid manufacturing of metallic objects. *Rapid Prototyping Journal*, 18(4):264–280, 2012.
- [7] Panagiotis Kazanas, Preetam Deherkar, Pedro Almeida, Helen Lockett, and Stewart Williams. Fabrication of geometrical features using wire and arc additive manufacture. *Proceedings of the Institution of Mechanical Engineers, Part B: Journal of Engineering Manufacture*, 226(6):1042–1051, 2012.
- [8] Jayaprakash Sharma Panchagnula et al. *Additive manufacturing of complex metallic objects with overhanging features: slicing and path planning strategies*. PhD thesis, Indian institute of technology Hyderabad, 2017.
- [9] I Pinto. Additive manufacturing of nickel components using cmt process. 2015.
- [10] Gerhard Posch, Kerstin Chladil, and Harald Chladil. Material properties of cmt—metal additive manufactured duplex stainless steel blade-like geometries. *Welding in the World*, 61(5):873–882, 2017.
- [11] GE Reports. Laser metalz: Bionic design is the next frontier for 3d printing, 2017.
- [12] Sciaky. Advantages of wire am vs. powder am, 2016.
- [13] sciaky. Ebam® drives innovation for many applications and industries. <https://www.sciaky.com/additive-manufacturing/applications-industries>, 2016.

- [14] S Selvi, A Vishvaksenan, and E Rajasekar. Cold metal transfer (cmt) technology-an overview. *Defence technology*, 14(1):28–44, 2018.
- [15] Lewis E Shoemaker. Alloys 625 and 725: trends in properties and applications. *Superalloys*, 718:625–706, 2005.
- [16] Simon. Wire-feed additive manufacturing might be the future of metal-based 3d printing, 2015.
- [17] Yong-Ak Song, Sehyung Park, Doosun Choi, and Haesung Jee. 3d welding and milling: Part i—a direct approach for freeform fabrication of metallic prototypes. *International Journal of Machine Tools and Manufacture*, 45(9):1057–1062, 2005.
- [18] Simhambhatla Suryakumar, KP Karunakaran, U Chandrasekhar, and MA Somashekara. A study of the mechanical properties of objects built through weld-deposition. *Proceedings of the Institution of Mechanical Engineers, Part B: Journal of Engineering Manufacture*, 227(8):1138–1147, 2013.
- [19] Iván Tabernero, Amagoia Paskual, Pedro Álvarez, Alfredo Suárez, et al. Study on arc welding processes for high deposition rate additive manufacturing. *Procedia CIRP*, 2018.
- [20] Crainfield university. Have we 3d printed the biggest metal part ever, 2017.
- [21] Stewart W Williams, Filomeno Martina, Adrian C Addison, Jialuo Ding, Goncalo Pardal, and P Colegrove. Wire+ arc additive manufacturing. *Materials Science and Technology*, 32(7):641–647, 2016.
- [22] Jun Xiong, Yanjiang Li, Rong Li, and Ziqiu Yin. Influences of process parameters on surface roughness of multi-layer single-pass thin-walled parts in gmaw-based additive manufacturing. *Journal of Materials Processing Technology*, 252:128–136, 2018.
- [23] Zhaodong Zhang, Chengshuai Sun, Xinkun Xu, and Liming Liu. Surface quality and forming characteristics of thin-wall aluminium alloy parts manufactured by laser assisted mig arc additive manufacturing. *International Journal of Lightweight Materials and Manufacture*, 2018.
- [24] Huihui Zhao, Guangjun Zhang, Ziqiang Yin, and Lin Wu. A 3d dynamic analysis of thermal behavior during single-pass multi-layer weld-based rapid prototyping. *Journal of Materials Processing Technology*, 211(3):488–495, 2011.